BERICHTE
aus dem Fachbereich Geowissenschaften
der Universität Bremen

Nr. 135

Schmieder, Frank

MAGNETIC CYCLOSTRATIGRAPHY OF SOUTH ATLANTIC SEDIMENTS

Berichte, Fachbereich Geowissenschaften, Universität Bremen, Nr. 135,
82 Seiten, Bremen 1999

ISSN 0931-0800

Die "Berichte aus dem Fachbereich Geowissenschaften" werden in unregelmäßigen Abständen vom Fachbereich 5, Universität Bremen, herausgegeben.

Sie dienen der Veröffentlichung von Forschungsarbeiten, Doktorarbeiten und wissenschaftlichen Beiträgen, die im Fachbereich angefertigt wurden.

Die Berichte können bei:

Frau Gisela Boelen

Sonderforschungsbereich 261

Universität Bremen

Postfach 330 440

D 28334 BREMEN

Telefon: (49) 421 218-4124

Fax: (49) 421 218-3116

angefordert werden.

Zitat:

Schmieder, F.

Magnetic Cyclostratigraphy of South Atlantic Sediments.

Berichte, Fachbereich Geowissenschaften, Universität Bremen, Nr. 135, 82 Seiten, Bremen, 1999.

ISSN 0931-0800

Magnetic Cyclostratigraphy of South Atlantic Sediments

Dissertation

zur Erlangung des

Doktorgrades der Naturwissenschaften

im Fachbereich Geowissenschaften

der Universität Bremen

vorgelegt von

Frank Schmieder

Bremen 1999

Tag des Kolloquiums:

12.2.1999

Gutachter:

Prof. Dr. Ulrich Bleil
Prof. Dr. Gerold Wefer

Prüfer:

Prof. Dr. Volkhard Spieß
Prof. Dr. Heinrich Miller

„So ergibt sich ... ein Bild des Eiszeitalters, welches sich mit den Ergebnissen der geologischen Forschung vollständig deckt. Mit dieser erfreulichen Schlußfolgerung soll nicht das Bekenntnis unterdrückt werden, daß durch die vorliegende Lösung des Eiszeitenproblems ein neues Problem entstanden ist, nämlich jenes, warum der säkulare Bestrahlungsgang, welcher sich durch alle Zeugnisse des Quartärs so unzweideutig zu erkennen gab, während der vorhergehenden geologischen Zeiten in Europa nicht zu solchen Vereisungen geführt habe wie während der letzten 800 Jahrtausende."

Milutin Milankovitch, 1936

Contents

Introduction

Milankovitch theory and cyclostratigraphy

The biggest breakthrough in understanding the Pleistocene ice ages was the discovery that climatic changes are strongly influenced by orbitally induced variations in solar insolation received on Earth. Although the seminal idea has been expressed earlier this theory is inseparably associated with the name of Milutin Milankovitch (1879-1958). He was the first to compute in great mathematical detail the elements of Earth's orbit and their effect on changes in insolation (Figure 1). His complete astronomical theory of Pleistocene ice ages (e.g., Milankovitch, 1936) fundamentally supported the basic idea that cold summers in northern high latitudes are necessary for the build up of large ice shields (for a historical review of the astronomical theory of paleoclimate see Milankovitch, 1936; Berger, 1988 and Schwarzacher, 1993a).

Variations in insolation mainly result from changes in obliquity of the Earth's rotational axis and in precession of the equinoxes (Figure 2). Hays et al. (1976) showed that the corresponding periods around 41 (obliquity), 23 and 19 kyr (precession) can be identified in oxygen isotope records of marine sediments together with the near 100 kyr ice age cycle dominating the late Pleistocene. For each of these periods the coherency between orbital and isotopic signals is statistically highly significant (Imbrie et al., 1984; Figure 3). The discovery that paleoclimatic variations can be traced to exactly predictable periodical fluctuations of the Earth's orbit opened formerly unequaled possibilities for detailed age modeling. Today, the once visionary idea of cyclostratigraphy is realized by quantitatively correlating paleoclimate signals or filtered components to target records constructed from orbital variations. During the last two decades this 'astronomical tuning' has proven to be one of the most powerful tools for high resolution chronostrati-

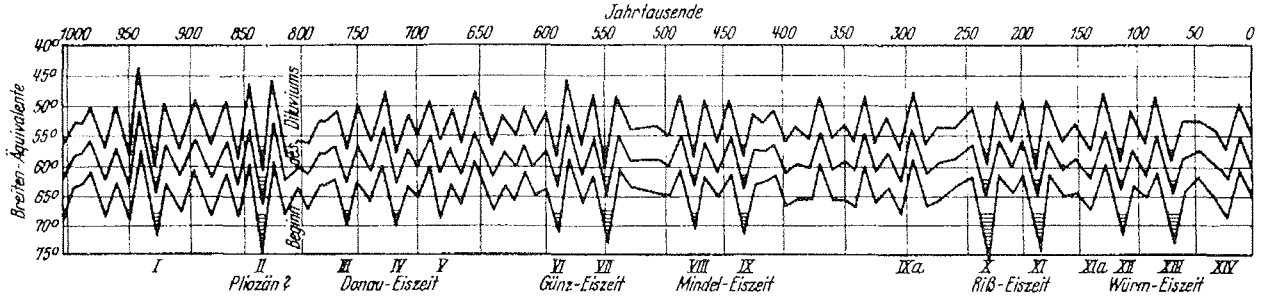

Fig. 16. Strahlungsdiagramm von M. Milankovitch

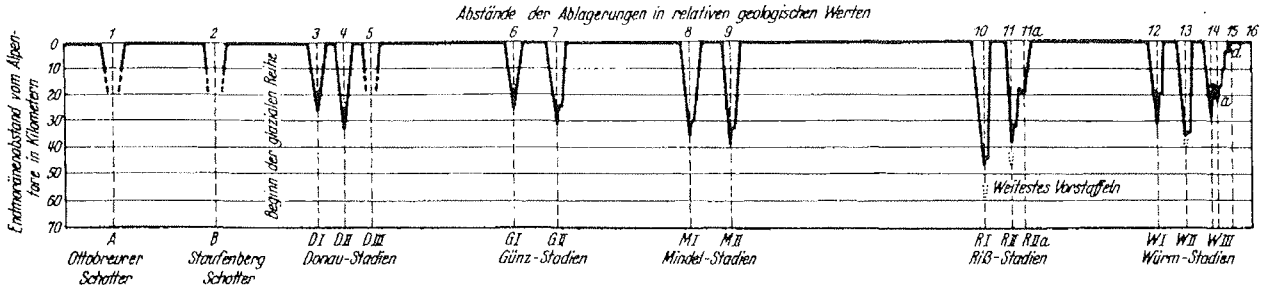

Fig. 17. Stratigraphisches Diagramm von B. Ebel

Figure 1. Milutin Milankovitch's radiation estimates for latitude 50, 55 and 65°N for the past 1000 kyr (top) compared to a stratigraphic interpretation of European ice ages (Würm, Riß, Mindel, Günz, Donau) by B. Eberl (bottom). From Köppen & Geiger (1936).

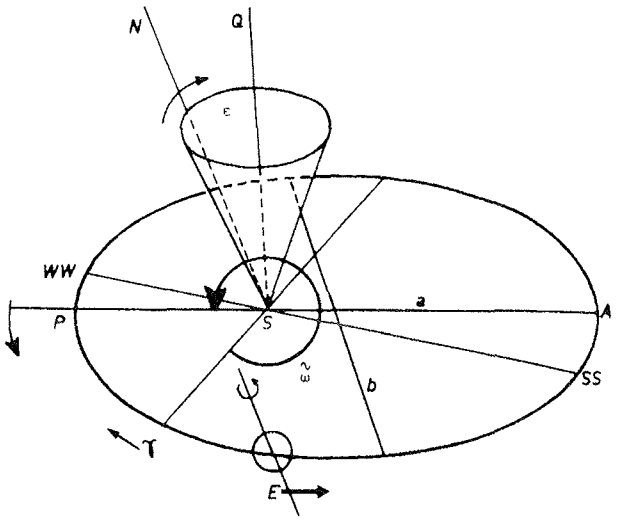

Figure 2. Insolation received on Earth depends on several elements of the Earth's (E) orbit around the sun (S) varying due to gravitational effects of the planets and the moon. Eccentricity $e = \sqrt{a^2 - b^2} / a$ defines the elliptical shape of the orbit (presently $e = 0.016$). Obliquity (ε, presently 23°27') measures the angle between the Earth's axis of rotation (SN) and the perpendicular to the ecliptic (SQ) and is mainly responsible for the seasonal contrasts and the latitudinal gradient of insolation. WW and SS denote winter and summer solstice, respectively, γ indicates the vernal equinox. The inclination ε of the Earth's axis follows a complex precessional movement along the cone shaped surface that produces a migration of the equinoxes scaled to the longitude of the perihelion $\tilde{\omega}$. Today, the Earth is about at the perihelion (P, closest approach between Earth and Sun) during the northern hemisphere winter solstice. From Berger (1988).

graphy, especially for the late Pliocene and Pleistocene but by no means restricted to these epochs (e.g., Schwarzacher, 1993a, b; Shackleton et al., 1995; D'Argenio et al., 1998).

The tardy triumph of the Milankovitch theory over long-standing criticism (see Berger, 1988) is documented impressively in the delayed acceptance of the orbitally tuned age of the Brunhes/Matuyama boundary. Although earlier proposed by Johnson (1982), the age of 780-790 ka became widely accepted only after the 'second attempt' of Shackleton et al. (1990) and Hilgen (1991). Cande and Kent (1992) for example revised their magnetic polarity time scale in 1995 (Cande and Kent, 1995) and made it consistent with astrochronology, also in older sections of the record. In the meantime, Wilson (1993) showed that astronomical calibration results in a more concordant sea-floor spreading history when applied to spacings of magnetic anomaly pattern in the Pacific Ocean. Still assuming an age of 730 ka for the Brunhes/Matuyama boundary - and therefore somewhat inaccurate in the older part - Imbrie et al. (1984) published their epoch-making SPECMAP time scale for the last about 800 kyr and started a systematic documentation of the Earth's paleoclimatic history which since then has been extended and refined gradually by astronomically calibrated $\delta^{18}O$ time scales (e.g., Ruddiman et al., 1986; Martinson et al., 1987; Ruddiman et al., 1989; Raymo et al., 1989; Shackleton et al., 1990; Tiedemann et al., 1994; Berger and Jansen, 1994a).

The ratio of oxygen isotopes ^{18}O and ^{16}O has been applied as a paleoclimatic indicator for quite some time (e.g., Emiliani, 1955). In most cases it is mainly a measure of global ice volume (e.g., Shackleton, 1967). In the context of cyclostratigraphy oxygen isotopes are by far the most frequently used and best studied proxy. But measuring detailed $\delta^{18}O$ records is very time consuming and involves an immense laboratory work. In low sedimentation rate, predominantly terrigenous and/or deposits below the CCD (carbonate compensation depth) detailed analyses may be seriously hampered as it is necessary to collect a sufficient number of calcareous tests from each sample. Consequently, mainly cores from regions with high (carbonate) sedimentation rates are used to achieve detailed paleoclimatic records. This strategy excludes large parts of the worlds oceans holding valuable paleoenvironmental information.

The outlined restrictions of oxygen isotope stratigraphy led marine scientists to explore adequate alternatives. Since the discovery that paleoclimatic patterns are often mirrored by physical properties like magnetic susceptibility (e.g., Robinson, 1990; Tarduno et al., 1991) and GRAPE (Gamma Ray

Attenuation Porosity Evaluator) density records (e.g., Herbert and Mayer, 1991; Grützner et al., 1997) numerous chronostratigraphies have been established on basis of these continuously measurable proxies (e.g., Shackleton et al., 1995; Chi and Mienert, 1996; Shackleton and Crowhurst, 1997; Bickert et al., 1997). The measurements are very rapid and nondestructive and the high resolution reachable makes these parameters especially suitable both for the analyses of high frequency variability and low sedimentation rate deposits.

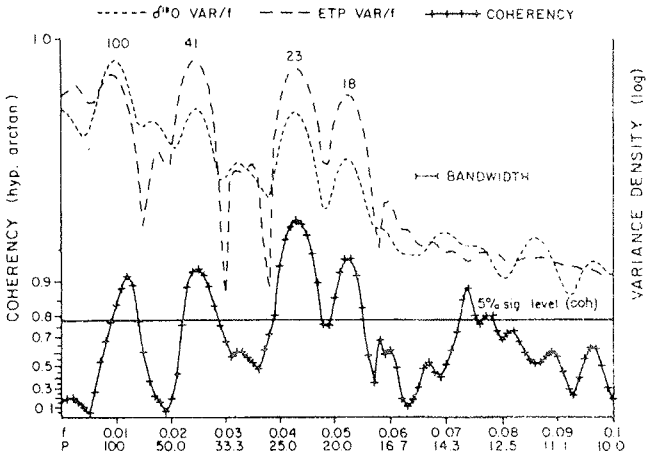

Figure 3. Coherency and variance spectra calculated from records of climatic and orbital fluctuations spanning the last 780 kyr (Imbrie et al., 1984). The ETP signal combines normalized variations of Eccentricity, obliquity (Tilt) and Precession. $\delta^{18}O$ is the unsmoothed SPECMAP stack. From Berger et al. (1984).

Main objectives

During recent years Marine Geophysics in the Department of Geosciences at Bremen University successfully established magnetic cyclostratigraphy as a very efficient dating tool for marine sediment sequences in addition to long-proven magnetostratigraphic technique (e.g., Bleil and Gard, 1989; Nowaczyk, 1991; Thießen, 1993; Nowaczyk et al., 1994; Frederichs, 1995; Gersonde et al., 1997). The age models for the sediment series presented in this thesis are all based on orbitally tuned high-resolution magnetic susceptibility records, partly combined with oxygen isotope data or based on Quaternary magnetostratigraphies. Advantages, difficulties and restrictions of using rock magnetic records for dating purposes are discussed in full detail in Chapter 2.

Although today Milankovitch's theory of a linkage between Earth's climate and orbital variations is widely accepted and successfully applied chronostratigraphically, the history of Pleistocene climate variability still holds numerous unresolved puzzles. To resolve its cyclicity, located within the main but also in the adjacent frequency bands above and below the principal Milankovitch frequencies, requires particularly adapted statistical methods. Extensions of time series analyses into the super- and sub-Milankovitch bands are described in Chapter 2.

The central paleoceanographic topic of this thesis (Chapters 2, 3 and 4) is the mid-Pleistocene transition (MPT) of the global climate system (Pisias and Moore, 1981; Prell, 1982; Ruddiman et al., 1989, Berger and Wefer, 1992; Berger and Jansen, 1994b), the change from a predominantly 41 kyr cyclicity in early Pleistocene to the late Quaternary 100 kyr ice age cycles. Variance in climate indices at periods of precession of the equinoxes (with periods in the range of 19 to 24 kyr) and obliquity or tilt (with major cycles around 41 kyr) can be explained in the framework of Milankovitch theory as linear responses to changes in solar insolation (e.g., Imbrie et al., 1992). In contrast, the origin of the 100 kyr ice age cycle dominating the late Pleistocene (Figure 3) calls for more complex explanations because the direct influence of eccentricity (with major periods at about 95 and 124 kyr in addition to a somewhat stronger 413 kyr component) on insolation is by far too small to produce the corresponding climate style (e.g., Imbrie et al., 1993).

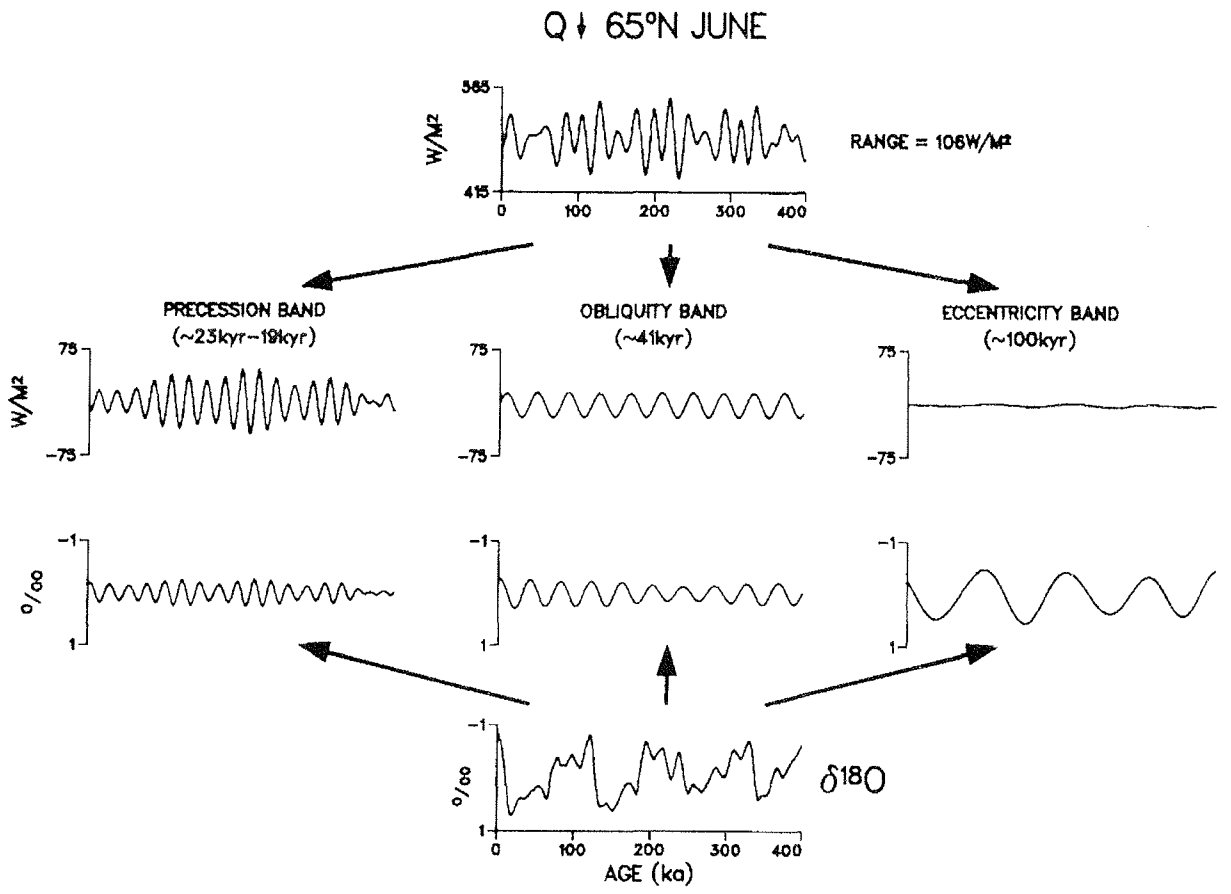

Figure 4. The 100 kyr cycle problem. Partitioning radiation (top, data from Berger, 1978) and climate time series (bottom, data from Imbrie et al., 1984) into their dominant periodic components reveals a large discrepancy in the eccentricity band. While the three frequencies contribute to the insolation signal in proportion to 1, 0.2 and 0.02, the respective ratios for climate variations amount to 1, 2.5 and 11. From Imbrie et al. (1993).

This discrepancy between driving force and response is illustrated in Figure 4.

Besides its pure existence, another enigma is the more or less abrupt onset of the 100 kyr cycle approximately 650 kyr ago (e.g., Berger et al., 1994; Mudelsee and Schulz, 1997). Build up of major ice shields on the northern hemisphere already started at about 2.5 Ma (e.g., Shackleton et al., 1984). While late Pliocene to early Pleistocene paleoclimate records reveal a mainly obliquity and precession related variance (e.g., Raymo et al., 1989; Ruddiman et al., 1989; Bloemendal and deMenocal, 1989), variations with a period near 100 kyr are the primary rhythm of late Pleistocene climatic change although insolation variations remained almost identical. The exact timing of the MPT and the question whether the transition from 41 to 100 kyr cyclicity was gradual ('mid-Pleistocene evolution', Ruddiman et al., 1989) or abrupt ('mid-Pleistocene revolution', Berger and Wefer, 1992) were subject of multiple studies and attempts to model this shift with different statistical techniques (e.g., Maasch, 1988; DeBlonde and Peltier, 1991; Park and Maasch, 1993; Mudelsee and Schulz, 1997; Mudelsee and Stattegger, 1997; Clark and Pollard, 1998). Of the diverse explanations proposed for the 100 kyr cycle, models invoking a pCO_2 controlled insolation threshold for the melting of large ice shields (e.g., Saltzman and Verbitsky, 1993; Berger and Jansen, 1994b) currently yield the best approximation of $\delta^{18}O$ signal pattern. As illustrated in Figure 5, these models accomplish a reconstruction of the MPT timing and the development of 100 kyr cycles by introducing a decreasing atmospheric pCO_2 level (Raymo, 1997; Paillard, 1998).

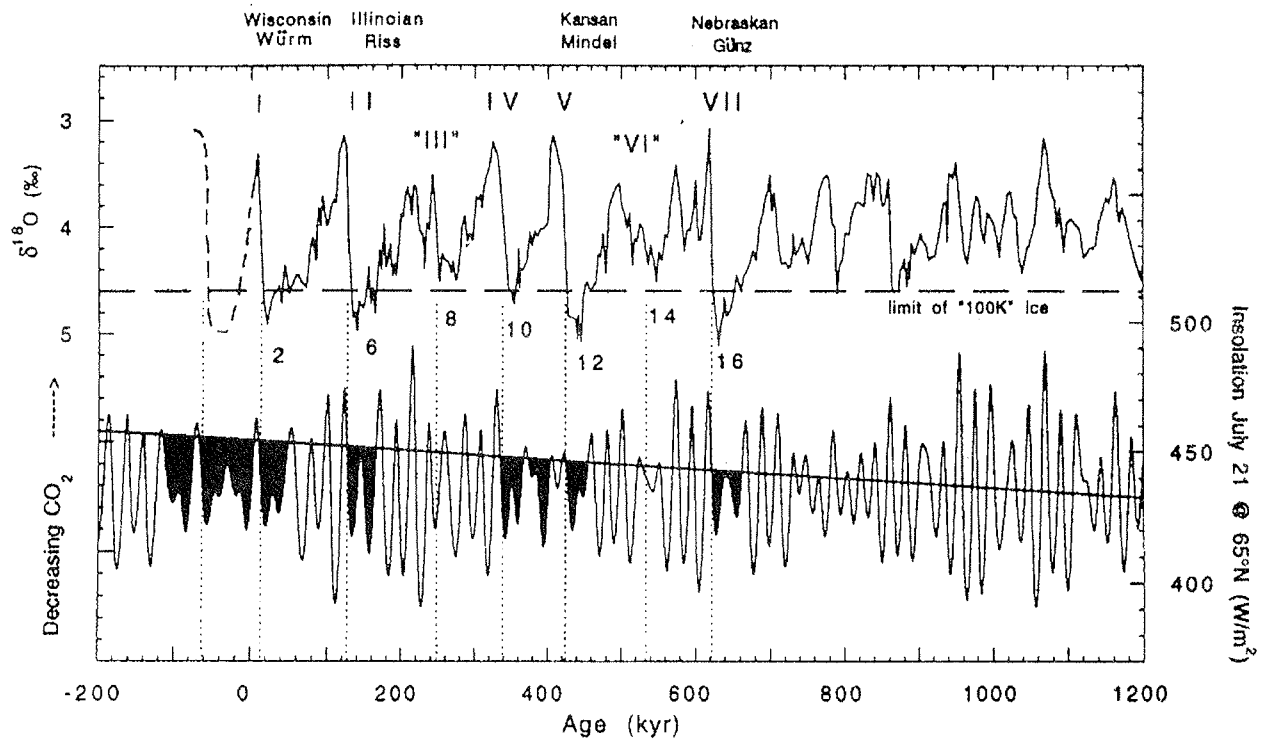

Figure 5. Benthic oxygen isotope data from Pacific ODP Site 849 compared to insolation at 65°N on July 21. The horizontal dashed line in the $\delta^{18}O$ record indicates the level below which 'excess 100 kyr ice' is observed during glacials. The vertical dotted lines mark the midpoint of terminations. Assuming a long-term drawdown of the atmospheric pCO_2 level, outlined by the sloping line in the insolation record, results in a changing threshold for the melting of large ice shields. During late Pleistocene a sufficiently high insolation is only attained at times of positive interaction of obliquity and precession at the end of the black shaded regions. Because the amplitude of precession is modulated by eccentricity, 100 kyr cycles are produced, coinciding with several of the terminations. From Raymo (1997).

With a few exceptions (e.g., Raymo et al., 1997) so far all investigations of the MPT were based on oxygen isotope records. The rock magnetic view presented in this thesis adds some completely new aspects for the understanding of this fundamental enigma of Quaternary climate evolution. A series of sediment sequences from submarine ridges of the subtropical South Atlantic Ocean located in a water depth alternately affected by North Atlantic Deep Water (NADW) and Lower Circumpolar Deep Water (LCDW) have been studied which recorded the paleoceanographic history in a region of strategic importance for the global thermohaline circulation (e.g., Berger and Wefer, 1996).

Individual studies

This thesis comprises four manuscripts which are in press or have been submitted for publication. The studies were performed in the Marine Geophysics Section of the Department of Geosciences in the framework of the Graduiertenkolleg 221 "Stoff-Flüsse in marinen Geosystemen", associated with the Sonderforschungsbereich 261 "Der Südatlantik im Spätquartär: Rekonstruktion von Stoffhaushalt und Stromsystemen". Both research projects are funded by the Deutsche Forschungsgemeinschaft. The work has been supervised by Prof. Dr. Ulrich Bleil.

A stratigraphic synthesis of twelve sediment cores covering the deep subtropical South Atlantic Ocean was established using magnetostratigraphic and cyclostratigraphic methods. This regional

chronostratigraphic framework forms the basis for various research strategies and scientific co-operations - most intensely with Dr. Tilo von Dobeneck, co-author of all four papers.

A first, methodological treatise introduces advanced signal analytical techniques enabling paleoceanographic interpretations in the super- to sub-Milankovitch ranges. Their immense potential is exemplified by susceptibility records from the subtropical and western tropical South Atlantic, the latter dated by von Dobeneck (1998).

In the course of the mid-Pleistocene climate transition (MPT) the dominant periodicity of the climate system response changed from 41 to 100 kyr. Rock magnetic investigations identify this period as an interim state of reduced carbonate accumulation in the subtropical South Atlantic. The second paper interprets the MPT as a separate climate state of reduced NADW influence, terminated by an ocean-wide event at 530 ka.

The third manuscript compares the temporal evolution of climatic cycles in environmental magnetic proxy records to driving orbital variations. Reciprocal exchange of spectral energy between the 41 and 100 kyr bands supports models invoking a pCO_2-controlled insolation threshold for the occurrence of 100 kyr glaciation cycles in late Pleistocene.

The final study is concerned with the terrigenous input in the Rio Grande Rise area and primarily based on clay mineral investigations by the first author, Dr. Franz X. Gingele. My own contribution to this study consisted in establishing age models for the cores and statistical analyses of clay mineral data. Additional, previously unpublished results were provided by Dr. Rainer Petschick (clay minerals) and Dr. Carsten Rühlemann (oxygen isotopes).

In the following the four manuscripts are briefly summarized. All data used in the thesis are archived in the information system PANGAEA/SEPAN (www.pangaea.de).

T. von Dobeneck and F. Schmieder
Using rock magnetic proxy records for orbital tuning and extended time series analyses into the super- and sub-Milankovitch bands
In: G. Fischer and G. Wefer
Use of Proxies in Paleoceanography: Examples from the South Atlantic
Springer-Verlag, in press.

This paper outlines the methodical background of the thesis. Two case studies are presented, both based on a several sediment sequences dated by orbital tuning of their high-resolution magnetic susceptibility records. Extended time series analyses focus on the statistical evaluation of different paleoclimatic aspects documented in the frequency bands above and below the main Milankovitch cycles. The Subtropical South Atlantic Susceptibility (SUSAS) stack extents back to 1.5 Ma and thus provides ideal conditions to study various superstructures, e.g., amplitude modulations of proxy responses. Comparatively elevated sedimentation rates in the Ceará Rise Susceptibility (CEARIS) stack allow an examination of high-frequency sub-Milankovitch phenomena. Paleoceanographic implications are only briefly discussed in this publication.

F. Schmieder, T. von Dobeneck and U. Bleil
Mid-Pleistocene climate transition: initiation, interim state and terminal event
submitted to *Nature*

The article addresses a fundamental enigma of Quaternary climate evolution which recently has been subject of several inspiring scientific publications. So far, most investigations of the mid-Pleistocene climate transition were based on oxygen isotope records reflecting global ice volume. The analysis of rock magnetic parameters presented here focuses

on changes in deep water chemistry. The data suggest that the mid-Pleistocene climate transition from about 920 to 640 ka does not represent a gradual change from a 41 to a 100 kyr world, but rather a third, quite different climate state confined by brief shifts at both boundaries. Moreover, many of the sediment series studied document an unusual terminal event at the end of the mid-Pleistocene climate transition, possibly related to other yet unexplained findings in numerous paleoclimatic records at around this time.

F. Schmieder, T. von Dobeneck and U. Bleil
Cycles, trends and events of Pleistocene sedimentation in the oligotrophic subtropical South Atlantic Ocean
to be submitted to *Paleoceanography*

The submarine ridges of the South Atlantic Ocean provide ideal opportunities to study paleoclimatically driven temporal and spatial alternations of NADW and LCDW as they intersect the vertically fluctuating broad transition zone separating these two deep water masses during glacial as well as interglacial times. Sediment series recovered at twelve sites on these ridges were investigated for cyclic fluctuations and trends of Quaternary deposition. The results imply a linkage between changes of predominant cyclicity, long-term trends in carbonate accumulation and a paleoceanographic event at about 530 ka documented at several locations.

F.X. Gingele, F. Schmieder, T. von Dobeneck, R. Petschick and C. Rühlemann
Terrigenous flux in the Rio Grande Rise area during the past 1500 ka: evidence of deepwater advection or rapid response to continental rainfall patterns?
Paleoceanography, 14, 84-95, 1999

The main objective of this study is to investigate the usability of kaolinite as a tracer for NADW in the Rio Grande Rise area. A comparison of kaolinite/chlorite ratios in surface sediment samples from the mid-Atlantic Ridge and the Rio Grande Rise region reveals that in the continental realm the Rio Doce (Brazil) is a major source of kaolinite in marine sediments whereas the supply of kaolinite by NADW is of minor importance. Time series analyses evince cyclic variations of kaolinite/chlorite ratios in one of the SUSAS cores coherent with global ice volume in the 41 and 100 kyr bands. They are interpreted to have recorded fluctuations in discharge of the Rio Doce and to mirror humidity conditions in the South American hinterland.

References

Berger, A., Long-term variations of caloric insolation resulting from Earth's orbital elements, *Quat. Res.*, 9, 139-167, 1978.

Berger, A., J. Imbrie, J. Hays, G. Kukla and B. Saltzman, Milankovitch and Climate Part 1, Reidel, Dordrecht, 510 pp, 1984.

Berger, A., Milankovitch theory and climate, *Rev. Geophys.*, 26, 624-657, 1988.

Berger, W.H. and E. Jansen, Fourier stratigraphy: spectral gain adjustment of orbital ice mass models as an aid in dating late Neogene deep-sea sediments, *Paleoceanography*, 9, 693-703, 1994a.

Berger, W.H. and E. Jansen, Mid-Pleistocene climate shift-the Nansen connection, in: *The polar oceans and their role in shaping the global environment*, edited by O.M. Johannessen, R.D. Muench and J.E. Overland, Geophys. Monogr. Ser., 85, AGU, Washington, pp 295-311,1994b.

Berger, W.H. and G. Wefer, Klimageschichte aus Tiefseesedimenten, *Naturwissenschaften* 79, 541-550, 1992.

Berger, W.H., M.K. Yasuda, T. Bickert, G. Wefer, T. Takayama, Quaternary time scale for the Ontong Java Plateau: Milankovitch template for Ocean Drilling Program Site 806, *Geology*, 22, 463-467, 1994.

Berger, W.H. and G. Wefer, Central themes of South Atlantic circulation, in *The South Atlantic: present and past circulation*, edited by G. Wefer, W.H. Berger, G. Siedler and D.J. Webb, Springer, Berlin, pp 1-11, 1996.

Bickert, T., W.B. Curry and G. Wefer, Late Pliocene to Holocene (2.6-0 Ma) western equatorial Atlantic deep-water circulation: inferences from benthic stable isotopes, *Proc. ODP, Sci. Results*, 154, 239-254, 1997.

Bleil, U. and G. Gard, Chronology and correlation of Quaternary magnetostratigraphy and nannofossil biostratigraphy in Norwegian-Greenland Sea sediments, *Geol. Rundschau*, 78, 1173-1187, 1989.

Bloemendal, J. and P. deMenocal, Evidence for a change in the periodicity of tropical climate cycles at 2.4 Myr from whole-core magnetic susceptibility measurements, *Nature*, 342, 897-900, 1989.

Cande, S.C. and D.V. Kent, A new geomagnetic polarity time scale for the Late Cretaceous and Cenozoic, *J. Geophys. Res.*, 97, 13917-13951, 1992.

Cande, S.C. and D.V. Kent, Revised calibration of the geomagnetic polarity timescale for the Late Cretaceous and Cenozoic, *J. Geophys. Res.*, 100, 6093-6095, 1995.

Chi, J. and J. Mienert, Linking physical property records of Quaternary sediments to Heinrich events, *Mar. Geology*, 131, 57-73, 1996.

Clark, P.U. and D. Pollard, Origin of the middle Pleistocene transition by ice sheet erosion of regolith, *Paleoceanography*, 13, 1-9, 1998.

D'Argenio, B.D., A.G. Fischer, G.M. Richter, G. Longo, N. Pelosi, F. Molisso and M.L. Duarte Morais, Orbital cyclicity in the Eocene of Angola: visual and image-time series analysis compared, *Earth Planet. Sci. Lett.*, 160, 147-161, 1998.

DeBlonde, G. and W.R. Peltier, A one-dimensional model of continental ice volume fluctuations through the Pleistocene: implications for the origin of the Mid-Pleistocene climate transition, *J. Clim.*, 4, 318-344, 1991.

Emiliani,C., Pleistocene temperature, *J. Geol.*, 63, 538-578, 1955.

Frederichs, T., Regionale und altersabhängige Variation gesteinsmagnetischer Parameter in marinen Sedimenten der Arktis, *Ber. Polarforschung*, 164, 212 pp, 1995.

Gersonde, R., F.T. Kyte, U. Bleil, B. Diekmann, J.A. Flores, K. Gohl, G. Grahl, R. Hagen, G. Kuhn, F.J. Sierro, D. Völker, A. Abelmann and J.A. Bostwick, Geological record and reconstruction of the late Pliocene impact of the Eltanin asteroid in the Southern Ocean, *Nature*, 390, 357-363, 1997.

Grützner, J., F.C. Bassinot and J. Mienert, High-resolution compressional-wave velocity measurements in Pleistocene sediments of the Ceará Rise (western equatorial Atlantic): implications for orbital driven sedimentary cycles, *Proc. ODP, Sci. Results*, 154, 135-149, 1997.

Hays, J.D., J. Imbrie and N.J. Shackleton, Variations in Earth's orbit: pace-maker of the ice ages, *Science* 194, 1121-1132, 1976.

Herbert, T.D. and L.A. Mayer, Long climatic time series from sediment physical property measurements, *J. Sediment. Petrol.*, 61, 1089-1108, 1991.

Hilgen, F.J., Extension of the astronomically calibrated (polarity) time scale to the Miocene/Pliocene boundary, *Earth Planet. Sci. Lett.*, 107, 349-368, 1991.

Imbrie, J., J.D. Hays, D.G. Martinson, A. McIntyre and A.C. Mix, The orbital theory of Pleistocene climate: support from a revised chronology of the marine $\delta^{18}O$ record, in *Milankovitch and Climate Part 1*, edited by A. Berger, J. Imbrie, J. Hays, G. Kukla and B. Saltzman, Reidel, Dordrecht, pp 269-305, 1984.

Imbrie, J., A. Berger, E.A. Boyle, S.C. Clemens, A. Duffy, W.R. Howard, G. Kukla, J. Kutzbach, D.G. Martinson, A. McIntyre, A.C. Mix, B. Molfino, J.J. Morley, L.C. Peterson, N.G. Pisias, W.L. Prell, M.E. Raymo, N.J. Shackleton and J.R. Toggweiler, On the structure and origin of major glaciation cycles 1. Linear responses to Milankovitch forcing, *Paleoceanography*, 7, 701-738, 1992.

Imbrie, J., A. Berger, E.A. Boyle, S.C. Clemens, A. Duffy, W.R. Howard, G. Kukla, J. Kutzbach, D.G. Martinson, A. McIntyre, A.C. Mix, B. Molfino, J.J. Morley, L.C. Peterson, N.G. Pisias, W.L. Prell, M.E. Raymo, N.J. Shackleton and J.R. Toggweiler, On the structure and origin of major glaciation cycles 2. The 100,000-year cycle, *Paleoceanography*, 8, 699-735, 1993.

Johnson, R.G., Brunhes-Matuyama magnetic reversal dated at 790,000 yr B.P. by marine-astronomical correlations, *Quat. Res.*, 17, 135-147, 1982.

Köppen, W. and R. Geiger, Handbuch der Klimatologie, Verlag von Gebrüder Borntträger, Berlin, 1936.

Maasch, K.A., Statistical detection of the mid-Pleistocene transition, *Clim. Dyn.*, 2, 133-143, 1988.

Martinson, D.G., N.G. Pisias, J.D. Hays, J. Imbrie, T.C. Moore Jr. and N.J. Shackleton, Age dating and the orbital theory of the ice ages: development of a high-resolution 0 to 300,000-year chronostratigraphy, *Quat. Res.*, 27, 1-29, 1987.

Milankovitch, M., Die astronomische Theorie der Klimaschwankungen, in *Handbuch der Klimatologie*, edited by Köppen, W. and R. Geiger, Verlag von Gebrüder Borntträger, Berlin, 1936.

Mudelsee, M. and M. Schulz, The mid-Pleistocene climate transition: onset of 100 ka cycle lags ice volume build-up by 280 ka, *Earth. Planet. Sci. Lett.*, 151, 117-123, 1997.

Mudelsee, M. and K. Stattegger, Exploring the structure of the mid-Pleistocene revolution with advanced methods of time-series analysis, *Geol. Rundschau*, 86, 499-511, 1997.

Nowaczyk, N., Hochauflösende Magnetostratigraphie spätquartärer Sedimente arktischer Meeresgebiete, *Ber. Polarforschung*, 78, 187 pp, 1991.

Nowaczyk, N., T.W. Frederichs, A. Eisenhauer and G. Gard, Stratigraphy of late Quaternary sediments from the Yermak Plateau, Arctic Ocean: evidence for four geomagnetic polarity events within the last 170 kyr of the Brunhes epoch, *Geophys. J. Int.*, 117, 453-471, 1994.

Paillard, D., The timing of Pleistocene glaciations from a simple multiple-state climate model, *Nature*, 391, 1998.

Park, J. and K.A. Maasch, Plio-Pleistocene time evolution of the 100-kyr cycle in marine paleoclimate records, *J. Geophys. Res.*, 98, 447-461, 1993.

Pisias, N.G. and T.C. Moore, The evolution of Pleistocene climate: a time series approach, *Earth Planet. Sci. Lett.*, 52, 450-458, 1981.

Prell, W.L., Oxygen and carbon isotope stratigraphy for the Quaternary of Hole 502B: evidence for two modes of isotopic variability, *Initial Rep. DSDP*, 68, 455-464, 1982.

Raymo, M.E., The timing of major climate transitions, *Paleoceanography*, 12, 577-585, 1997.

Raymo, M.E., W.F. Ruddiman, J. Backman, B.M. Clement and D.G. Martinson, Late Pliocene variation in northern hemisphere ice sheets and North Atlantic deep water circulation, *Paleoceanography*, 4, 413-446, 1989.

Raymo, M.E., D.W. Oppo and W. Curry, The mid-Pleistocene climate transition: a deep-sea carbon isotopic perspective, *Paleoceanography*, 12, 546-559, 1997.

Robinson, S.G., Applications for whole-core magnetic susceptibility measurements of deep-sea sediments, *Proc. ODP, Sci. Results*, 115, 737-771, 1990.

Ruddiman, W.F., M.E. Raymo and A. McIntyre, Matuyama 41,000-year cycles: North Atlantic Ocean and northern hemisphere ice sheets, *Earth. Planet. Sci. Lett.*, 80, 117-129, 1986.

Ruddiman, W.F., M.E. Raymo, D.G. Martinson, B.M. Clement and J. Backman, Pleistocene evolution: northern hemisphere ice sheets and North Atlantic ocean, *Paleoceanography*, 4, 353-412, 1989.

Saltzman, B. and M.Y. Verbitsky, Multiple instabilities and modes of glacial rhythmicity in the Plio-Pleistocene: a general theory of late Cenozoic climatic change, *Clim. Dyn.*, 9, 1-15, 1993.

Schwarzacher, W., Cyclostratigraphy and the Milankovitch theory, Elsevier, Amsterdam, 225 pp, 1993a.

Schwarzacher, W., Milankovitch cycles in the pre-Pleistocene stratigraphic record: a review, in *High resolution stratigraphy*, edited by E.A. Hailwood and R.B. Kidd. *Geol. Soc. Spec. Publ.*, 70, 187-194, 1993b.

Shackleton, N.J., Oxygen isotope analyses and Pleistocene temperatures re-assessed, *Nature*, 215, 15-17, 1967.

Shackleton, N.J., J. Backman, H. Zimmermann, D.V. Kent, M.A. Hall, D.G. Roberts, D. Schnitker, J.G. Baldauf, A. Desprairies, R. Homrighausen, P. Huddlestun, J.B. Keene, A.J. Kaltenback, K.A.O. Krumsiek, A.C. Morton, J.W. Murray and J. Westberg-Smith, Oxygen isotope calibration of the onset of ice-rafting and history of glaciation in the North Atlantic region, *Nature*, 307, 620-623, 1984.

Shackleton, N.J., A. Berger, W.R. Peltier, An alternative astronomical calibration of the lower Pleistocene timescale based on ODP Site 677, *Trans. Royal Soc. Edinburgh: Earth Sci.*, 81, 251-261, 1990.

Shackleton, N.J., S. Crowhurst, T. Hagelberg, N.G. Pisias and D.A. Schneider, A new Late Neogene time scale: application to Leg 138 sites, *Proc. ODP, Sci. Results*, 138, 73-101, 1995.

Shackleton, N.J. and S. Crowhurst, Sediment fluxes based on an orbital tuned time scale 5 Ma to 14 Ma, site 926, *Proc. ODP, Sci. Results*, 154, 69-82, 1997.

Tarduno, J.A., L.A. Mayer, R. Musgrave and Shipboard Scientific Party, High resolution, whole-core magnetic susceptibility data from Leg 130, Ontong Java Plateau, *Proc. ODP, Init. Rep.*, 130, 541-548, 1991.

Thießen, W., Magnetische Eigenschaften von Sedimenten des östlichen Südatlantiks und ihre paläozeanographische Relevanz, Ph.D. thesis, *Ber. FB Geow. Univ. Bremen*, 170 pp, 1993.

Tiedemann, R., M. Sarnthein and N.J. Shackleton, Astronomic timescale for the Pliocene Atlantic $\delta^{18}O$ and dust flux records of Ocean Drilling Program site 659, *Paleoceanography*, 9, 619-638, 1994.

von Dobeneck, T., Analytical strategies in environmental magnetism - a South Atlantic perspective, Habilitation thesis, FB Geowissenschaften, Univ. Bremen, 1998.

Wilson, D.S., Confirmation of the astronomical calibration of the magnetic polarity timescale from sea-floor spreading rates, *Nature*, 364, 788-790, 1993.

Using Rock Magnetic Proxy Records for Orbital Tuning and Extended Time Series Analyses into the Super- and Sub-Milankovitch Bands

T. von Dobeneck* and F. Schmieder

Fachbereich Geowissenschaften, Universität Bremen, Postfach 33 04 40, D-28334 Bremen, Germany
**corresponding author (e-mail): dobeneck@uni-bremen.de*

Abstract: High-resolution rock magnetic proxy records of marine sediments, in particular magnetic susceptibility logs, delineate variations of sediment lithology and mirror climatic and oceanographic changes of different duration. Most commonly, Milankovitch cyclicity resulting from orbital forcing of carbonate dissolution and terrigenous sedimentation prevails. Extracted by bandpass filtering, these signal components can serve for multiple core correlation, cyclostratigraphic analyses and orbital tuning. Phase relations between astronomical obliquity and precession cycles and their equivalents in rock magnetic records depend on regional sedimentological settings. Two case studies are developed to demonstrate specific aims, strategies, strengths and restrictions of rock magnetic time series analyses and their extension into the super- and sub-Milankovitch bands. In the first example, twelve Pleistocene susceptibility records spanning the oligotrophic subtropical South Atlantic (SUSAS stack) were successfully tuned to obliquity and precession despite their low average sedimentation rates < 1cm/kyr. Multiple bandpass filtering and evolutionary spectral analysis reveal two major base line shifts at around 0.95 and 0.6 Ma and various superstructures (e.g., amplitude modulations) of orbital proxy response. Compared to analogous analyses of an adapted astronomical target curve, converse residue patterns in the 41 kyr and 100 kyr bands indicate that Pleistocene ice age cycles were mainly triggered by obliquity before 1.25 Ma and from 1.05 to 0.7 Ma, while eccentricity modulation of precession predominated between 1.25 and 1.05 Ma and during the last 0.6 Ma. In the second example, eight susceptibility records from the western equatorial Atlantic Ceará Rise (CEARIS stack) were tuned to a lagged precession index signal. Subsequently, a high resolution core correlation scheme was established on basis of their coherent high-frequency (< 15 kyr) signal patterns. Basic harmonics and intermodulation frequencies of obliquity, and, predominately, precession resulting from nonlinear proxy response were detected by sub-Milankovitch spectral and bispectral analyses. Twin susceptibility peaks corresponding to a tropical double precession cycle appear even in the unfiltered records. Millennial signal variations (< 7 kyr) seem to coincide with Bond- and Dansgaard-Oeschger cycles.

Introduction

Many marine rock magnetic records exhibit Milankovitch cyclicities - sometimes in striking agreement with $\delta^{18}O$, $\delta^{13}C$ or $\%CaCO_3$ profiles. This phenomenon is generally explained by climatic impact on the fluxes of magnetically enriched terrigenous and 'non-magnetic' biogenic sedimentary components. They are increasingly employed as a data base for high-resolution core correlation, orbital age modelling and paleoceanographic time series analysis of marine sediments. Unlike ice-shield mediated climate proxies, magnetic records sustain their periodicity deep into pre-Quaternary times (Park et al. 1993; Hilgen et al. 1995; Shackleton and Crowhurst 1997). Paleoclimatic signatures of magnetic susceptibility and various remanence parameters have been described and stratigraphically exploited in paleoceanographic studies from all major oceans (e.g., Radhakrishnamurty et al. 1968; Kent 1982; Robinson 1986; Bloemendal et al. 1988; deMenocal et al. 1991; Bickert et al. 1997).

From FISCHER G, WEFER G (eds), 1999, *Use of Proxies in Paleoceanography: Examples from the South Atlantic.* Springer-Verlag Berlin Heidelberg, pp 601-633.

The article on marine 'Environmental Magnetism' by Frederichs et al. (this volume) outlines the physical and sedimentological principles of rock magnetic climate proxies. Lithological changes in sediment series can be traced by a range of specific rock magnetic parameters which indicate concentrations of para-, ferri- and antiferromagnetic minerals, discriminate among remanence-carrying minerals (various iron oxides, oxyhydroxides and sulfides), estimate average ferrimagnetic grain sizes, or quantify additional magnetic properties such as coercivity or anisotropy.

There is no universal rationale for the linkage of climate and sedimentary magnetic mineral inventories, but detailed rock magnetic studies usually provide the means to identify prevailing orbital forcing mechanisms within a regional context. Pronounced climate dependence has been observed for eolian dust load, ice-rafted debris, ocean current transport and sea-level related shelf erosion - all important sources or pathways of magnetic mineral deposition. The likewise cyclic accumulation of calcareous and siliceous microfossils plays a complementary and often dominant role in generating magnetic signals by modulating the concentration of the magnetic mineral fraction. Magnetic signal patterns can be obscured by too stable or too complex sedimentation conditions, discontinuous deposition (bottom current erosion, debris flows), intercalated high- or low-magnetic (tephra, fossil) layers, and, most severely, by reductive diagenesis of primary ferrimagnetic minerals in sub- or anoxic marine environments (Tarduno 1994; Tarduno and Wilkison 1996; Frederichs et al., this volume).

Isothermal magnetic parameters are determined by measuring the magnetic moment of artificially magnetized, but otherwise untreated bulk sediment samples. They represent averaged volume properties, are precise and well reproducible. Because of the ubiquity of magnetic iron minerals in nature and the availability of highly sensitive magnetometers, virtually every lithology can be investigated and characterized by magnetic parameter sets. The attainable speed and spatial resolution of whole-core measurements convinced a growing number of marine geoscientists to integrate rock magnetic methods, especially magnetic susceptibility logging, into their methodical repertory.

This paper intends to explain and illustrate standard and advanced concepts of Quaternary cyclostratigraphy with emphasis on marine rock magnetic records. The three main sections are concerned with

- stepwise refinement of multiple core correlation schemes, phase analysis, and orbital tuning,
- evolutionary spectral analysis of Milankovitch and super-Milankovitch signal variations covering long-periodic (> 100 kyr) amplitude modulations and transitions of basic climate cycles
- higher-order spectral analysis of sub-Milankovitch signal components related to climate variations of short duration (< 18 kyr).

As necessary restriction and tribute to the most popular rock magnetic parameter in paleoceanography, our case studies will exclusively focus on magnetic susceptibility records.

Experimental Methods

Traditional single sample measurements in rock magnetism are increasingly replaced by faster non-destructive techniques. High-resolution whole-core or half-core logging of magnetic susceptibility κ (Robinson 1990) is now a routine procedure in marine sediment studies. The lateral sensor characteristics of the widely used 'Bartington' susceptometer have half-widths of 50 to 25 mm for loop sensors of various diameters and of 12 to 4 mm for different spot sensors. These values also represent conservative minimum estimates for the attainable spatial resolution.

Modern pass-through SQUID magnetometers equipped with additional magnetization coils measure isothermal and anhysteretic remanent magnetization at resolutions ranging from 80 mm for whole core logging down to 30 mm for 'U-channel' (axial subcore) measurements (Weeks et al. 1993). A 10 mm resolution for surface remanence measurements is obtained by a newly developed high-T_c SQUID 'Rock Magnetic Micro-Scanner' (von Dobeneck et al. 1996).

Spatial resolutions down to 1 mm at the expense of a laborious single sample preparation are achieved by measuring magnetic hysteresis loops. The concept of the 'Alternating Gradient Force Magnetometer' (AGFM) allows to determine high-

quality hysteresis data from miniature 10-20 mg samples (Flanders 1988; von Dobeneck 1996).

Typical data sampling densities for high-resolution rock magnetic core-logging are 0.5-2 measurements/cm, which is more than the effective spatial resolution of most sensors. This over-sampling results in smooth, well-defined and complete records - an important prerequisite for the performance of signal analysis techniques. In this paper we present susceptibility records acquired with a 'Bartington F type' spot sensor at a 1 cm spacing.

Orbital Tuning Strategies

Milankovitch's (1941) visionary idea of synchronizing geological records to orbital variations has evolved into a widely accepted chronostratigraphic method (Imbrie and Imbrie 1980; Imbrie et al. 1984; Martinson et al. 1987). Applied to records of isotopic or lithologic characteristics, 'orbital tuning' can yield unmatched precision and consistency in dating Quaternary sediment series. Ideally it takes just three steps to align a proxy record to its orbital pacemaker:
- establish a rough initial chronology and detect spectral characteristics of Milankovitch cyclicity,
- choose an astronomic target curve and shift it by postulated or empirically determined phase lags,
- filter the proxy signal in the appropriate frequency band and match it with its model record.

In practice this approach bears numerous pitfalls. Rock magnetic records, like most proxy signals, depend more on regional sedimentation conditions than on global equilibria. They are not, in principle, safe bets for orbital tuning purposes and their patterns can be anything from a 'SPECMAP (Imbrie et al. 1984) double' to 'random wiggles'. Cyclostratigraphic age models critically rely on the initial and thus very consequential age model. Simple peak-to-peak correlation of proxy and target records is highly susceptible to erroneous matches (Shackleton et al. 1995), which have their origin in ordinary stratigraphic problems such as undetected hiati or turbidites, condensed or extended sections, bioturbation, lithologic and diagenetic effects. Algorithms such as signal slotting (Thompson and Clarke 1993) or complex demodulation (Pisias et al. 1990) have been used to find the statistically most probable proxy-target-correlation. Yet a combination of magneto- and biostratigraphic, eventually radiometric ages should be the most reliable basis to start from. Specific regional settings and scientific objectives may require adaptation of orbital tuning schemes into flexible, case-wise adapted strategies.

Two contrasting examples illustrate the scope of possible approaches at different interpretation levels. They are based on two series of FS METEOR gravity cores collected within a long-term Quaternary South Atlantic research project (SFB 261) at the University of Bremen. The coring sites are located in the subtropical and in the western tropical South Atlantic. The two study areas differ greatly in size as well as in prevailing sedimentation conditions and rates. The first example outlines the possibilities and limits of signal correlation and orbital tuning in low accumulation environments. Covering nearly the full Quaternary, these susceptibility records are rewarding targets for evolutionary spectral analysis. The particular interest of the second example lies in a much higher sedimentation and signal detail opening the possibility of analyzing periodic sub-Milankovitch signal components. We will primarily focus at the methodical aspects of these magnetic time series analyses.

Subtropical South Atlantic

The Subtropical South Atlantic Susceptibility (SUSAS) Stack stretches over the total width of the pelagic South Atlantic (Fig. 1) at around 25-35°S, connects its four major basins (Argentine, Brazil, Angola and Cape Basin) and crosses three submarine ridges (Rio Grande Rise, Mid Atlantic and Walvis Ridge). Via two deep water passages in the western South Atlantic, Vema and Hunter Channel, carbonate undersaturated Antarctic Bottom Water flows northward into the Brazil Basin, from where only a minor part reaches the Angola Basin through the Romanche Fracture Zone. Today, the slightly carbonate supersaturated North Atlantic Deep Water (NADW) flows southward at depths below 2000 m and controls the bottom water conditions in the Angola Basin. Therefore, the carbonate lysocline is much deeper in the Angola Basin (4700 to 4900 m) than in the Argentine, Bra-

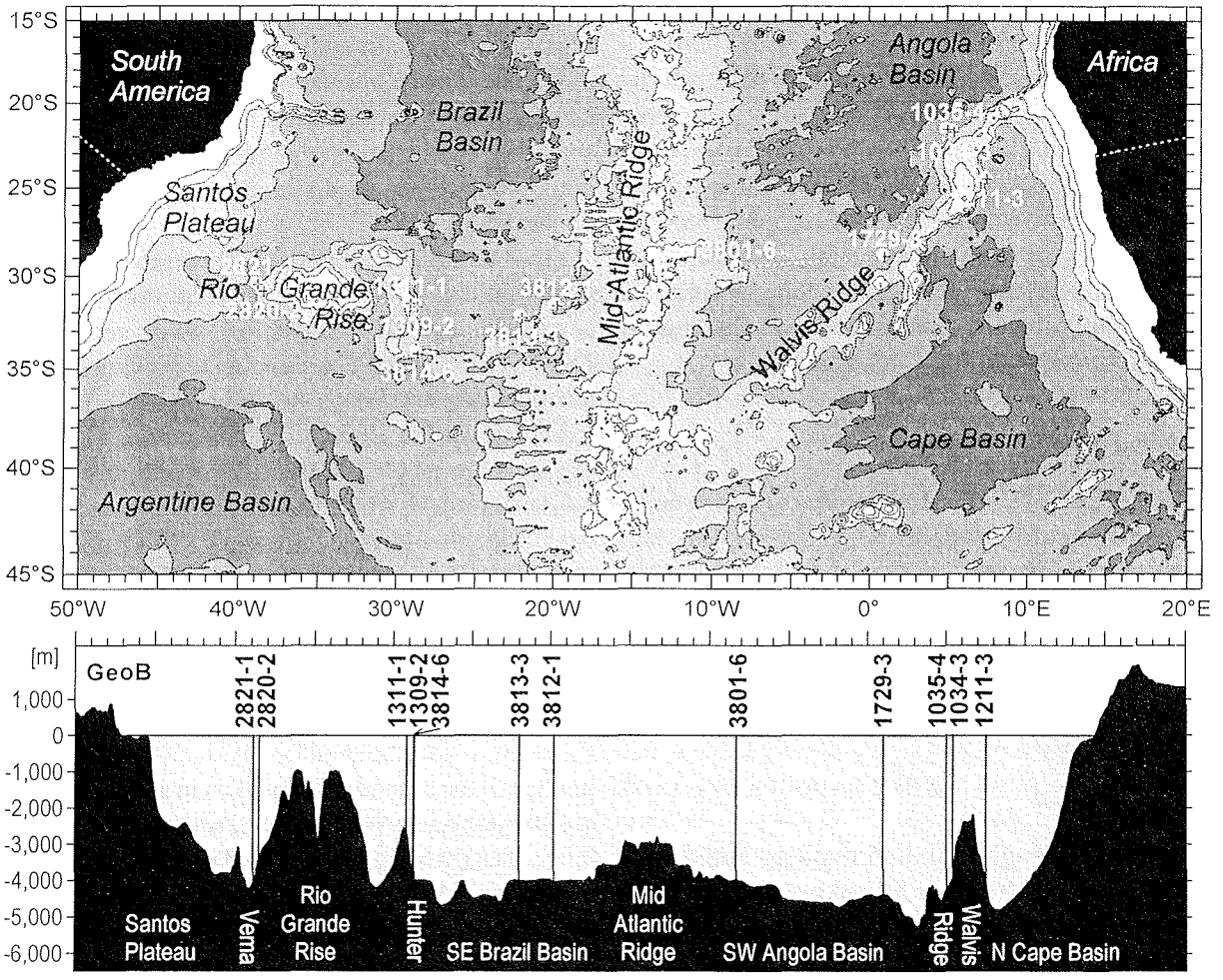

Fig. 1. GeoB core locations defining the SUSAS transect. The depth profile follows the white dashed line in the map and is plotted against longitude to depict the cores' affinities to the four major pelagic basins and their deep water bodies. It is not suitable to identify the positions and depths of deep water passages.

zil, and Cape Basins (4000 m). This west-east asymmetry of carbonate preservation diminishes during glacial times, when NADW production is reduced and the lysocline rises to about 3800 m in all four basins (Bickert and Wefer 1996).

Due to oligotrophic conditions along the profile the average sedimentation rates over the last 1.5 Ma range between 0.4 and 1.2 cm/kyr (Fig. 5). Susceptibility core means range from 18.5 to 470×10^{-6} SI. They increase with depth and show a drastic west to east decline originating from a much higher terrigenous influx to the western parts of the subtropical South Atlantic (Lisitzin 1996). All SUSAS logs exhibit distinct periodic oscillations primarily in the 100 kyr and 41 kyr band reflecting carbonate accumulation variations, with coherent long-term signal shifts superposed.

Oxygen isotope records exist for four SUSAS cores, GeoB 1034-3, 1035-4, 1211-3 (Bickert 1992; Bickert and Wefer 1996) and 1309-2 (W. Hale, pers. comm.). Their stratigraphic interpretability is limited by very low sedimentation rates, particularly in the deeper, obliquity-dominated (41 kyr cycles; e.g., Ruddiman et al. 1986) sections. Magnetostratigraphic dating at 5-10 cm spacing (Fig. 2) provided three or four reliable tie points in ten of twelve cores. By attributing these ages to the respective magnetic susceptibility logs, some spectral characteristics of Milankovitch cyclicity become apparent (Figs. 3a, 4a) suggesting climatic forcing.

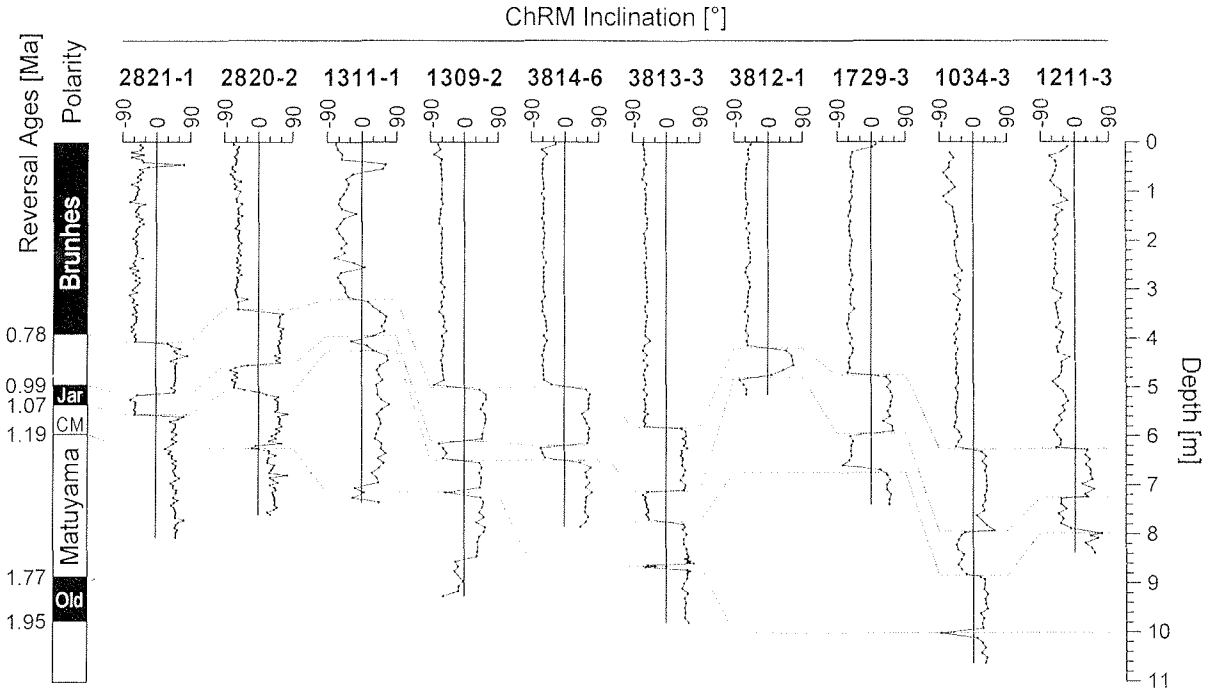

Fig. 2. Combined magnetostratigraphies (ChRM: Characteristic Remanent Magnetization) of SUSAS cores comprising the Brunhes/Matuyama boundary and the Jaramillo event (Jar). The Cobb Mountain (CM) event cannot be clearly identified at all sites. The Olduvai (Old) event is not reached in any of the cores. Reversal ages are given according to Shackleton et al. (1990). Data of cores GeoB 1034-3 and 1211-3 are from Thießen (1993).

Lomb-Scargle Fourier transform (LSFT; Lomb 1976; Scargle 1982, 1989) embedded in the SPECTRUM program (Schulz and Stattegger 1997) was used throughout all spectral analyses unless indicated, as it can be directly applied to unevenly spaced times series. The widely applied Blackman-Tukey method of spectral analysis (Blackman and Tukey 1958) employs Fourier Transform of the truncated and tapered autocovariance function and requires evenly spaced time series. The necessary interpolation procedure not only fails at age gaps, but inevitably underestimates high-frequency components and thereby 'reddens' the spectrum (Horowitz 1974). Moreover, interpolated data are statistically dependent (Mudelsee and Stattegger 1994) complicating the assessment of the significance of computed spectra.

Another important concern is spectral leakage, a mathematical consequence of the finite length of time series. Due to this effect dominant orbital cycles generate spectral ripples at higher frequencies, which may form misleading interference patterns. Tapering records with suitable window functions such as a Welch or Hanning window reduces this leakage effect at the expense of attainable resolution (Harris 1978). Individual compromises are found by comparing results from different tapers. A second 'spurious peak problem' arises from random fluctuations related to stochastic processes. A relatively simple counterstrategy is 'Welch's overlapped segment average' (WOSA) procedure (Welch 1967). By dividing a proxy record into overlapping segments and averaging their raw spectra, 'noise' peaks are gradually suppressed, but again resolution decreases.

Here a combination strategy of tapering and WOSA is applied. Following signal analytical nomenclature, spectra by Fourier transform of raw data are called 'periodograms', tapering yields 'modified periodograms' and segment averaging 'averaged periodograms'. Solely 'autospectra' give a complete spectral representation of time-dependent processes. They cannot be determined on basis of finite discrete time series, but only estimated within increasingly narrow confidence limits by the above defined spectra.

All initial spectra display significant maxima at around 40 kyr as core GeoB 3814-6 (Fig. 4a), but show little or no indications of a precessional signal component. As a spectrum represents an average over the integral record, it would be overly optimistic to infer that all obliquity-related oscillations can be extracted at this stage by filtering the record in the respective frequency band. Instead, all susceptibility records were mutually correlated to identify missing or expanded intervals. This comparison enables to estimate the extent of some short gaps and two laminated diatom ooze layers (Fig. 5), which had obviously been deposited in very short time. Core to core correlation revealed that simply removing these sections from the sequence results in complete records.

A pattern matching to standard $\delta^{18}O$ records, e.g. from equatorial Pacific ODP Site 677 (Shackleton et al. 1990) was feasible over most signal sections, but remained ambiguous between oxygen isotope stages 16 and 13 between about 0.65 and 0.5 Ma. Continuously high similarities, including long-term fluctuations of about 500 kyr duration, exist between all SUSAS susceptibility signals and the benthic $\delta^{13}C$ record at Pacific ODP Site 806 (Bickert et al. 1998), based on an orbitally tuned $\delta^{18}O$ stratigraphy (Berger et al. 1994). The complete and undisturbed susceptibility record of core

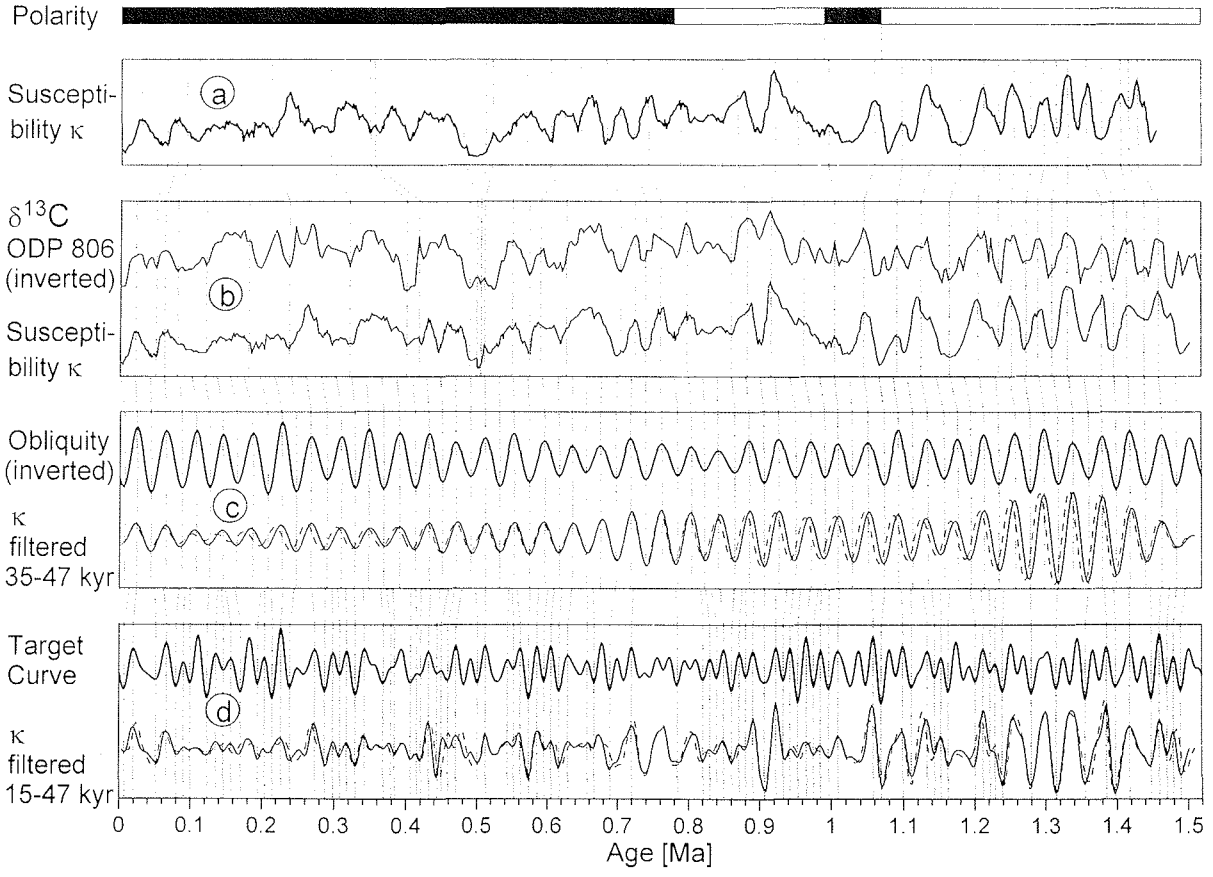

Fig. 3. Four step refinement of the age model for core GeoB 3814-6. **(a)** Susceptibility record dated by magnetostratigraphy (3 tie points). **(b)** Signal pattern correlation to the tuned $\delta^{13}C$ record of ODP Site 806 (44 tie points). In critical intervals other SUSAS records were inspected for supplementary information **(c)** Susceptibility filtered (35-47 kyr) in the obliquity range (dashed line) and tuned (solid line) to an astronomical obliquity signal shifted by -4.5 kyr (73 tie points). **(d)** Susceptibility filtered (15-47 kyr) and tuned to an astronomical (obliquity and precession) target curve (95 tie points).

GeoB 3814-6 (Fig. 3b) correlates particularly well and helped to substantiate the other eleven matches (Fig. 5). The improved spectral definition of Milankovitch frequencies owing to this correlation procedure is obvious (Fig. 4b).

The most widely used orbital tuning procedure assumes a phase lock between climate and metronome record (Martinson et al. 1987). In order to assess the absolute lag of any proxy record with respect to astronomical obliquity and precession, an independent and precise absolute chronology is required. $\delta^{18}O$ phase lags have been determined on basis of radiometric ages (Hays et al. 1976: 9 kyr for obliquity, 3 kyr for precession) and assumptions on the coupling of insolation and ice mass (Imbrie et al. 1984: 7.9 (7.4-8.2) kyr for obliquity, 5.0 (4.8-5.1) kyr and 4.2 (4.1-4.3) kyr for precession). To estimate orbital phase lags for regional proxy parameters such as susceptibility it is therefore sufficient to know the phase lags relative to a $\delta^{18}O$ curve from the same core.

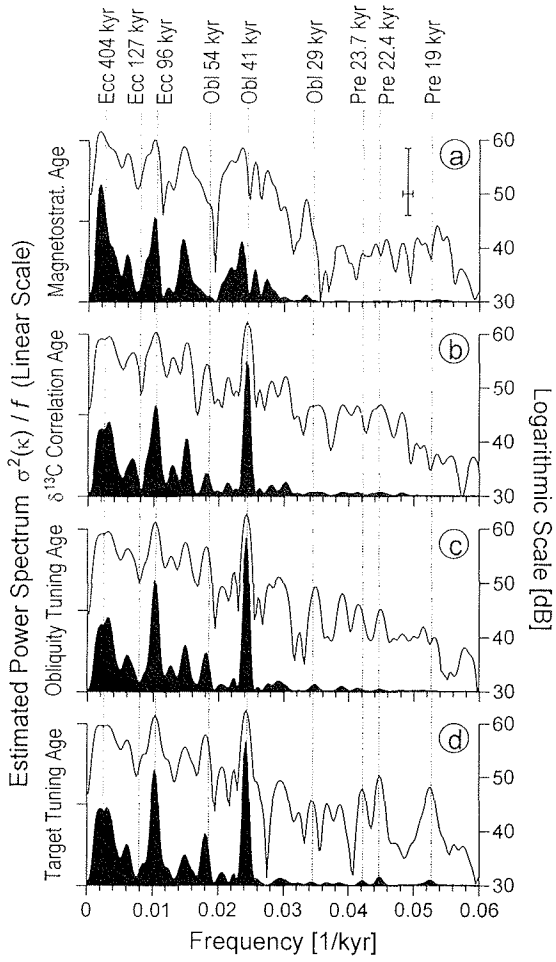

Fig. 4a-d. Estimated spectra (Hanning taper, WOSA: 2 segments) of the GeoB 3814-6 susceptibility signal on linear (solid black) and logarithmic (line) scales at each age model stage of Fig.3a-d. The cross is related to the logarithmic scale and delineates 6 dB bandwidth and 90 % confidence interval of all estimated spectra. The dotted lines depict orbital periods of eccentricity (Ecc), obliquity (Obl) and precession (Pre).

Here we use a revised $\delta^{18}O$ time scale of core GeoB 1211-3 (Bickert 1992) based on correlation to the SPECMAP stack (Imbrie et al. 1984). Cross spectral analysis of $\delta^{18}O$ and κ yields a coherence of 0.99 and 0.96 for the 100 kyr and 41 kyr cycles and reasonable phase angles of -41° and -30°. This implies that susceptibility leads $\delta^{18}O$ by 3.4 kyr in the obliquity band and therefore lags the obliquity forcing function by 7.9 kyr-3.4 kyr=4.5 kyr. The temporal resolution of the $\delta^{18}O$ record was too low to determine the precessional phase lag with an acceptable error margin. The subsequent orbital tuning process was performed in two stages:

At first the obliquity-related signal component was extracted applying a 1st order butterworth bandpass (35-47 kyr) filter in forward and reverse direction. This 'zero-phase-filtering' avoids phase distortion of the resulting sequence (Oppenheim and Schafer 1989) and was therefore used in all instances. It effectively doubles the filter order. A low filter order results in a short filter length and produces little reverberation. Its soft transition between stopband and passband limits the risk of signal loss in record sections, which are unduly compressed or stretched (and hence shifted in frequency) by imperfect initial age models.

Each maximum and minimum in the filtered signal was assigned the age (+4.5 kyr) of its postulated equivalent in the astronomical record (Berger and Loutre 1991), starting from the most uncritical sections near magnetostratigraphic or other reliable tie points. As illustrated in Fig. 3c, relative changes in the correlation age model are small, typically less than a half-cycle of obliquity. In the frequency domain (Fig. 4c) one notes just a small rise of peak amplitudes.

The second tuning step proceeds from the observation that faintly visible precessional peaks in

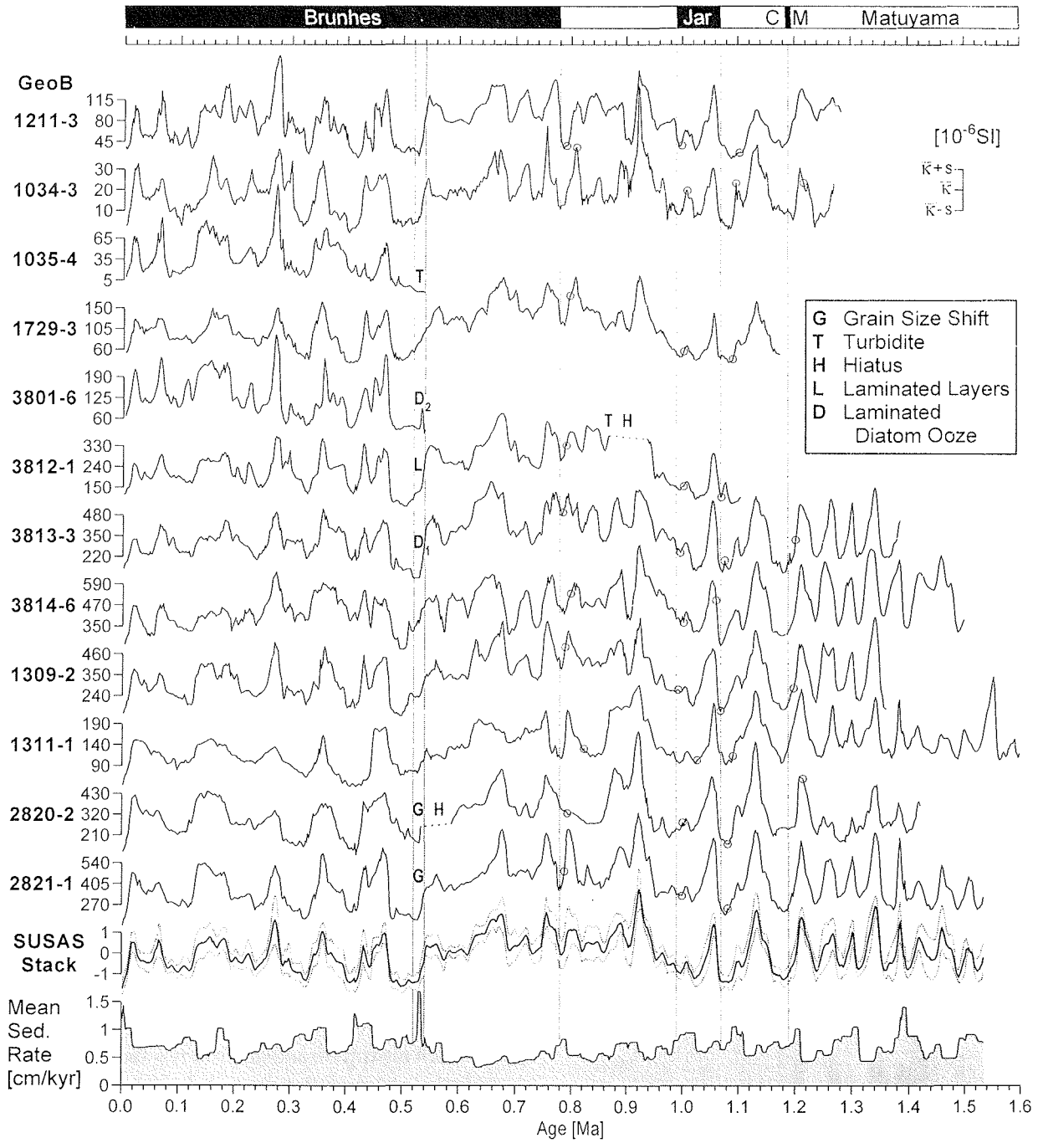

Fig. 5. Individually tuned SUSAS records and resulting stack (arithmetic mean with standard deviation band). To compensate for different mean amplitudes, each record was standardized by subtracting its mean and dividing by the standard deviation s. Dots mark identified paleomagnetic reversals (Jar: Jaramillo; CM: Cobb Mountain). They are generally located deeper in the cores than the corresponding reference ages of Shackleton et al. (1990), depicted by dotted lines. The resulting average lock-in depth is 12±9 cm. There is an obvious east-west trend (top to bottom) of increasing signal amplitude, but less detailed signal features. The gray vertical bar marks a zone of peculiar lithologies in six cores related to a conspicuous increase of averaged sedimentation rate (bottom, individual sedimentation rate records were previously normalized to the overall 0.5-0 Ma average of 0.75 cm/kyr).

the logarithmic spectra gradually sharpened at both refinements of the age model. To benefit from this precessional signal component, a target curve of normalized obliquity and precession index (mixing ratio of 2:3 chosen by visual evaluation) and 4.5 kyr lag was calculated, comprising not just more, but also more prominent signal features than either single orbital parameter. The obliquity-tuned primary susceptibility record was filtered using a wide bandpass (15-47 kyr) to include obliquity and precession cycles. As many extrema as possible were matched (Fig. 3d), admittedly at the resolution limit of these records. The resulting final age models are again just slight modifications of the previous models and possibly not even more precise in absolute ages as the precession time lag is undetermined. Nevertheless, this higher-frequency tuning leads to a better mutual signal correlation of the SUSAS records and therefore to an improved conservation of signal details in the SUSAS stack (Fig. 5). Because of the very different amplitude ranges, the stack was determined as an arithmetic mean of normalized (subtraction of core mean and division by standard deviation), interpolated (Δt=2 kyr) records.

Bioturbation should be responsible for the comparatively low spectral power in the precession band. Its effect can be assessed from the fact that sections of higher sedimentation rate (e.g. interval 0.6-0.2 Ma) clearly coincide better with precession patterns. A precessional cycle at a typical sedimentation rate of r=0.5 cm/kyr corresponds to roughly 10 cm core depth, twice the minimum estimate for the pelagic mixed layer thickness L (Peng et al. 1977). Mathematical models of vertical mixing (Berger and Heath 1968; Dalfes et al. 1984) permit to quantify the frequency selective amplitude damping. Under the stated sedimentation conditions the 'gain factor' G at an averaged precession frequency of f= 1/21 kyr^{-1} is

$$G(f) = \frac{1}{1 + 4\pi^2 (L/r)^2 f^2} = 0.10 \,.$$

Less intense damping of the obliquity related paleosignal (G=0.30) and nearly negligible damping of 100 kyr (G=0.72) and 400 kyr (G=0.98) cycles account for a relative loss of spectral intensity in the precession band. Bioturbation also influences phase relations to some extent (Dalfes et al. 1984) and can bias orbital tuning ages.

Fig. 5 summarizes the combined results of magnetic age modelling for the complete transect. A few question marks remain in core sections, where individual signal features seem to be missing or incomplete (e.g., GeoB 1311-1 at 0.42 Ma, GeoB 2820-2 at 0.8 Ma). The SUSAS stack is free of such local effects and therefore representative for the whole Quaternary oligotrophic deep South Atlantic Ocean.

Ceará Rise

The Ceará Rise Susceptiblity (CEARIS) Stack comprises two short transects on the northern flank of the Ceará Rise, a submarine elevation 700 km north-east off the Amazon Delta (Fig. 6). A steady, but highly variable deposition of terrigenous particles strongly modulates the susceptibility signal. Several pathways are involved. The sea-level fall in glacial periods causes erosion of the inner continental shelf, channeling of the Amazon discharge directly into the Amazon Canyon (Milliman et al. 1975; Damuth 1977) and intensification of mass-flow events on the slopes of the Amazon Fan (Maslin and Mikkelsen 1997). These mechanisms enhance the suspended particle load at different water depths reaching the Ceará Rise either by surface transport via the retroflection of the North Brazil Current into the North Equatorial Countercurrent (Johns et al. 1990) or by intensified nepheloid transport via the southeastward directed NADW flow (Kumar and Embley 1977; Francois and Bacon 1991). Increased eolian input from Africa in glacial periods (Sarnthein et al. 1981; Matthewson et al. 1995) and possibly enhanced sediment yield of the Amazon in glacials are further factors which contribute to the susceptibility variations.

This rather complex scenario of competing sediment fluxes might be suspected of producing complex composite susceptibility signals. Yet all CEARIS records are perfectly suitable for orbital tuning and exhibit very consistent patterns not only in the Milankovitch band, but also down to periods of 2-5 kyr.

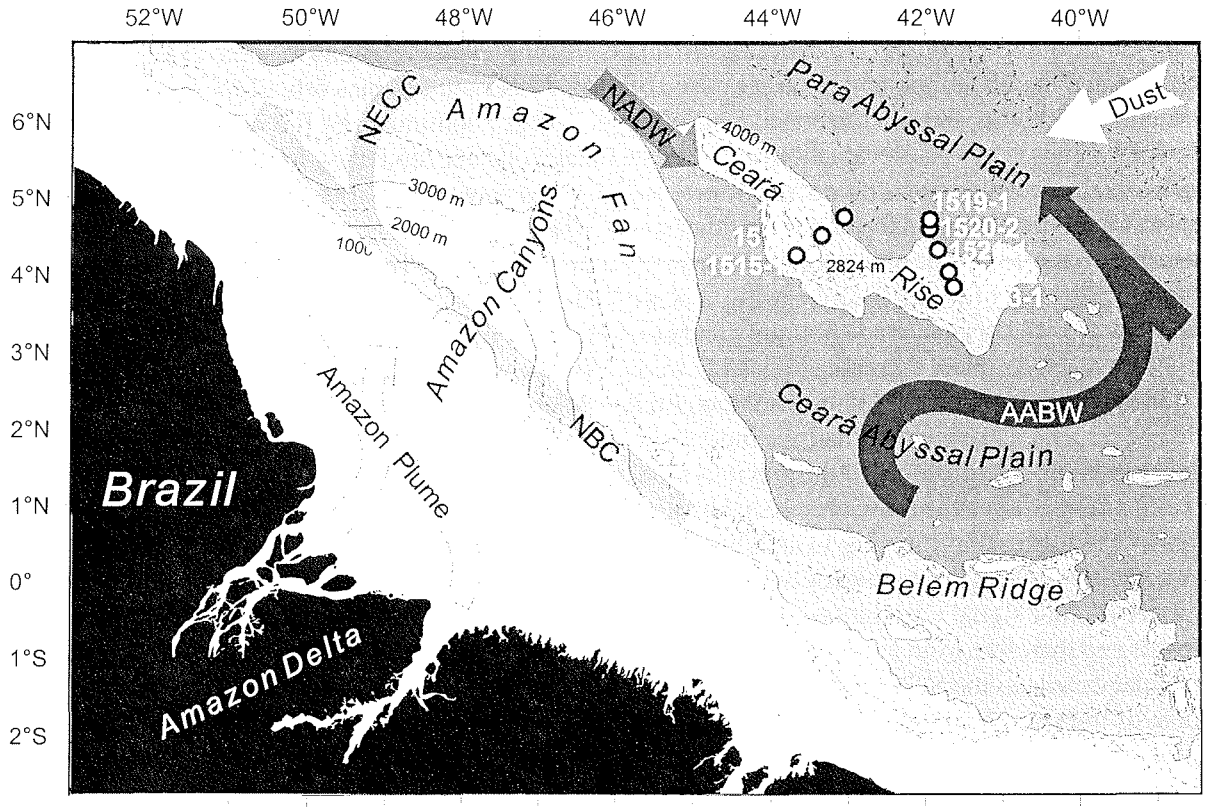

Fig. 6. Simplified hydrography of the Ceará Rise region and GeoB core locations included in the CEARIS stack. The retroflection of the North Brazil Current (NBC) into the North-Equatorial Countercurrent (NECC) is activated from June to January (Muller-Karger et al. 1988). The North Atlantic Deep Water (NADW) flows directly over the Ceará Rise, while the Antarctic Bottom Water (AABW) fully circumvents this bathymetric high.

Although no CEARIS core was believed to reach the Matuyama chron, all were submitted to systematic paleomagnetic analysis (Bleil and von Dobeneck, this volume). Several reversed intervals, some with multiple rebounds, were detected in each polarity record. Dating these features, which just vaguely coincide with previously reported Brunhes polarity events (e.g., Nowaczyk et al. 1994) seems difficult.

Oxygen isotope stratigraphies are available for two of eight CEARIS cores (Mulitza 1994; Rühlemann et al. 1996). These chronologies (Fig. 7) were based on a SPECMAP (Imbrie et al. 1984) correlation and represent convincing initial age models. They were adopted for the two respective susceptibility records (Fig. 7) and transferred to the other six cores (Fig 10a) by graphic correlation.

The pronounced similarity of $\delta^{18}O$ and susceptibility records and their obvious agreement with SPECMAP testify to the climatic dependence of both parameters during late Quaternary glacial/interglacial cycles. It is interesting to note that the synchrony of oxygen isotope and susceptibility variations is disturbed by varying peak lags and incoherent sections (Fig. 7). These effects are too large to be simply explained by the higher spatial resolution of the magnetic (1 cm) versus the isotopic (5 cm) record. Potential causes are

- proxy- and cycle-specific gain and lag values resulting from different signal formation mechanisms (Martinson et al. 1987),
- harmonic and intermodulation frequencies generated by (coupled) nonlinear response to orbital forcing (e.g. saw-toothed curves),

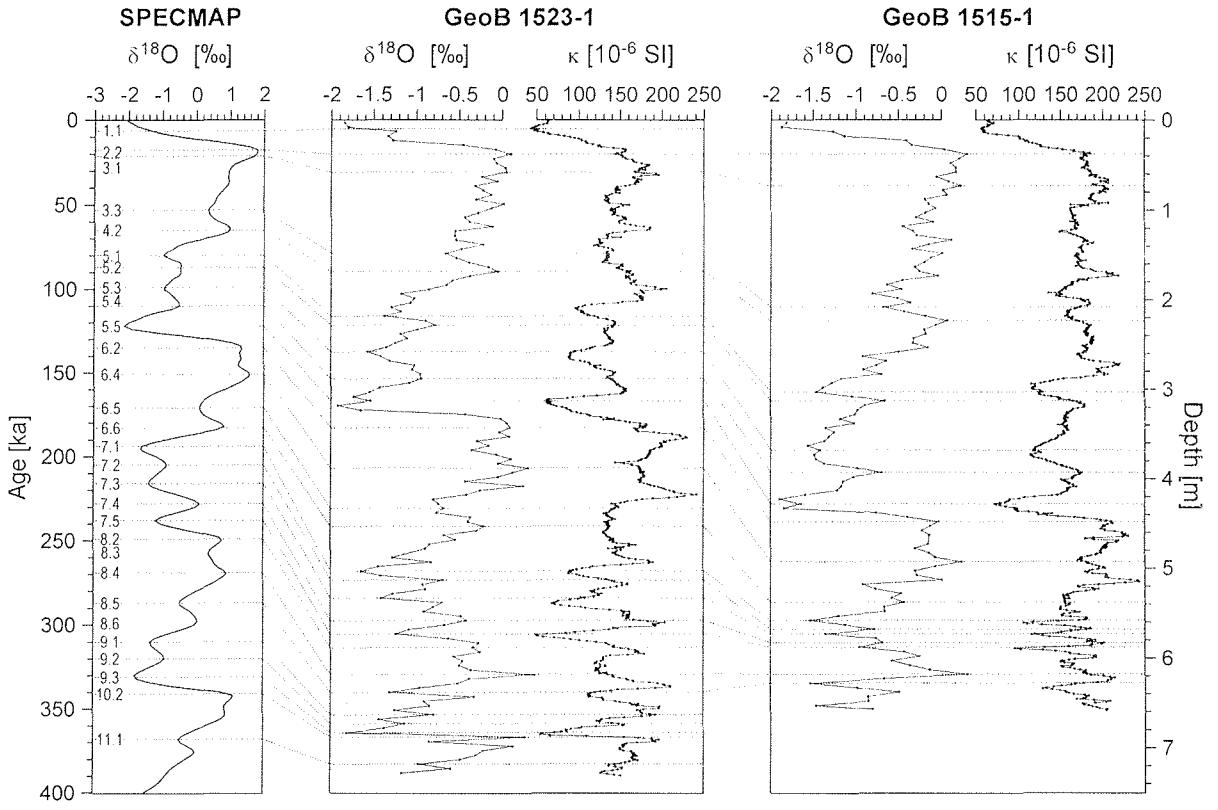

Fig. 7. Initial age model for CEARIS cores. *Globigerinoides sacculifer* $\delta^{18}O$ records of cores GeoB 1523-1 (Mulitza 1994) and GeoB 1515-1 (Rühlemann et al. 1996) were graphically correlated to SPECMAP (Imbrie et al. 1984) substages (dotted lines). Their ages provide 27 (19) tie points for the respective susceptibility records. Note inconsistent lead (stages 4.2, 5.4, 6.2, 8.4) and lag (stage 5.1) of κ to $\delta^{18}O$.

- the influence of extraneous (non-Milankovitch) forcing signals.

All possibilities are realistic and have important implications for the tuning strategy, particularly for choosing the most suitable target record.

The spectral representations of Fig. 8 reveal some information in this respect. Both $\delta^{18}O$-based spectra exhibit well-defined and similar, albeit not identical orbital characteristics. The susceptibility spectrum has considerably more precessional power and some additional peaks. Reasons for the differing distribution of spectral power will be given later. In the context of orbital tuning, it is sufficient to state that magnetic susceptibility chiefly follows precession and retains a rather stable phase lag (Fig. 9a, c). A shifted astronomical precession record is therefore the most evident tuning target.

SPECMAP determines the phase lag of our initial age model. According to cross-spectral analyses of both proxy parameters and the precession index (PI), the lags at the three main precession frequencies amount to 3-8 kyr for $\delta^{18}O$ and 0-5 kyr for κ (Fig. 9c). Since there are more than three orbital precession frequencies (the periods 23.7 kyr, 22.4 kyr and 19 kyr are only the three largest amplitude terms in the trigonometric expansion of astronomical precession; Berger and Loutre 1991), the applicable lag should be represented by a weighted average combining these phase angles, period lengths and spectral power. The time-domain equivalent of cross-spectral density, the cross-covariance function c_{xy}, supplies this weighted average lag. As both compared records are band-limited (precession by nature, susceptibility by band-

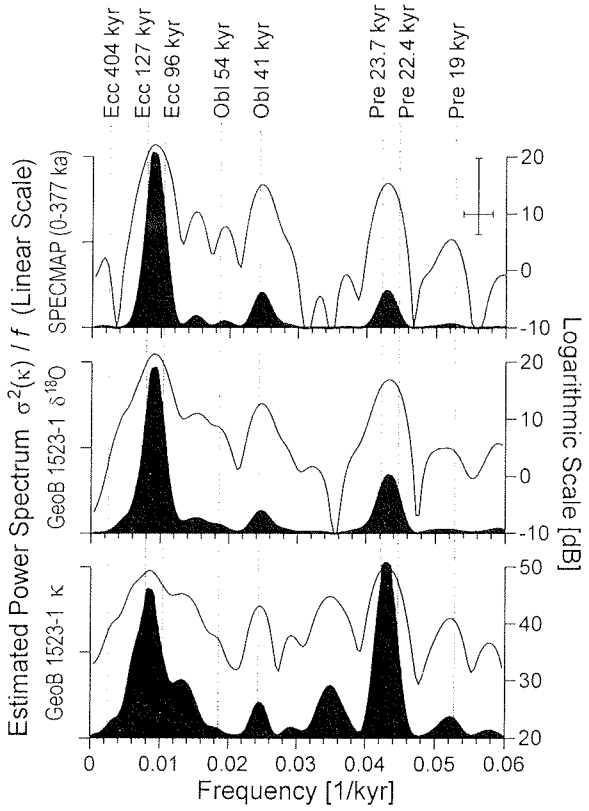

Fig. 8. Spectra (0-377 ka, Welch taper) of SPECMAP and GeoB 1523-1 $\delta^{18}O$ and κ records according to the correlation age model of Fig. 7 on linear (solid black) and logarithmic (line) scales. The cross is related to the logarithmic scale and delineates 6 dB bandwidth and 90 % confidence interval of all estimated spectra. The dotted lines mark basic orbital periods. Note the various influence of precession forcing in each spectrum and additional peaks in the κ record. The lower spectral resolution in comparison to Fig. 4 is a mathematical consequence of the much shorter time series.

pass filtering), the horizontal shift of the central maximum of the cross-covariance function (Fig. 9b, d) corresponds to the requested lag (Fig. 9c). According to this analysis, the susceptibility record of core GeoB 1523-1 lags precessional forcing by 1.77 kyr and leads $\delta^{18}O$ by 3.90 kyr which adds up to a plausible total delay of 5.67 kyr between PI and $\delta^{18}O$.

Starting out from the $\delta^{18}O$ based correlation age (Fig. 10a), precession tuning is a straightforward, but typically iterative procedure (Fig. 10b). Each step starts with filtering the time series in an extended precession band (15-28 kyr to include erroneously compressed or stretched signal sections), proceeds with identification and correlation of clearly developed maxima and minima to the shifted precession signal and ends with releasing the preceding and adopting the improved age model. These age modifications averaged 1.3-2.2 kyr in the first and 0.4-0.9 kyr in the second tuning step.

While the initial pattern correlation scheme was essentially based on matching individual peaks, the orbital tuning procedure relies on the maxima and minima of a filtered signal, to which, due to the necessary filter length, entire record sections numerically contribute. Consequentially, a tuned age model relies more on the continuous evolution than on singularities of a paleoceanographic record. On the other hand, narrow peaks and steep slopes have a strong impact on filter-extracted signals and hence also on their dating. The origin of these signal components is a priori uncertain and provides no ties to external time scales unless convincing links to known high-frequency climate variations such as Heinrich events (Grousset et al. 1993; Robinson et al. 1995; Chi and Mienert 1996), Bond (Bond et al. 1993) or Daansgard-Oeschger cycles (Dansgaard et al. 1993; Moros et al. 1997) can be established.

Spike and slope features, which are well reproducible within a core collection, can nevertheless help to improve the internal coherence of combined age models. Extracted and emphasized by highpass filtering in the sub-Milankovitch band (here <15 kyr) the high-frequency patterns of the CEARIS core collection was graphically correlated at an average spacing of 3 kyr between tie points (Fig. 10c). Each tie point was set to a common mean age (CMA) assuming that relative delay times in the study area are negligible. The graphic correlation of high-frequency signal components results in mean age shifts of 0.8-1.5 kyr. From a statistical viewpoint, this procedure corrects for orbital tuning errors related to core-specific features and therefore improves the precision of each age model. Because all correlated cores were previously dated by the same proxy and principles, the cumulative age shift equals zero for the total core collection and, for statistical reasons, also for each core.

At this refinement stage, it is justified to demand, how precise this tuned age model might be. A major

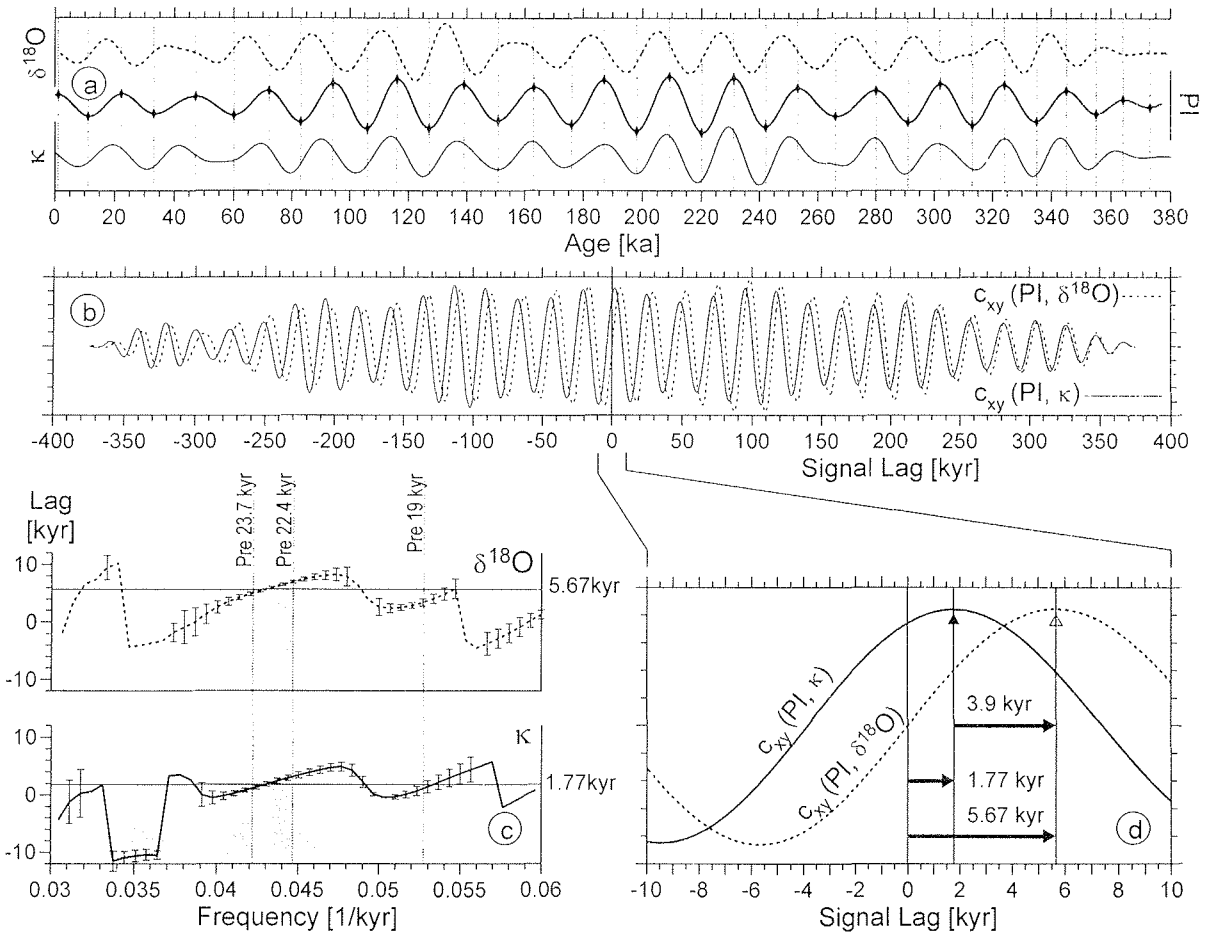

Fig. 9. Quantification of the $\delta^{18}O$ and κ signal lags in relation to precession forcing (example: GeoB 1523-1). **(a)** Based on the SPECMAP correlation age model (Fig. 7), $\delta^{18}O$ and κ were zero-phase filtered in the precession band (3rd order butterworth 15-28 kyr) and compared to the precession index (PI) of Berger and Loutre (1991). All signals exhibit similar amplitude modulation and fairly stable phase relations. **(b)** Comparison of cross-covariance functions of PI and precession-filtered proxies. The central maximum (shown magnified in (d)) indicates the best match of delayed metronome record and proxy response. Estimated lag values are 1.77 kyr for susceptibility and 5.67 kyr for $\delta^{18}O$. **(c)** The phase spectra of PI and unfiltered proxy records (derived from cross-spectral analysis) were converted to 'lag spectra' to show their frequency-dependence and good coincidence with lag values obtained from (b). Error bars represent 80% confidence intervals, corresponding auto-spectrum amplitudes are shaded gray. **(d)** Close-up at cross-covariance functions of (b).

error source is age-depth-nonlinearity (Schiffelbein and Dorman 1986). The applied (linear) age interpolation does not consider fluctuations of the sedimentation rate between tie points. The relative age discrepancies between CEARIS cores due to this effect should on average be less than 1 kyr, as the matched signal features are densely spaced and their high resemblance implies regionally uniform sedimentation conditions. A quasi-continuous pattern correlation (Martinson et al. 1982) may further reduce this margin. The synchronism with the external forcing signal is potentially more affected by interpolation errors. Its precision can be roughly estimated from cross spectral analyses and is in the order of 2 kyr. The absolute error margins of orbital tuning are even larger, but difficult to quantify. They result from uncertain and unstable phase relations (Martinson et al. 1987), vertical mixing by

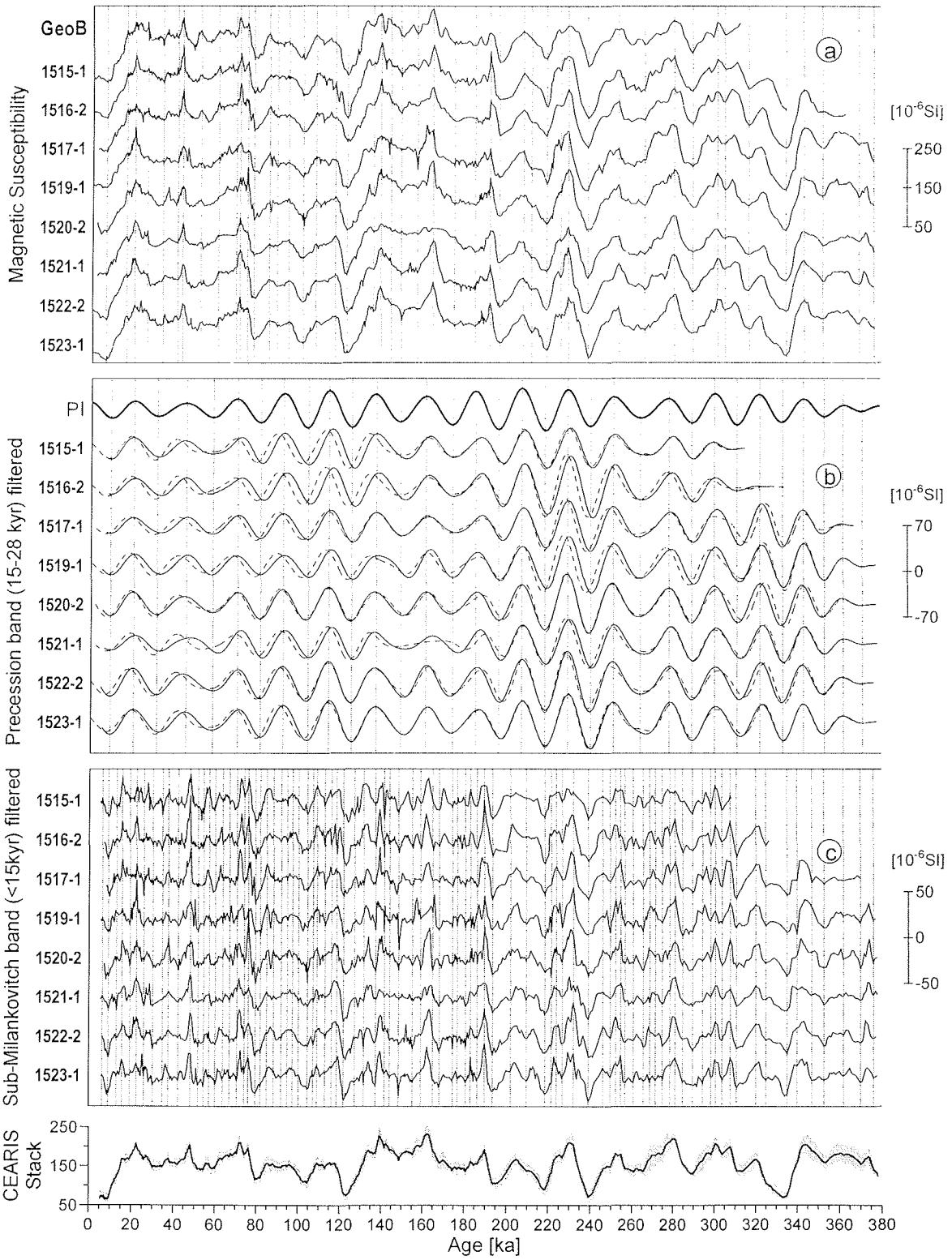

Fig. 10. Three step refinement of age models for CEARIS cores. **(a)** Graphic correlation to $\delta^{18}O$ age model of core GeoB 1523-1 (48 tie points). **(b)** Initial (dashed) and subsequent stage (solid) of synchronizing all bandpass filtered susceptibility signals to the astronomical precession index (lag 1.77 kyr, 33 tie points). **(c)** Graphic correlation of sub-Milankovitch band (<15 kyr) features to their common mean age (90 tie points). **(d)** CEARIS stack.

bioturbation (Berger and Heath 1968) and an increasing error of astronomical calculations with age (Berger and Loutre 1992).

Specific Aspects of Tuning Rock Magnetic Records

Orbital tuning of proxy records implies the assumption that a parameter is almost exclusively responding to primary orbital forcing and that the response function is not misleading the correlation of proxy and target signals. Saturation effects, competing anticorrelated orbital response mechanisms and secondary overprinting will bias the tuning approach and eventually make it pointless. It may be possible to master such problems with specifically designed target curves (e.g., Berger and Jansen 1994a), but this strategy requires a deep understanding of all processes involved. Obviously there is a need for simpler criteria defining which sediments are appropriate for orbital tuning. A few general rules for rock magnetic age modelling in various depositional environments can be outlined.

Of all rock magnetic records those from sub- or anoxic sediments are the most precarious as they are usually affected by magnetite reduction. The second example in the paper by Frederichs et al. (this volume) illustrates, how multi-parametric magnetic methods can be used to reconstruct a susceptibility record which has been diagenetically overprinted during temporary suboxic conditions.

An abrupt coarsening or fining of the magnetic mineral fraction as indicated by magnetogranulometric proxies such as M_{ar}/M_{ir} (ibid.) reveals changes in the sedimentation modus, that probably also mask paleoceanographic informations of other proxy parameters. Whatever may cause this disturbance - erosion, winnowing, reductive diagenesis, slumping or intercalated turbidite or tephra layers - the respective sections should be carefully studied and eventually dissected. The remaining record can still be reassembled and tuned, if a pattern correlation with undisturbed records permits a convincing quantification of resulting age gaps.

We found the simultaneous orbital tuning of 5-20 regionally related cores much more conclusive than a treatment of individual records, because it gives a better impression of pattern variability in problematic sections and clues for correlation uncertainties. Parallel core processing is supported by the speed of experimental data acquisition in environmental magnetism.

Partial or total carbonate dissolution does not affect the stability of the magnetic mineral fraction. However, without carbonate or opal sedimentation (pelagic clay) the most important mechanism of susceptibility modulation, the mutual dilution of terrigenous and biogenic sediment fractions (Robinson 1990; Diester-Haass 1991; Mienert and Chi 1995) is missing. Unless orbital variations induce compositional changes within the lithogenic fraction, concentration-dependent magnetic parameters will merely reflect consolidation with depth. In this as well as other cases of purely terrigenous sedimentation, it is advisable to base orbital tuning upon magnetomineralogic (e.g., hematite-magnetite ratio) or -granulometric parameters (e.g., $S_{-0.3\,T}$ or M_{ar}/M_{ir}). These records often carry a climatic signal related to varying source regions or transport (oscillating eolian or glaciomarine fluxes, bottom current activity).

In oceanic regions with very low, irregular or high sedimentation rates, rock magnetic records deviate more or less severely from standard patterns (as do other types of records). A promising age modelling strategy is to start out with establishing susceptibility-based core-to-core correlation frameworks. When all inconsistencies in this multiple correlation scheme are resolved, the most convincing and complete record is dated by the best available method and may then serve as initial age model for subsequent tuning of the entire collection.

In principle, magnetostratigraphy provides ideal initial age models for orbital tuning of rock magnetic parameters. Paleo- and rock magnetic investigations can share the same sample set which is advantageous for cross-validation. At least one core reaching Matuyama age within a set of magnetically paralleled cores is needed to assign a rough age frame to all others. Although numerous short inverse polarity events of the Brunhes Chron (< 0.78 Ma) have been detected (Nowaczyk et al. 1994) their chronostratigraphic use is severely hampered by lithology-dependent lock-in effects (Bleil and von Dobeneck, this volume).

Extended Time Series Analyses

Having tuned a rock magnetic record to basic astronomical cycles in the Milankovitch range gives access to time series analyses into the adjacent frequency bands. These are essential to investigate the temporal evolution and physical principles of proxy response to orbital forcing. Suitable methods to analyze super- (> 100 kyr) and sub-Milankovitch (< 18 kyr) signal variations with and without the viewpoint of orbital forcing are presented in the following.

Evolutionary spectral analysis requires long time series and is therefore demonstrated for the SUSAS stack covering the last 1.5 m.y. The high temporal resolution of the CEARIS stack makes it a suitable exercise for spectral analyses in the sub-Milankovitch frequency range.

Super-Milankovitch Signal Variations of the SUSAS Stack

Linear orbital forcing through insolation variations can only account for proxy oscillations in the precession and obliquity band (Imbrie et al. 1992). The 96 kyr, 127 kyr and 404 kyr eccentricity cycles modulate the precession amplitude, but produce negligible insolation changes in their own frequency range (Fig. 12a). Yet, the SUSAS stack like other Pleistocene climate records exhibits strong 100 kyr variance (Fig. 12c).

Many attempts have been made to explain this '100 kyr cycle problem', frequently invoking nonlinear processes channeling energy into the 100 kyr band (for a summary see Imbrie et al., 1993). In rejecting the assumption that variations in insolation alone are responsible for the observed climatic changes, Muller and MacDonald (1995) explain the 100 kyr cycle by inclination changes of the Earth's orbital plane relative to the symmetry plane of the solar system. Liu (1992; 1995) concludes that frequency variations of the obliquity cycle can give rise to strong 100 kyr forcing of climate. Like various others, Raymo (1997) favors the idea that eccentricity modulation of the precession index amplitude generates quasi-periodic 100 kyr ice age cycles. The climate changes from ice shield growth to decay, when summer insolation exceeds a certain threshold value. A long-term reduction of the atmospheric pCO_2 level (Saltzman and Verbitsky 1993), eventually caused by tectonic processes (Raymo et al. 1988; Raymo and Ruddiman 1992), is thought to have induced a steady rise of the insolation threshold for large-scale melting in Quaternary times. This may explain, why late Pliocene to early Pleistocene paleoclimate records exhibit mainly obliquity and precession related variance (e.g., Raymo et al. 1989; Bloemendal and deMenocal 1989; deMenocal 1995), while late Pleistocene climate fluctuations, in spite of similar insolation variations, are dominated by 100 kyr cycles (e.g., Hays et al. 1976; Ruddiman et al. 1989). The exact timing of this mid-Pleistocene climate transition and the question whether it was a gradual ('mid-Pleistocene evolution', Ruddiman et al. 1989) or a sudden change ('mid-Pleistocene revolution', Berger et al. 1994) have been subject of many studies (Shackleton and Opdyke 1976; Pisias and Moore 1981; Prell 1982; Ruddiman et al. 1989; Berger and Jansen 1994b; Mudelsee and Stattegger 1997) and attempts to model or characterize the transition with different statistical techniques (e.g., DeBlonde and Peltier 1991; Park and Maasch 1993; Mudelsee and Schulz 1997).

Fig. 11. Temporal analysis of varying frequency content of the SUSAS stack. From bottom to top: Lowpass filtering of the normalized susceptibility stack reveals three distinct periods with different base levels and transitions centered at around 0.95 and 0.6 Ma. Extracting the basic Milankovitch cycles by bandpass filtering depicts frequency shifts within the eccentricity band and fading of the obliquity related variance in early Pleistocene. Precessional amplitudes are generally low due to bioturbation damping, particularly in periods of lower sedimentation rates. The envelopes were derived by Hilbert transformation (Bendat and Piersol 1986). For the evolutionary spectral analysis (see text) 500 kyr sections of the highpass filtered SUSAS signal (purple) progressing in 10 kyr steps are tapered and transformed into the frequency domain. Related to the center of each section, the resulting spectra are color-coded and form a so-called 'spectrogram'. The colored horizontal bars represent the limits used in the bandpass analyses below.

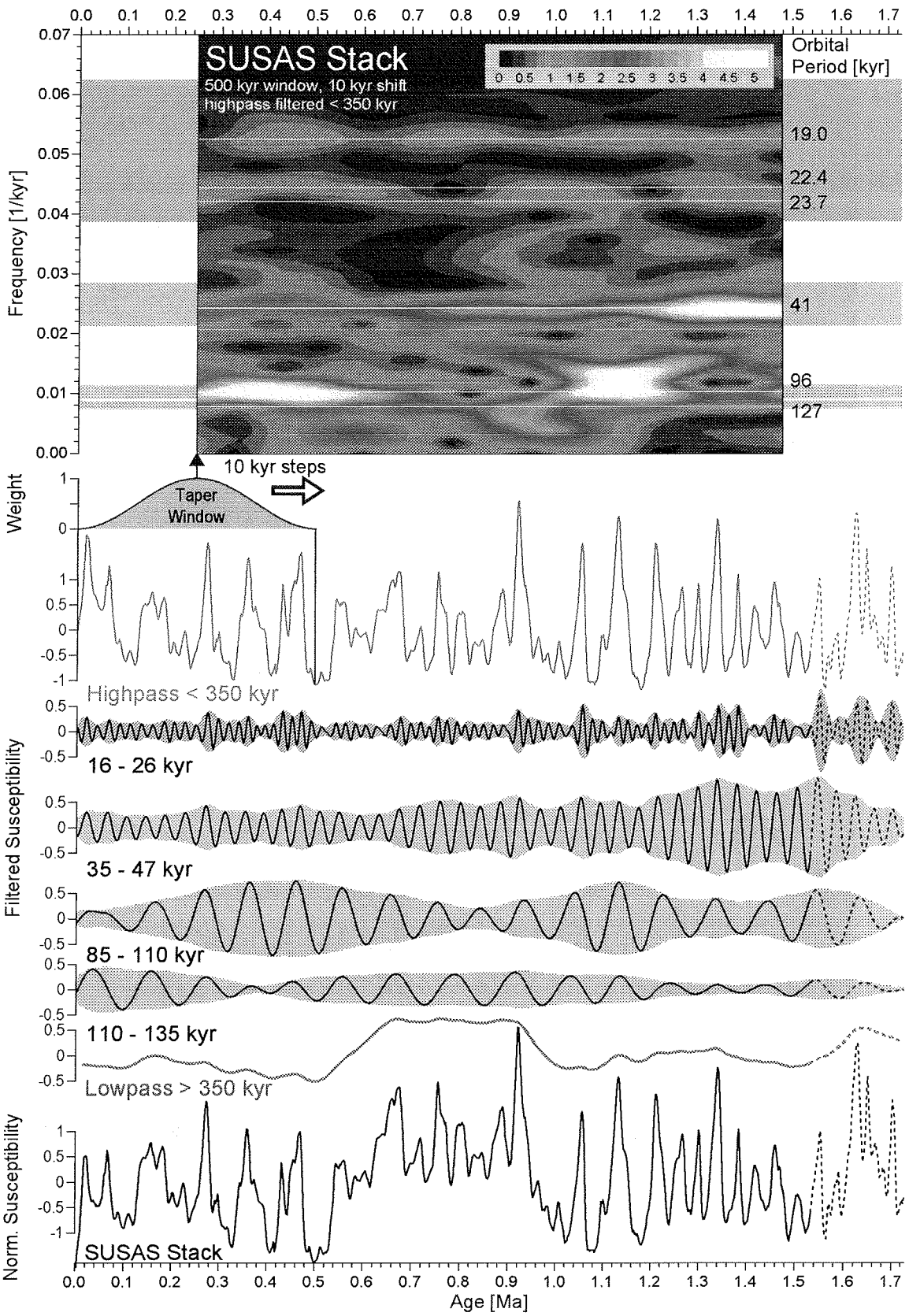
SUSAS Stack
500 kyr window, 10 kyr shift
highpass filtered < 350 kyr
Orbital Period [kyr]
19.0
22.4
23.7
41
96
127
Frequency [1/kyr]
10 kyr steps
Taper Window
Weight
Highpass < 350 kyr
16 - 26 kyr
35 - 47 kyr
85 - 110 kyr
110 - 135 kyr
Lowpass > 350 kyr
Filtered Susceptibility
SUSAS Stack
Norm. Susceptibility
Age [Ma]

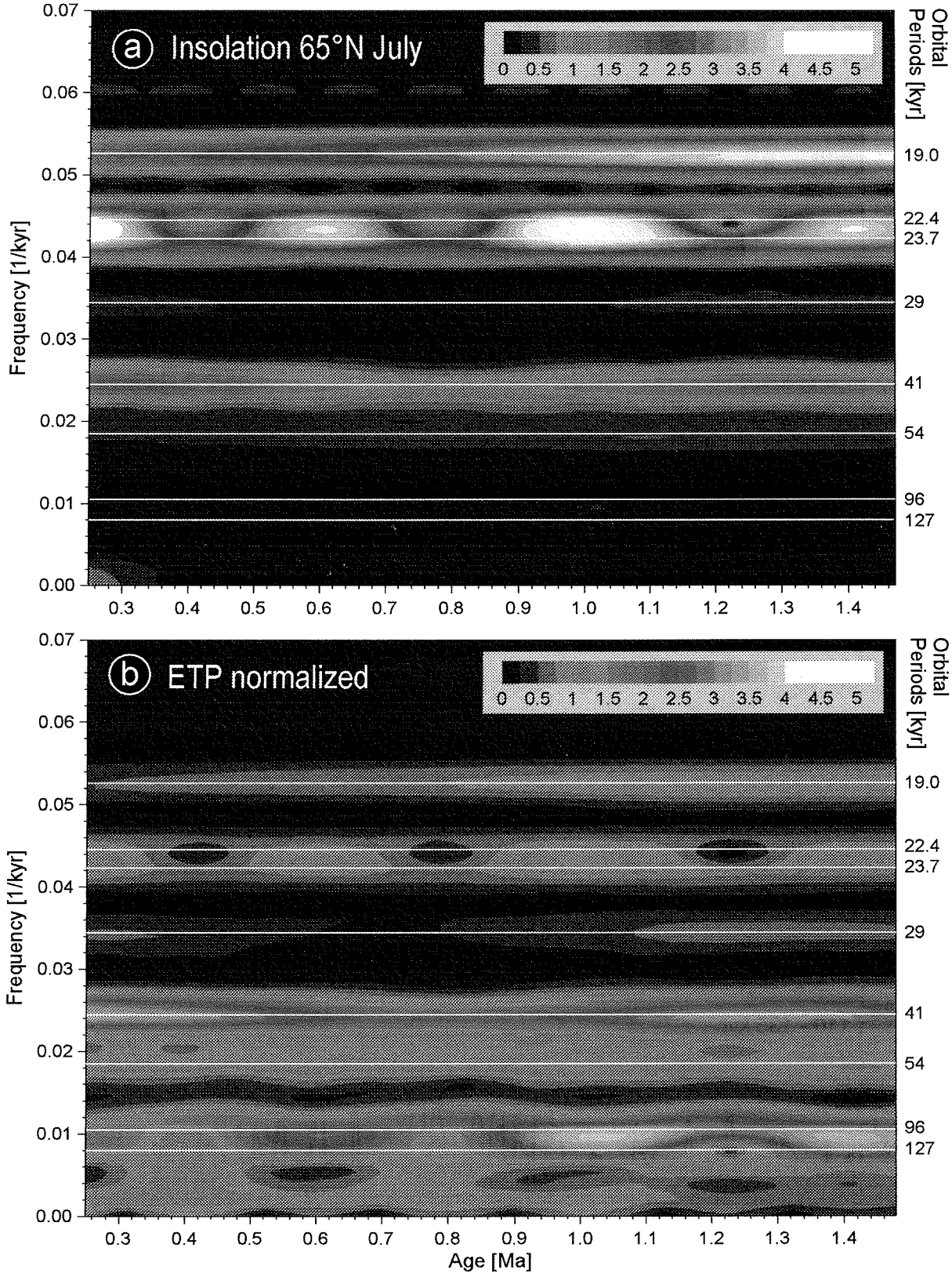

Fig. 12. Evolutionary spectral analysis of **(a)** insolation and **(b)** adapted ETP signal (see text for explanations).

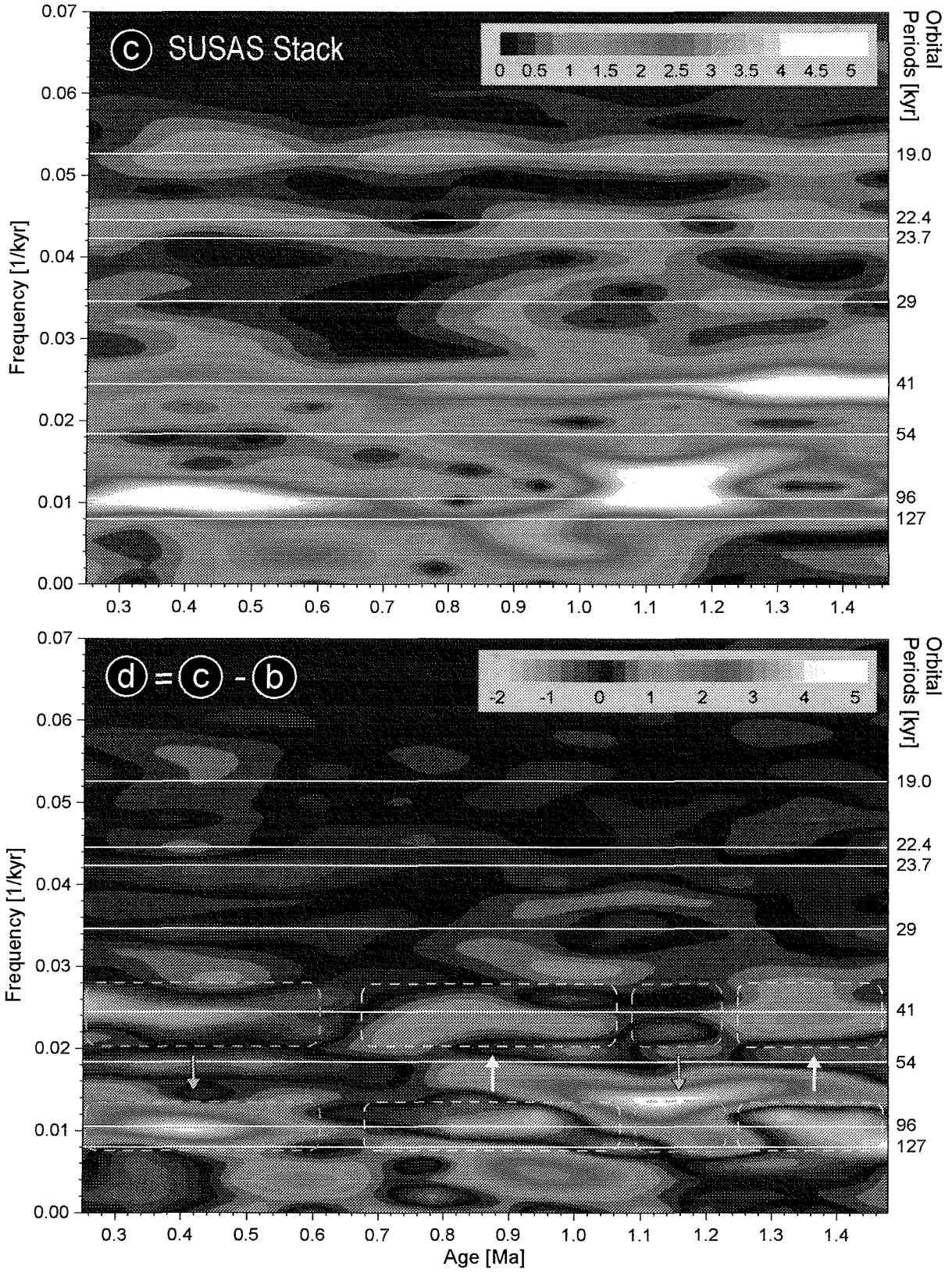

Fig. 12. Evolutionary spectral analysis of **(c)** SUSAS stack and **(d)** SUSAS-ETP residue (see text for explanations).

These controversies of 100 kyr cyclicity and Pleistocene climate transitions essentially address the issue, whether long-term paleoceanographic variations are related to basic Milankovitch cycles and their superstructures (e.g. envelopes), or rather to extraneous (forced by non-Milankovitch mechanisms) or free oscillations. A simple, frequently applied method to analyze proxy signals in this context is multiple bandpass filtering. In the lower half of Fig. 11 five signal components of particular interest are extracted from the SUSAS record.

The prominent long-term trend obtained from lowpass filtering (1st order Butterworth >350 kyr) is a remarkable feature not found in oxygen isotope signals and therefore not directly related to global ice volume. It is mirrored by the sedimentation rate stack (Fig. 5) and also by $CaCO_3$ concentration (P. Müller, unpublished data), hence by carbonate accumulation. Resembling more a double base line shift than a cycle, this signal marks two transitions:

- a first from 1.0 to 0.9 Ma corresponds to the age of the mid-Pleistocene (r)evolution,
- a second from 0.65 to 0.5 Ma culminates in the large-scale sedimentation event outlined in Fig. 5.

Their duration may have been shorter, since lowpass filtering inevitably broadens step functions.The three age intervals delimited by these two transitions show different spectral characteristics in the Milankovitch bands. The precession-related signal (16-26 kyr) is poorly documented due to bioturbation damping with the exception of sections of higher sedimentation rates and enhanced forcing. Apart from superimposed amplitude fluctuations, the influence of obliquity (35-47 kyr) on the SUSAS stack diminishes continuously with a major decrease near 1.2 Ma. The analysis in the 100 kyr range was subdivided into two bands from 85 kyr to 110 kyr and from 110 kyr to 135 kyr to distinguish the 96 kyr and 127 kyr eccentricity cycles. These periods clearly dominate the signal in late Pleistocene, but also give important contributions to older sections. As the amplitude variations in the 41 kyr and 100 kyr bands resemble in great detail the patterns found in $\delta^{18}O$ records of Pacific and Atlantic sites (Park and Maasch 1993), we conclude that the observed features are of a global nature and closely related to changes in ice volume.

Evolutionary spectral analysis is an excellent method to visualize the variability of cyclic climate characteristics in a record through time (e.g., Pestiaux and Berger 1984; Bloemendal and deMenocal 1989; Mwenifumbo and Blangy 1991). Spectra generated within a moving window are depicted in three-dimensional 'spectrograms' combining frequency and time domain (top of Fig. 11). These calculations were made using the 'SPECGRAM' algorithm embedded in the 'MATLAB Signal Processing Toolbox'. A 500 kyr frame was advanced at 10 kyr steps and, in order to minimize cut-off effects, tapered with a Hanning window, thereby focusing to the central section at each step. Long-term trends (periods >350 kyr) were previously removed by highpass filtering (purple curve) to avoid disturbance by these unresolved signal components. The resulting data matrix was normalized to an average spectral density of 1 by dividing all values by the total matrix mean. This procedure merely scales all spectrograms uniformly and enables their comparison, but does not alter relative variations in the time or frequency domain.

In Figs. 12a-d spectrograms of forcing and responding variables are related. The July mid-month insolation signal at 65°N (Berger and Loutre 1991) and a normalized ETP curve are shown as reference. ETP curves are artificial, but often employed target records composed by calibrating and adding the time series of Eccentricity, Tilt (obliquity) and Precession (Imbrie et al. 1984). Here, the cumulative spectral intensity in each band of the ETP spectrogram was calibrated to equal that of the SUSAS spectrogram. Being based on the same orbital variations, both reference signals exhibit identical amplitude modulation patterns, but very different spectral power in each band. In the eccentricity band this difference amounts to several orders of magnitude - an expression of the 100 kyr cycle problem. Characteristic Milankovitch superstructures as the cyclic 400 kyr modulation of the 100 kyr, 54 kyr and 23 kyr cycles and the synchronous decay of the 100 kyr and 19 kyr cycles are clearly illustrated in Fig. 12b. The faint 29 kyr cycle is a subordinate component of the obliquity signal and shows similar modulation as the main periods near 41 kyr.

The numerical difference between the spectrograms of the SUSAS record and the ETP curve is displayed in Fig. 12d. For the two precessional bands at 19 kyr and 23 kyr, the assumption of a constant proxy response appears justified, as both records largely compensate. In contrast, the residues in the 41 kyr band show a variable response to obliquity forcing. Two marked spectral intensity declines at 1.2-1.1 and 0.7-0.6 Ma (Fig. 12c) cannot be explained as a result of steady response to orbital forcing (Fig. 12b) and suggest that the potential of obliquity to drive the observed carbonate dissolution cycles decreased stepwise during Pleistocene times. This finding is in accordance with analyses made for $\delta^{18}O$ records (e.g., Ruddiman et al. 1989; Joyce et al. 1990) and implies that the climatic system was less sensitive to obliquity forcing during the late Pleistocene. The coincidence of target and proxy records in the 100 kyr band is even lower, as indicated by larger residues and steeper gradients. While the ETP model looses 100 kyr power (Fig. 12b), the SUSAS stack, like most climate records, documents an intensification of 100 kyr oscillations in late Pleistocene.

This trend is interrupted by an early Pleistocene 100 kyr maximum appearing between 1.2 and 1.1 Ma. This 'premature 100 kyr incident', also observed in $\delta^{18}O$ records (e.g., Mudelsee and Stattegger 1997), merges with a phase of strong 70 kyr cyclicity (Fig. 12c) which has also been found in other paleoceanographic records (e.g., Ruddiman et al. 1989; Robinson 1990; Bassinot et al. 1994; Bolton et al. 1995). Two low-frequency positive maxima centered at 0.95 and 0.6 Ma in the SUSAS and the residual spectrogram (Fig. 12c, d) result from remainders of the earlier discussed base line transitions of the long-term susceptibility trend (Fig. 11 bottom).

The most striking result of the residual spectrogram is the reciprocity of spectral intensities in the 41 and 100 kyr bands (dashed outlines in Fig. 12d). In relation to the stationary ETP model, the SUSAS 100 kyr cyclicity develops over-proportionally in sections with reduced response to obliquity (blue outline) and retreats, where the response to obliquity is strong (yellow outline). These findings imply an exchange of spectral energy between obliquity and eccentricity in overall accordance with insolation threshold models (e.g., Saltzman and Verbitsky 1993; Raymo 1997). Intensified northern hemisphere summer insolation capable of triggering major deglaciations hence should result from an interference of obliquity maxima with precession index minima. At times, when the insolation threshold is relatively low, obliquity maxima alone will trigger the withdrawal of continental ice shields and 41 kyr cyclicity prevails. When the insolation threshold is higher, the required peak insolation is only reached by optimum interaction of obliquity and precession. As eccentricity modulates the precession amplitude, sufficiently large precessional peaks occur only during 100 kyr eccentricity maxima causing the observed 100 kyr climate cycles.

Raymo (1997) assumes a linear, pCO_2 controlled rise of the insolation threshold over the past 1.2 m.y. and obtained a single transition from 41 kyr to 100 kyr predominance at about 0.7 Ma. Our evolutionary spectral analyses (Figs. 12c, d) imply, that this turnover was predated by a 100 kyr episode around 1.2 Ma.

Sub-Milankovitch Signal Variations of the CEARIS Stack

A most interesting feature of all CEARIS records are consistent high-frequency variations in the sub-Milankovitch to millennial range. As shown in Fig. 10c, the < 15 kyr signal components extracted by high-pass filtering can be matched in all detail. Again, spectral analysis is a promising strategy to detect the environmental factors causing this unusually regular pattern. Stochastic processes would yield smeared 'colored noise' spectra with poorly defined maxima, while periodic signals are represented by much sharper peaks appearing at characteristic frequencies - under the premise that a record is undisturbed, accurately dated, and covering enough time to provide ample spectral resolution. Because these conditions are never fully met in practice, elaborate statistical techniques have been developed to distinguish harmonic and random signal oscillations (e.g., Thomson 1982; for applications see Yiou et al. 1991; Nobes et al. 1991; Cortijo et al. 1995).

Since all fundamental Milankovitch periods exceed 18 kyr (e.g., Berger and Loutre 1992;

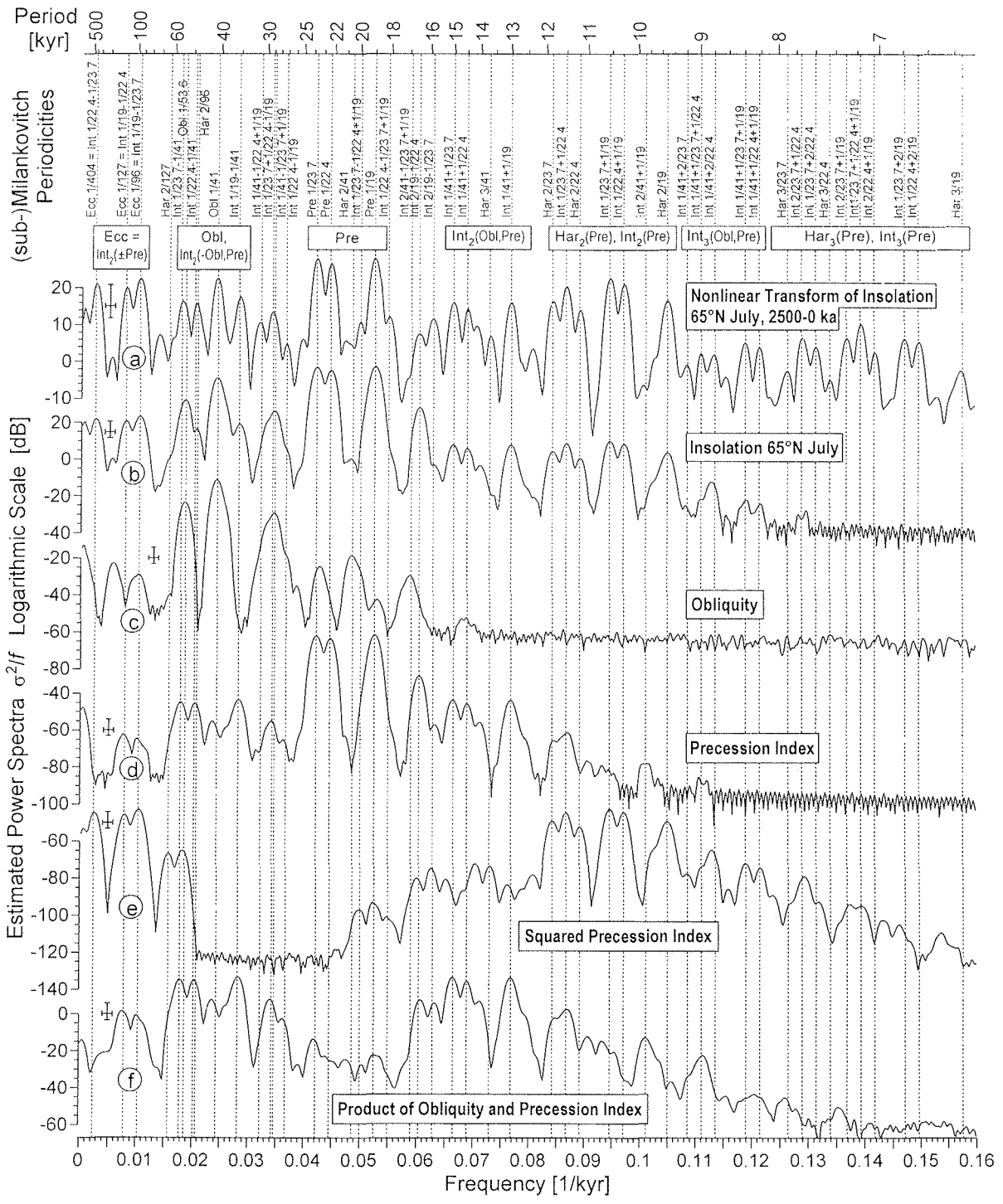

Fig. 13. Reference spectra (Blackman-Harris taper, WOSA: 3 segments) of fundamental orbital frequencies and their low-order (≤3) combinations based on astronomical time series (2500-0 ka; Berger and Loutre 1991). (Sub-) Milankovitch periodicities (vertical dotted lines) are classified in groups (gray bars) of common order (index numbers) and origin (intermodulations (Int) and harmonics (Har)). Crosses depict 6dB bandwidths and 90 % confidence intervals. **(a)** A simple nonlinear transform of **(b)** the 65°N July insolation signal shows spectral characteristics in common with (b), **(c)** obliquity and **(d)** precession signal, even in the sub-Milankovitch 8-18 kyr range. Other higher-order cycles of (a) coincide with **(e)** squared precession and **(f)** coupled obliquity and precession.

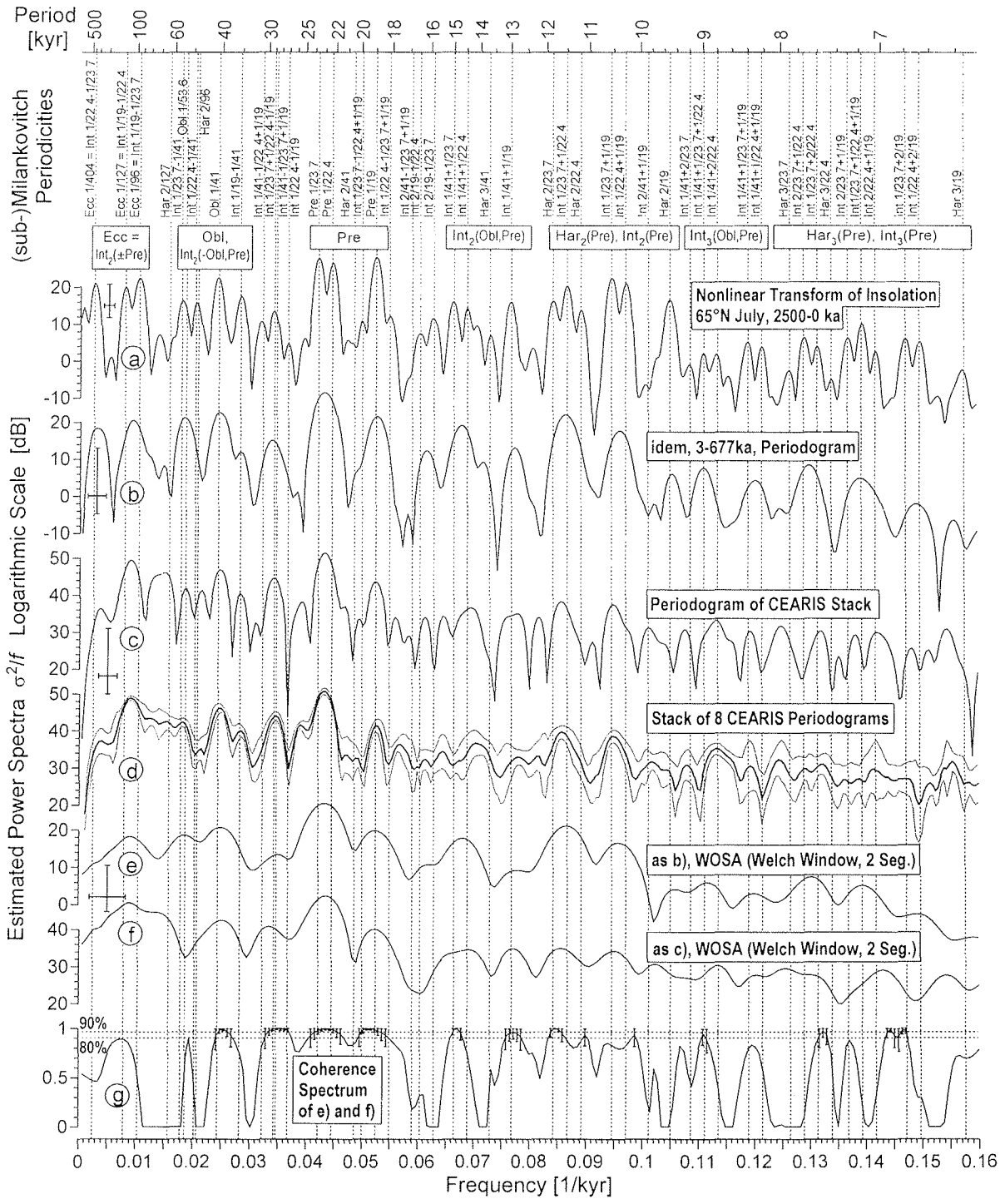

Fig. 14. Extended spectral analysis of CEARIS stack. References are **(a)** spectrum of Fig. 13a, **(b)** raw and **(e)** averaged periodogram of signal section spanning the CEARIS age range (377-6 ka). Analogously, **(c)** and **(f)** depict the raw and averaged periodogram of CEARIS stack. In **(d)** the eight individual CEARIS periodograms are stacked. The initially narrow standard deviation band widens towards higher frequencies. The coherency spectrum **(g)** of reference (e) and proxy signal (f) yields high squared coherencies not only for the basic Milankovitch periods but also for spectral maxima near 30 kyr, 15 kyr, 13 kyr, 11.5 kyr, 10.5 kyr, and 9 kyr. Combined with the overall coincidence of spectral patterns this identifies these CEARIS sub-Milankovitch peaks as the hypothesized combination tones.

Schwarzacher 1993) and known solar activity cycles (e.g. sunspot, Hale and Gleissberg cycles) frequently detected in varved sediments have periods <200 years (Glenn and Kelts 1991), which periodicities may actually be expected in the spectral range from 1 to 18 kyr? Besides free, quasi-periodic climate fluctuations, the most likely candidates are multiples and combination tones of Milankovitch frequencies originating from nonlinear transformations in the response chain of insolation, climate, proxy physics and sedimentation.

'Harmonics' result from nonlinear response to a single orbital cycle, while 'intermodulation frequencies' arise from nonlinear coupling of two or more basic orbital cycles. The frequencies of these additional modes are simply integer $(k, l, m, n, ...)$ combinations of the fundamental forcing frequencies $f_1, f_2, f_3, f_4, ...$ (Le Treut and Ghil 1983):

$$f(k,l,m,n,...) = kf_1 + lf_2 + mf_3 + nf_4 + ...;$$
$$k,l,m,n,... \in \{..., -1, 0, 1, 2, ...\};$$
$$\text{order} = |k| + |l| + |m| + |n| + ..$$

The number of potential combination tones within an investigated frequency band can be boosted ad lib by admitting high order combinations involving negative coefficients. Concerning orbital forcing, only the lowest order combinations within a given frequency range are bound to represent substantial spectral power (e.g., Yiou et al. 1991). All low-order (≤ 3) combination tones calculated from obliquity and precession and their realization and significance in the spectra of various astronomical time series are shown in Fig. 13. The five most important eccentricity frequencies can be obtained as linear combinations of the basic precession frequencies (e.g., 1/404 kyr^{-1} = 1/22.4 kyr^{-1} - 1/23.7 kyr^{-1}; Berger and Loutre 1992). It is therefore unnecessary to include them separately in the calculation of potential orbital combination tones. However, it is essential to distinguish not just two, but all three major precession frequencies.

Even pure obliquity and precession signals (Fig. 13c, d) and their transformation into latitude dependent insolation (Berger and Loutre 1994) involve (slightly) nonlinear process (Berger and Pestiaux 1984) and display sub-Milankovitch peaks above the noise floor of numerical precision (Fig. 13b). From the viewpoint of physical climate models, non-linear response is rather the rule than the exception. Not just ice-sheet dynamics (Le Treut and Ghil 1983), but also factors controlling monsoon intensity (Short et al. 1991; Crowley et al. 1992) favor the generation of orbital harmonics. Periods of 10-12 kyr, corresponding to a doubled precession cycle (simulated here by squaring the precession index; Fig. 13e), appear in insolation (Fig. 13b; Berger and Loutre 1997) and proxy spectra (Pestiaux et al. 1988; Park et al. 1993; Hagelberg et al. 1994), particularly at low latitudes. The coupling of obliquity and precession (Fig. 13f) generates characteristic peaks in the 13-15 kyr band, which are also found in sediments (e.g., Berger et al. 1991) and ice core records (Yiou et al. 1991). A simple non-linear mathematical transform of an astronomical insolation signal (Berger and Loutre 1991) yields a nearly complete spectrum of all theoretically derived orbital combination tones (Fig. 13a) and may be used as unbiased reference to identify significant sub-Milankovitch peaks of proxy spectra. (Fig. 14a). In order to provide equivalent frequency resolution with respect to the CEARIS spectra, the underlying time series was reduced to the same time range (377 - 6 ka; Fig. 14b,e).

The spectral amplitudes of insolation (Fig. 13b) fade steeply in the sub-Milankovitch range, while those of its nonlinear transform (Fig.13a/14a) and the CEARIS record (Fig. 14c) decrease much less. This discrepancy implies spectral power channeling into the sub-Milankovitch band. By visual comparison of the synthetic spectra (Fig. 14b,e) with those of the CEARIS stack (Fig. 14c,f) and the stack of the eight individual CEARIS spectra (Fig. 14d) many analogous peaks can be detected. The most prominent sub-Milankovitch peaks appear near 9, 10.5, 11.5, 13 and 15 kyr. They coincide with the earlier mentioned low-order combination tones and harmonics of obliquity and precession. A combined evaluation of model and proxy spectra and their coherence spectrum (Fig. 14g) indicates, that the coherence at these four sub-Milankovitch frequencies is significant at an 80% level and thus nearly as high as at the basic Milankovitch frequencies. This result is statistically valid, but is based upon a synthetic and somewhat arbitrary reference curve.

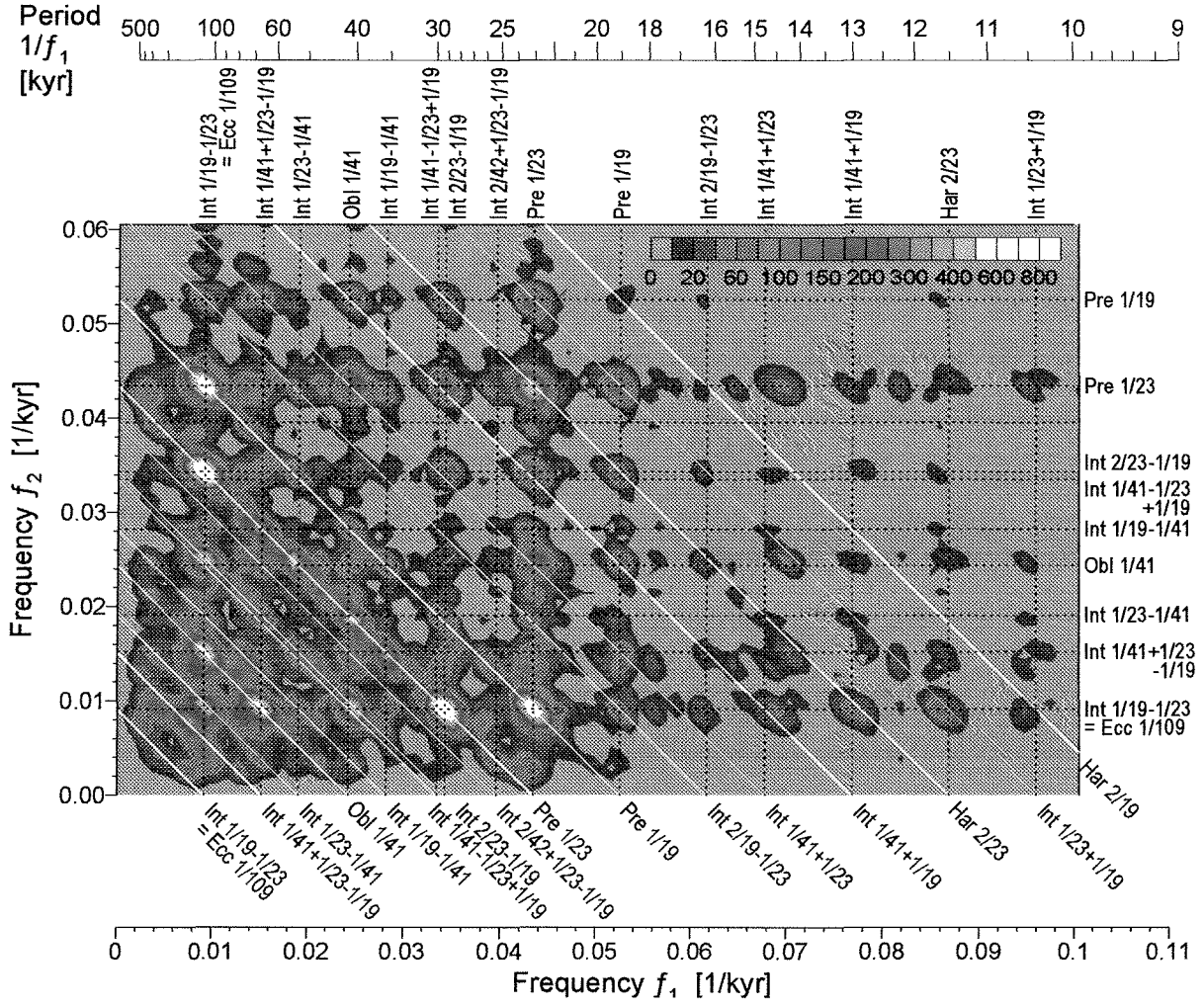

Fig. 15. Bispectral analysis of CEARIS stack (see text for explanation).

A more direct approach is bispectral analysis (e.g., Rao and Gabr 1984; Nikias and Raghuveer 1987). This higher-order statistical method was employed by Muller and MacDonald (1997) to analyze 100 kyr cyclicity and by Hagelberg et al. (1991) for detection of sub-Milankovitch climate variations. In contrast to power and cross spectra, which regard individual or compare equal frequencies, bispectra are capable of detecting non-linear coupling of different frequencies. A phase-lock between a hypothetical combination frequency f_3 and its assumed generating frequencies f_1 and f_2 is condition for a peak in the mirror-symmetric, two-dimensional diagram. Noise components and random oscillations are efficiently suppressed.

The bispectrum of the CEARIS stack (Fig. 15) displays a considerable number of peaks, mostly at the intersections of grid lines representing a simplified set of basic Milankovitch frequencies and their low-order combinations. A combination frequency f_3 can result from different pairs (f_1,f_2). For evident mathematical reasons these realizations are positioned along diagonal lines. Besides basic obliquity and precession peaks resulting from combinations of their own intermodulation frequencies, various low-order harmonics (as 2/23 kyr^{-1}) and intermodulations (as (1/41+1/23) kyr^{-1}) are detected. The four major sub-Milankovitch peaks of the coherence spectrum (Fig. 14g) are validated as phase-locked combination tones of obliquity and preces-

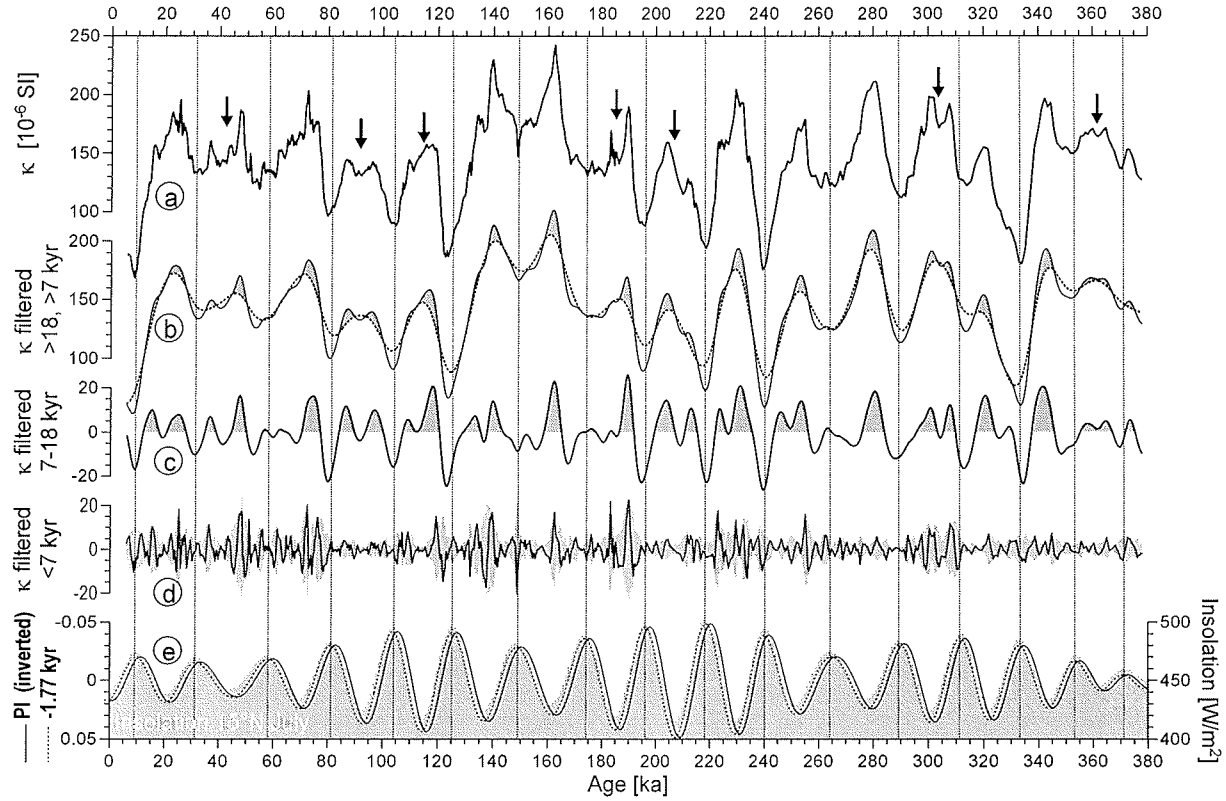

Fig. 16. (a) Susceptibility record of GeoB 1523-1 (arrows mark twin peaks corresponding to precession harmonics). **(b)** idem, lowpass filtered (2nd order Butterworth) to exclude (> 18 kyr, dotted line) and include (> 7 kyr, solid line) sub-Milankovitch harmonics. **(c)** The residue of both filtered signals (7-18 kyr) frequently shows deep minima in phase with insolation maxima (dotted vertical lines), followed by twin maxima (shaded as in b) before and after insolation minima. **(d)** The millennial band (< 7 kyr) signal component appears to be aperiodic, although in some sections, its envelope (shaded) resembles curve c (see also Fig. 16) **(e)** Precession index (solid line), shifted by -1.77 kyr (dashed line), and 15°N July insolation curve (shaded) by Berger and Loutre (1991).

sion. Two further peak chains near 65 kyr and 30 kyr are identified as third-order intermodulations ((1/41+1/23-1/19) kyr^{-1} and (1/41-1/23+1/19) kyr^{-1}) within the Milankovitch band. Their important climatic implication will be discussed below.

In essence these results suggest that large parts of the observed sub-Milankovitch signal components down to periods of at least 10 kyr can be explained by non-linear climate response to orbital variations. Below 10 kyr 'subtone dispersion' comes into play (Fig. 14). Precession and obliquity cycles are given as trigonometric expansions of several sinusoidal signals, most of them with very similar frequencies (Berger and Loutre 1992; Schwarzacher 1993). The frequencies of their second and third order harmonics are still close enough for their peaks to merge. With increasing order, the differences become larger and each intermodulation peak splits up into a peak chain, eventually interfering with other peak chains... so that even prominent and significant spectral peaks are no more safely identified. Considering that for the CEARIS cores the estimated age uncertainty is in the order of 2 kyr, there is no sense in searching for orbital effects much below periods of 7 kyr. The relative increase of the noise component with higher frequency, resulting from climatic and depositional random processes and stratigraphic error, is documented by the widening of the standard deviation band in Fig. 14d.

In view of paleoceanographic interpretation, signal phase and regularity are almost as important as frequency and amplitude. A band selective time domain representation of the susceptibility record

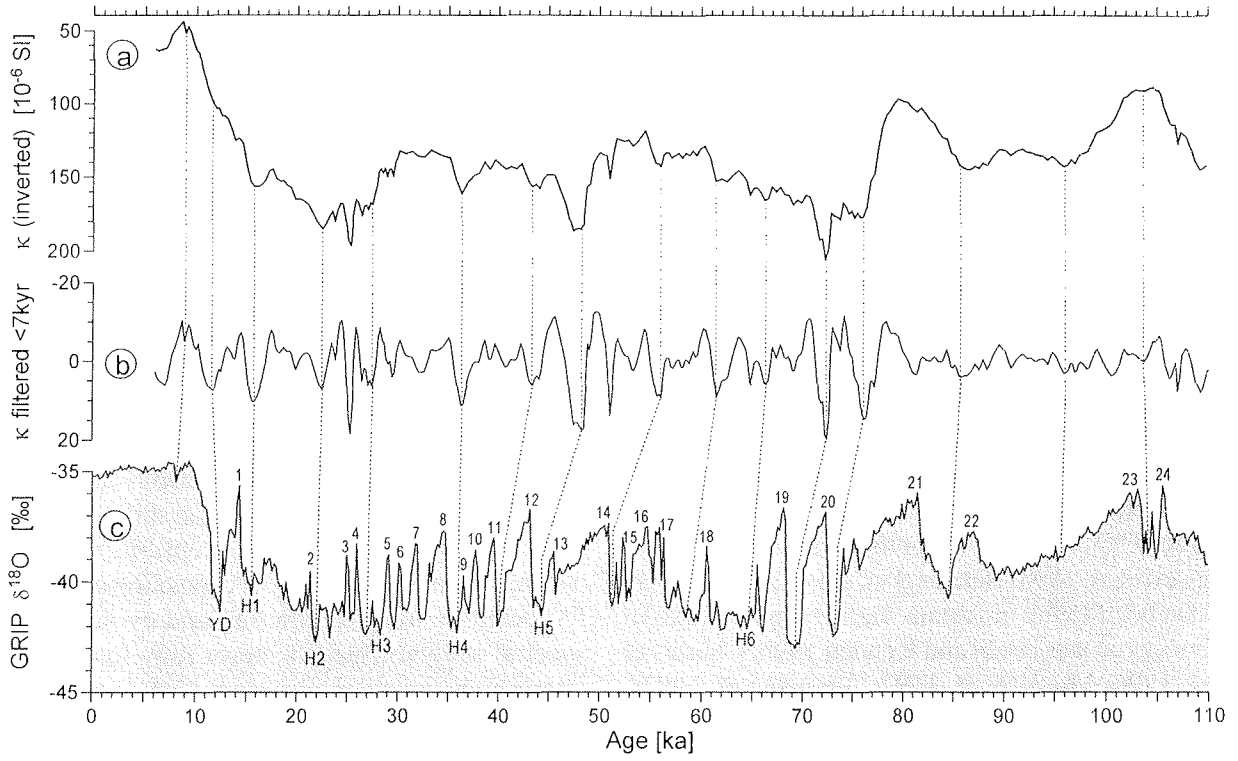

Fig. 17. Tentative correlation of 110-0 ka section of **(a)** susceptibility record of GeoB 1523-1, **(b)** idem, highpass filtered (2nd order Butterworth < 7 kyr) to extract millennial scale variations, to **(c)** GRIP $\delta^{18}O$ record on Dansgaard et al. (1993) age model. Labels mark Dansgaard-Oeschger cycles 1-24, Younger Dryas, and Heinrich events H1-H6. As considerable disagreement over details of the GRIP timescale persists (e.g., Hammer et al. 1997; Johnsen et al. 1997; Adkins et al. 1997), the correlation ages are not sufficiently reliable to evaluate the precision of orbital tuning.

of core GeoB 1523-1 is shown in Fig. 16 for the Milankovitch (> 18 kyr), sub-Milankovitch range (18 to 7 kyr) and millennial range (< 7 kyr). The 7 kyr boundary is clearly a statistical and not a paleoclimatic limit.

The coherent orbital periodicities in the Milankovitch band (Figs.14b, c, 16b) suggest that global glacial interglacial sea-level changes modulate the flux of (Fe-rich) Amazon sediments from the shelf region into the adjacent pelagic realm. Only tropical insolation variations can explain the much higher 23 kyr spectral power of κ compared to $\delta^{18}O$ (Fig. 8) and precessional susceptibility variations prior to Northern hemisphere glaciation at the Ceará Rise (Harris et al. 1997). At low latitudes precession largely controls insolation (Fig. 16e, Berger and Pestiaux 1984) and modulates sea surface temperature, monsoon intensity and nutricline depth (e.g., McIntyre et al. 1989). Periods of elevated summer insolation result in increased carbonate accumulation (Rühlemann et al. 1996) and reduced Saharan dust deposition (Sarnthein et al 1981; Balsam et al. 1995) in the western equatorial Atlantic. Both effects lower the precessional susceptibility signal (Fig. 16c,e). In periods of reduced insolation, 'twin peaks' of susceptibility are frequently observed - not just in the filtered (Fig. 16c), but also in the raw signal (arrows in Fig. 16a). They are therefore authentic paleoceanographic features and not artefacts of signal distortion by varying sedimentation rates (Martinson et al. 1982; Schiffelbein and Dorman 1986). Detailed rock magnetic analyses (T. von Dobeneck, unpublished data) indicate that the earlier of both peaks carries more Saharan, the second more Amazonian characteristics. Together they reflect the double precession cycle of monsoon intensity.

Further support to pCO_2 threshold models ('100 kyr cycle problem'), discussed in the context of SUSAS time series analyses, comes from the

extraordinarily high bispectral intensities of the intermodulation frequencies (1/41+1/23-1/19) kyr^{-1} and (1/41-1/23+1/19) kyr^{-1}. Both combination tones express nonlinear interaction of obliquity with the envelope of the composed precession signal, which has a frequency of (-1/23+1/19) kyr^{-1}, corresponding to an (averaged) eccentricity frequency of 1/109 kyr^{-1}. This interaction provides the trigger mechanism for the late Quaternary 100 kyr ice age cycles.

Millennial climate cycles are believed to result from free, self-sustained glaciomarine oscillations as proposed by many coupled climate models (e.g., Birchfield et al. 1994; Paillard 1995). Large millennial temperature oscillations documented by ice core $\delta^{18}O$ studies from both hemispheres (Dansgaard et al. 1993; Bender et al. 1994) have recently also been found in various marine high-resolution proxy records (Behl and Kennett 1996; Charles et al. 1996; Moros et al. 1997; Adkins et al. 1997), with some reservations also at the Ceará Rise (Curry and Oppo 1997). It is therefore not overly ambitious to tentatively correlate the millennial signal component of GeoB 1523-1 (Fig. 16d) with the GRIP $\delta^{18}O$ record (Fig. 17). Although both patterns are not exactly mirror images, the similarity is quite reasonable given the fact that a 2.8 m and a 2800 m record from two climate extremes are compared.

Conclusions

The SUSAS and CEARIS studies demonstrate how the methods of cyclostratigraphy and environmental magnetism can be fruitfully combined. Other than most physical properties parameters, magnetic susceptibility depends linearly on the concentrations of a few (iron-bearing) minerals, predominately (titano-) magnetite. In most marine environments its mean value and climatic modulation primarily mirrors the ratio of terrigenous and biogenic sediment accumulation. Susceptibility variations can be closely related to carbonate dissolution cycles as in case of the SUSAS cores, but may also primarily respond to climatic cycles of terrigenous supply as in the CEARIS example. The basic mechanisms of these two cycles are well studied and largely understood. They are effects of deep water formation, sea level change, aridity and wind intensity, all intimately linked to orbital cycles. Although the phase relations of $\delta^{18}O$ and κ differ regionally, the orbital response of susceptibility to climatic change is often adequate for cyclostratigraphy and orbital tuning. Pilot spectral studies on selected cores yield applicable phase lags and indicate best tuning targets.

Particularly in low-accumulation environments phase settings are not as important as pattern reproducibility. Because susceptibility logging generates a complete low-noise image based on the sediment volume, subtle signal characteristics are resolved enabling pattern identification even in problematic sections. Aperiodic trends, shifts and amplitude fluctuations of the susceptibility record document modifications of the depositional system. Extracted by lowpass filtering and evolutionary spectral analysis, these features may have more interesting climatic implications than a perfect orbital correlation scheme. In the SUSAS example, analogue long term trends of subtropical South Atlantic κ and $\%CaCO_3$ and global $\delta^{13}C$ (but not $\delta^{18}O$) records indicate marked changes at around 0.95 and 0.6 Ma. Repeated converse shifts of 100 kyr and 41 kyr spectral power relative to an ETP model substantiate pCO_2 threshold concepts (e.g., Saltzman and Verbitsky 1993; Raymo 1997) of the mid-Pleistocene transition.

In addition, most high-resolution susceptibility records carry important signal components in the sub-Milankovitch and millennial bands. In case of the eight CEARIS records these high-frequency variations are largely coherent and can be used to improve the internal precision of the combined cyclostratigraphic age model. As shown by spectral and bispectral analysis, the signal modulation in the 7-18 kyr band is mainly due to periodic harmonics and combination tones of orbital frequencies such as the doubled precession cycle predicted for tropical climate by models (Short et al. 1991). Similar spectral interpretations in the < 7 kyr band are inhibited by the complexity of combination tones and uncertainty of the age model. A tentative correlation of millennial CEARIS variations to Dansgaard-Oeschger cycles (Dansgaard et al. 1993) yields quite convincing results within the limitations of both age models. Both categories of high-

frequency variations open attractive perspectives to improve chronostratigraphic precision beyond the present state of the art.

Acknowledgments

We thank U. Bleil for many helpful discussions and constructive criticism. Reviews and many valuable suggestions by W.H. Berger and M. Schulz are gratefully acknowledged. T. Bickert kindly provided unpublished $\delta^{13}C$ data of ODP Site 806. This study was funded by the Deutsche Forschungsgemeinschaft (Sonderforschungsbereich 261 at Bremen University, contribution No. 219). F. S. was supported by the Deutsche Forschungsgemeinschaft in the framework of Graduiertenkolleg 221.

Data are available under www.pangaea.de/Projects/SFB261.

References

Adkins JF, Boyle EA, Keigwin L, Cortijo E (1997) Variability of the North Atlantic thermohaline circulation during the last interglacial period. Nature 390:154-156

Balsam WL, Otto-Bliesner BL, Deaton BC (1995) Modern and last glacial maximum eolian sedimentation patterns in the Atlantic Ocean interpreted from sediment iron oxide content. Paleoceanography 10:493-507

Bassinot FC, Beaufort L, Vincent E, Labeyrie LD, Rostek F, Müller PJ, Quidelleur X, Lancelot Y (1994) Coarse fraction fluctuations in pelagic carbonate sediments from the tropical Indian Ocean: a 1500-kyr record of carbonate dissolution. Paleoceanography 9:579-600

Behl RJ, Kennett JP (1996) Brief interstadial events in Santa Barbara basin, NE Pacific, during the past 60 kyr. Nature 379:243-246

Bendat JS, Piersol AG (1986) Random data. Wiley, New York, pp 1-566

Bender M, Sowers T, Dickson ML, Orchardo J, Grootes P, Mayewski PA, Meese DA (1994) Climate correlations between Greenland and Antarctica during the past 100,000 years. Nature 372:663-666

Berger A, Pestiaux P (1984) Accuracy and stability of the Quaternary terrestrial insolation. In: Berger A, Imbrie J, Hays J, Kukla G, Saltzman B (eds) Milankovitch and Climate Part 1, Reidel, Dordrecht, pp 83-111

Berger A, Loutre MF (1991) Insolation values for the climate of the last 10 million years. Quat Sci Rev 10:297-317

Berger A, Melice JL, Hinnov L (1991) A strategy for frequency spectra of Quaternary climate records. Clim Dyn 5:227-240

Berger A, Loutre MF (1992) Astronomical solutions for paleoclimate studies over the last 3 million years. Earth Planet Sci Lett 111:369-382

Berger A, Loutre MF (1994) Precession, eccentricity, obliquity, insolation and paleoclimates. In: Duplessy JC, Spyridakis MT (eds) Long-term climatic variations. Springer, Berlin, pp 107-151

Berger WH, Heath GR (1968) Vertical mixing in pelagic sediments. J Mar Res 26:134-142

Berger WH, Yasuda MK, Bickert T, Wefer G, Takayama T (1994) Quaternary time scale for the Ontong Java Plateau: Milankovitch template for Ocean Drilling Program Site 806. Geology 22:463-467

Berger WH, Jansen E (1994a) Fourier stratigraphy: spectral gain adjustment of orbital ice mass models as an aid in dating late Neogene deep-sea sediments. Paleoceanography 9:693-703

Berger WH, Jansen E (1994b) Mid-Pleistocene climate shift - the Nansen connection. In: Johannessen OM, Muench RD, Overland JE (eds) The polar oceans and their role in shaping the global environment. Geophys Monogr Ser 85, AGU, Washington, pp 295-311

Bickert T (1992) Rekonstruktion der spätquartären Bodenwasserzirkulation im östlichen Südatlantik über stabile Isotope benthischer Foraminiferen. PhD thesis, Ber FB Geo Univ Bremen 27,pp 1-205

Bickert T, Wefer G (1996) Late Quaternary deep water circulation in the South Atlantic: reconstruction from carbonate dissolution and benthic stable isotopes. In: Wefer G, Berger WH, Siedler G, Webb DJ (eds) The South Atlantic: present and past circulation, Springer Verlag, Berlin, pp 599-620

Bickert T, Curry WB, Wefer G (1997) Late Pliocene to Holocene (2.6-0 Ma) western equatorial Atlantic deep-water circulation: inferences from benthic stable isotopes. Proc ODP, Sci Results 154:239-254

Bickert T, Berger WH, Wefer G (1998) The deep western equatorial Pacific in Plio-Pleistocene times: Results from Leg 130 (Ontong Java Plateau). Paleoceanography (subm)

Birchfield GE, Wang H, Rich JJ (1994) Century/millenium internal climate oscillations in an ocean-atmosphere-continental ice sheet model. J Geophys Res 99:12459-12470

Blackman RB, Tukey JW (1958) The measurement of power spectra. Dover Publ Inc, New York, pp 1-190

Bloemendal J, Lamb B, King J (1988) Paleoenvironmental implications of rock-magnetic properties of late Quaternary sediment cores from the Eastern Equatorial Atlantic. Paleoceanography 3:61-87

Bloemendal J, deMenocal P (1989) Evidence for a change in the periodicity of tropical climate cycles at 2.4 Myr from whole-core magnetic susceptibility measurements. Nature 342:897-900

Bolton EW, Maasch KA, Lilly JM (1995) A wavelet analysis of Plio-Pleistocene climate indicators: A new view of periodicity evolution. Geophys Res Lett 22:2753-2756

Bond G, Broecker W, Johnsen S, McManus J, Labeyrie L, Jouzel J, Bonani G (1993) Correlations between climate records from North Atlantic sediments and Greenland ice. Nature 365:143-145

Charles CD, Lynch-Stieglitz J, Ninnemann US, Fairbanks RG (1996) Climate connections between the hemisphere revealed by deep sea core/ice core correlations. Earth Planet Sci Lett 142:19-27

Chi J, Mienert J (1996) Linking physical property records of Quaternary sediments to Heinrich events. Mar Geology 131:57-73

Cortijo E, Yiou P, Labeyrie L, Cremer M (1995) Sedimentary record of rapid climatic variability in the North Atlantic Ocean during the last glacial cycle. Paleoceanography 10:911-926

Crowley TJ, Kim KY, Mengel JG, Short DA (1992) Modeling 100,000 year climate fluctuations in pre-Pleistocene time series. Science 255:705-707

Curry WB, Oppo DW (1997) Synchronous, high-frequency oscillations in tropical sea surface temperatures and North Atlantic Deep Water production during the last glacial cycle. Paleoceanography 12:1-14

Dalfes HN, Schneider SH, Thompson SL (1984) Effects of bioturbation on climatic spectra inferred from deep sea cores. In: Berger A, Imbrie J, Hays J, Kukla G, Saltzman B (eds) Milankovitch and Climate Part 1, Reidel, Dordrecht, pp 481-492

Damuth JE (1977) Late Quaternary sedimentation in the western equatorial Atlantic, Geol Soc America Bull 88:695-710

Dansgaard W, Johnsen SJ, Clausen HB, Dahl-Jensen D, Gundestrup NS, Hammer CU, Hvidberg CS, Steffensen JP, Sveinbjornsdottir AE, Bond G (1993) Evidence for general instability of past climate from a 250-kyr ice-core record. Nature 364:218-220

DeBlonde G, Peltier WR (1991) A one-dimensional model of continental ice volume fluctuations through the Pleistocene: implications for the origin of the Mid-Pleistocene climate transition. J Clim 4:318-344

deMenocal P (1995) Plio-Pleistocene African climate. Science 270:53-59

deMenocal P, Bloemendal J, King J (1991) A rock-magnetic record of monsoonal dust deposition to the arabian sea: evidence for a shift in the mode of deposition at 2.4 Ma. Proc ODP, Sci Results 117:389-401

Diester-Haass L (1991) Rhythmic carbonate content variations in Neogene sediments above the oceanic lysocline. In: Einsele G, Ricken W, Seilacher A (eds.) Cycles and events in stratigraphy, Springer Verlag, Berlin, pp 94-109

Flanders PJ (1988) An alternating gradient force magnetometer, J Appl Phys 63:3940-3945

Francois R, Bacon MP(1991) Variations in terrigenous input into the deep Equatorial Atlantic during the past 24,000 years, Science 251:1473-1475

Glenn CR, Kelts K (1991) Sedimentary rhythms in lake deposits. In: Einsele G, Ricken W, Seilacher A (eds.) Cycles and events in stratigraphy, Springer Verlag, Berlin, pp 188-221

Grousset FE, Labeyrie L, Sinko JA, Cremer M, Bond G, Duprat J, Cortijo E, Huon S (1993) Patterns of ice-rafted detritus in the glacial North Atlantic (40-55°N). Paleoceanography 8:175-192

Hagelberg TK, Pisias N (1991) Linear and nonlinear couplings between orbital forcing and the marine $\delta^{18}O$ record during the late neogene. Paleoceanography 6:729-746

Hagelberg TK, Bond G, deMenocal P (1994) Milankovitch band forcing of sub-Milankovitch climate variability during the Pleistocene. Paleoceanography 9:545-558

Hammer CU, Andersen KK, Clausen HB, Dahl-Jensen D, Hvidberg CS , Iversen P (1997) The stratigraphic dating of the GRIP ice core. Special Report of the Geophysical Department, Niels Bohr Institute for Astronomy, Physics and Geophysics, University of Copenhagen

Harris, FJ (1978) On the use of windows for harmonic analysis with the Discrete Fourier Transform. Proc IEEE 66:51-83

Harris SE, Mix AC, King T (1997) Biogenic and terrigenous sedimentation at Ceara Rise, western tropical Atlantic, supports Pliocene-Pleistocene deep-water linkage between hemispheres. Proc ODP, Sci Results 154:331-345

Hays JD, Imbrie J, Shackleton NJ (1976) Variations in Earth's orbit: pace-maker of the ice ages. Science 194:1121-1132

Hilgen FJ, Krijgsman W, Langereis CG, Lourens LJ, Santarelli A, Zachariasse WJ (1995) Extending the

astronomical (polarity) time scale into the Miocene. Earth Planet Sci Lett 136:495-510

Horowitz LL (1974) The effects of spline interpolation on power spectral density. IEEE Trans ASSP 22:22-27

Imbrie J, Imbrie JZ (1980) Modeling the climatic response to orbital variations, Science 207:943-953

Imbrie J, Hays JD, Martinson DG, McIntyre A, Mix AC (1984) The orbital theory of Pleistocene climate: support from a revised chronology of the marine $\delta^{18}O$ record. In: Berger A, Imbrie J, Hays J, Kukla G, Saltzman B (eds) Milankovitch and Climate Part 1, Reidel, Dordrecht, pp 269-305

Imbrie J, Berger A, Boyle EA, Clemens SC, Duffy A, Howard WR, Kukla G, Kutzbach J, Martinson DG, McIntyre A, Mix AC, Molfino B, Morley JJ, Peterson LC, Pisias NG, Prell WL, Raymo ME, Shackleton NJ, Toggweiler JR (1992) On the structure and origin of major glaciation cycles 1. Linear responses to Milankovitch forcing. Paleoceanography 7:701-738

Imbrie J, Berger A, Boyle EA, Clemens SC, Duffy A, Howard WR, Kukla G, Kutzbach J, Martinson DG, McIntyre A, Mix AC, Molfino B, Morley JJ, Peterson LC, Pisias NG, Prell WL, Raymo ME, Shackleton NJ, Toggweiler JR (1993) On the structure and origin of major glaciation cycles 2. The 100,000-year cycle. Paleoceanography 8:699-735

Johns WE, Schott FA, Zantopp RJ, Evans RH (1990) The North Brazil Current retroflection: seasonal structure and eddy variability, J Geophys Res 95:22103-22120

Johnsen SJ, Clausen HB, Dansgaard W, Gundestrup NS, Hammer CU, Andersen U, Andersen KK, Hvidberg CS, Dahl-Jensen D, Steffensen JP, Shoji H, Sveinbjörnsdóttir AE, White JWC, Jouzel J, Fisher D (1997) The $\delta^{18}O$ record along the Greenland Ice Core Project deep ice core and the problem of possible Eemian climatic instability. J Geophys Res 102:26397-26410

Joyce JE, Tjalsma LRC, Prutzman JM (1990) High resolution planktic stable isotope record and spectral analysis for the last 5.35 m.y.: Ocean Drilling Program Site 625, northeast gulf of Mexico. Paleoceanography 5:507-529

Kumar N, Embley RW (1977) Evolution and origin of Ceará Rise: an aseismic rise in the western equatorial Atlantic, Geol Soc America Bull 88:683-694

Kent DV (1982) Apparent correlation of paleomagnetic intensity and climatic records in deep-sea sediments. Nature 229:538-539

Le Treut H, Ghil M (1983) Orbital forcing, climatic interactions, and glaciation cycles. J Geophys Res 88:5167-5190

Lisitzin AP (1996) Oceanic sedimentation: lithology and geochemistry. AGU, Washington D.C.:400 pp

Liu HS (1992) Frequency variations of the Earth's obliquity and the 100-kyr ice-age cycles. Nature 358:397-399

Liu HS (1995) A new view on the driving mechanism of Milankovitch glaciation cycles. Earth Planet Sci Lett 131:17-26

Lomb NR (1976) Least-squares frequency analysis of unequally spaced data. Astrophys Space Sci 39:447-462

Martinson DG, Menke W, Stoffa P (1982) An inverse approach to signal correlation. J Geophys Res 87: 4807-4818

Martinson DG, Pisias NG, Hays JD, Imbrie J, Moore TC, Shackleton NJ (1987) Age dating and the orbital theory of the ice ages: development of a high-resolution 0 to 300,000-year chronostratigraphy. Quat Res 27:1-29

Maslin M, Mikkelsen N (1997) Amazon fan mass-transport deposits and underlying interglacial deposits: age estimates and fan dynamics. Proc ODP, Sci Results 155:353-365

Matthewson AP, Shimmield GB, Kroon D (1995) A 300 kyr high-resolution aridity record of the North African continent. Paleoceanography 10:677-692

McIntyre A, Ruddiman WF, Karlin K, Mix AC (1989) Surface water response of the equatorial Atlantic Ocean to orbital forcing. Paleoceanography 4:19-55

Mienert J, Chi J (1995) Astronomical time-scale for physical property records from Quaternary sediments of the northern North Atlantic. Geol Rundschau 84:67-88

Milankovitch M (1941) Kanon der Erdbestrahlung und seine Anwendung auf das Eiszeitenproblem. Roy Serb Acad Spec Publ 133:1-633

Milliman JD, Summerhayes CP, Barretto HT (1975) Quaternary sedimentation on the Amazon continental margin: a model, Geol Soc America Bull 86:610-614

Moros M, Endler R, Lackschewitz KS, Wallrabe-Adams HJ, Mienert J., Lemke W (1997) Physical properties of Reykjanes Ridge sediments and their linkage to high-resolution Greenland Ice Sheet Project 2 ice core data. Paleoceanography 12:687-695

Mudelsee M, Schulz M (1997) The Mid-Pleistocene climate transition: onset of 100 ka cycle lags ice volume build-up by 280 ka. Earth Planet Sci Lett 151:117-123

Mudelsee M, Stattegger, K (1994). Plio-/Pleistocene climate modelling based on oxygen isotope time series from deap-sea sediment cores: The Grassberger-Procaccia algorithm and chaotic climatic systems. Math Geol 26:799-815

Mudelsee M, Stattegger, K (1997) Exploring the structure of the mid-Pleistocene revolution with advanced methods of time-series analysis. Geol Rundschau 86:499-511

Mulitza S (1994) Spätquartäre Variationen der oberflächennahen Hydrographie im westlichen äquatorialen Atlantik. Berichte, Fachbereich Geowissenschaften, Universität Bremen 57, pp1-97

Muller RA, MacDonald GJ (1995) Glacial cycles and orbital inclination. Nature 377:107-108

Muller RA, MacDonald GJ (1997) Simultaneous presence of orbital inclination and eccentricity in proxy climate records from Ocean Drilling Program site 806. Geology 25:3-6

Muller-Karger F, McClain CR, Richardson PL (1988) The dispersal of the Amazon's water. Nature 333:56-59

Mwenifumbo CJ, Blangy JP (1991) Short-term spectral analysis of downhole logging measurements from Site 704. Proc ODP, Sci Results 114:577-585

Nikias CL, Raghuveer MR (1987) Bispectrum estimation: a digital signal processing framework. Proc. IEEE 75:869-891

Nobes DC, Bloomer SF, Mienert J, Westall F (1991) Milankovitch cycles and nonlinear response in the Quaternary record in the Atlantic sector of the southern oceans. Proc ODP, Sci Results 114:551-576

Nowaczyk NR, Frederichs T, Eisenhauer A, Gard G (1994) Magnetostratigraphic data from late Quaternary sediments from the Yermak Plateau, Arctic Ocean: evidence for four geomagnetic polarity events within the last 170 ka of the Brunhes Chron. Geophys J Int 117:453-471

Oppenheim AV, Schafer RW (1989) Discrete time signal processing. Englewood Cliffs, NJ, Prentice Hall, pp 311-312

Park J, D'Hondt SL, King JW, Gibson C (1993) Late Cretaceous precessional cycles in double time: a warm-Earth Milankovitch response. Science 261:1431-1434

Park J, Maasch KA (1993) Plio-Pleistocene time evolution of the 100-kyr cycle in marine paleoclimate records. J Geophys Res 98:447-461

Paillard D (1995) The hierarchical structure of glacial climatic oscillations: interactions between ice-sheet dynamics and climate. Clim Dyn 11:162-177

Peng TH, Broecker WS, Kipphut G, Shackleton N (1977) Benthic mixing in deep sea cores as determined by ^{14}C dating and its implications regarding climate stratigraphy and the fate of fossil fuel CO_2.In: Andersen NR, Malahoff A (eds) The fate of fossil fuel CO_2 in the oceans. Plenum Press, New York, pp 355-373

Pestiaux P, Berger A (1984) An optimal approach to the spectral characteristics of deep-sea climatic records In: Berger A, Imbrie J, Hays J, Kukla G, Saltzman B (eds) Milankovitch and Climate Part 1, Reidel, Dordrecht, pp 417-445

Pestiaux PI, van der Mersch I, Berger A, Duplessy JC (1988) Paleoclimatic variability at frequencies ranging from 1 cycle per 10,000 years to 1 cycle per 1000 years: evidence for nonlinear behaviour of the climate system. Clim Change 12:9-37

Pisias NG, Moore TC (1981) The evolution of Pleistocene climate: a time series approach. Earth Planet Sci Lett 52:450-458

Pisias NG, Mix AC, Zahn R (1990) Nonlinear response in the global climate system: Evidence from benthic oxygen isotopic record in core RC13-110. Paleoceanography 5:147-160

Prell WL (1982) Oxygen and carbon isotope stratigraphy for the Quaternary of Hole 502B: evidence for two modes of isotopic variability. Initial Rep DSDP 68:455-464

Radhakrishnamurty C, Likhite SD, Amin BS, Somayajulu BLK (1968) Magnetic susceptibility stratigraphy in ocean sediment cores, Earth Planet Sci Lett 4:464-468

Rao TS, Gabr M (1984) An introduction to bispectral analysis and bilinear time-series models. Springer, New York

Raymo ME (1997) The timing of major climate transitions. Paleoceanography 12:577-585

Raymo ME, Ruddiman WF, Froehlich PN (1988) Influence of late Cenozoic mountain building on ocean geochemical cycles. Geology 16:649-653

Raymo ME, Ruddiman WF, Backman J, Clement BM, Martinson DG (1989) Late Pliocene variation in northern hemisphere ice sheets and North Atlantic deep water circulation. Paleoceanography 4:413-446

Raymo ME, Ruddiman WF (1992) Tectonic forcing of late Cenozoic climate. Nature 359:117-122

Robinson SG (1986) The late Pleistocene paleomagnetic record of North Atlantic deep-sea sediments revealed by mineral-magnetic measurements. Phys Earth Planet Inter 42:22-47

Robinson SG (1990) Applications for whole-core magnetic susceptibility measurements of deep-sea sediments. Proc ODP, Sci Results 115:737-771

Robinson SG, Maslin MA, McCave IN (1995) Magnetic susceptibility variations in Upper Pleistocene deep-sea sediments of the NE Atlantic: implications for ice rafting and paleocirculation at the last glacial maximum. Paleoceanography 10:221-250

Ruddiman WF, Raymo ME, McIntyre A (1986) Matuyama 41,000-year cycles: North Atlantic Ocean and northern hemisphere ice sheets. Earth Planet Sci Lett 80:117-129

Ruddiman WF, Raymo ME, Martinson DG, Clement BM, Backman J (1989) Pleistocene evolution: northern hemisphere ice sheets and North Atlantic ocean. Paleoceanography 4:353-412

Rühlemann C, Frank M, Hale W, Mangini A, Mulitza S, Müller PJ, Wefer G (1996) Late Quaternary productivity changes in the western equatorial Atlantic: evidence from ^{230}Th-normalized carbonate and organic carbon accumulation. Mar Geology 135:127-152

Saltzman B, Verbitsky MY (1993) Multiple instabilities and modes of glacial rhythmicity in the Plio-Pleistocene: a general theory of late Cenozoic climatic change. Clim Dyn 9:1-15

Sarnthein MG, Tetzlaff G, Koopmann B, Wolter K, Pflaumann U (1981) Glacial and interglacial wind regimes over the eastern subtropical Atlantic and north-west Africa. Nature 293:193-196

Scargle JD (1982) Studies in astronomical time series analysis. II: statistical aspects of spectral analysis of unevenly spaced data. Astrophys J 263:835-853

Scargle JD (1989) Studies in astronomical time series analysis. III: Fourier transforms, autocorrelation functions, and cross-correlation functions of unevenly spaced data. Astrophys J 343:847-887

Schiffelbein P, Dorman LR (1986) Spectral effects of time-depth nonlinearities in deep sea sediment records: a demodulation technique for realigning time and depth scales. J Geophys Res 91:3821-3835

Schulz M, Stattegger K (1997) SPECTRUM: spectral analysis of unevenly spaced paleoclimatic time series. Comp Geosci 23:929-945

Schwarzacher W (1993) Cyclostratigraphy and the Milankovitch theory. Elsevier, Amsterdam, 225 pp

Shackleton NJ, Opdyke ND (1976) Oxygen-isotope and paleomagnetic stratigraphy of pacific core V28-239 late Pliocene to latest Pleistocene. In: Cline RM, Hays JD (eds) Investigations of Later Quaternary paleoceanography and paleoclimatology. Mem 145 Geol Soc Amer, Washington, pp 449-464

Shackleton NJ, Berger A, Peltier WR (1990) An alternative astronomical calibration of the lower Pleistocene timescale based on ODP Site 677. Trans Royal Soc Edinburgh: Earth Sci 81:251-261

Shackleton NJ, Hagelberg TK, Crowhurst SJ (1995) Evaluating the success of astronomical tuning: pitfalls of using coherence as a criterion for assessing pre-Pleistocene timescales. Paleoceanography 10:693-697

Shackleton NJ, Crowhurst S (1997) Sediment fluxes based on an orbital tuned time scale 5 Ma to 14 Ma, Site 926. Proc ODP, Sci Results 154:69-82

Short DA, Mengel JG, Crowley TJ, Hyde WT, North GR (1991) Filtering of Milankovitch cycles by Earth's geography. Quat Res 35:157-173

Tarduno JA (1994) Temporal trends of magnetic dissolution in the pelagic realm: gauging paleoproductivity? Earth Planet Sci Lett 123:39-48

Tarduno JA, Wilkison SL (1996) Non-steady state magnetic mineral reduction, chemical lock-in, and delayed remanence acquisition in pelagic sediments. Earth Planet Sci Lett 144:315-326

Thiessen W (1993) Magnetische Eigenschaften des östlichen Südatlantiks und ihre paläozeanographische Relevanz. PhD thesis, Ber FB Geo Univ Bremen, 41, pp 1-170

Thompson R, Clarke RM (1993) Quantitative marine sediment core matching using a modified sequence-slotting algorithm. In: Hailwood EA, Kidd RB (eds) High resolution stratigraphy. Spec Publ Geol Soc London 70, pp 39-49

Thomson, DJ (1982) Spectrum estimation and harmonic analysis. Proc IEEE 70:1055-1096

von Dobeneck T (1996) A systematic analysis of natural mineral assemblages based on modelling hysteresis loops with coercivity-related hyperbolic basis functions. Geophys J Int 124:675-694

von Dobeneck T, Frederichs Th, Fabian K, Bleil U (1996) Rock Magnetic Micro-Scanning mit HTSL-SQUID-Gradiometer, VDI-Technologiezentrum (eds) Supraleitung und Tieftemperaturtechnik 1996. VDI-Verlag Düsseldorf (Germany), pp 51-54

Weeks R, Laj C, Endignoux L, Fuller M, Roberts A, Manganne R, Blanchard E, Goree W (1993) Improvements in long-core measurement techniques: applications in paleomagnetism and paleoceanography. Geophys J Int 114:651-662

Welch PD (1967) The use of fast Fourier transform for the estimation of power spectra: a method based on time averaging over short, modified periodograms. IEEE Trans Audio, Electroacustics, AU-15:70-73

Yiou P, Genthon C, Ghil M, Jouzel J, Le Treut H, Barnola JM, Lorius C, Korotkevitch YN (1991) High-frequency paleovariability in climate and CO2 levels from Vostock ice core records. J Geophys Res 96:20365-20378

Mid-Pleistocene climate transition: initiation, interim state and terminal event *(submitted to Nature)*

F. Schmieder, T. von Dobeneck & U. Bleil

Fachbereich Geowissenschaften, Universität Bremen,

P.O. Box 330 440, 28334 Bremen, Germany

The mid-Pleistocene transition (MPT) of the global climate system[1-4], initiated by a shift towards much larger northern hemisphere ice shields at around 920 ka[5] and ending with predominance of 100 kyr ice age cyclicity since about 640 ka[6-8], is one of the fundamental enigmas in Quaternary climate evolution[9]. Of the diverse explanations proposed for the 100 kyr cycle, models invoking a pCO_2-controlled insolation threshold for the melting of large ice shields[10-14] currently yield the best reproduction of $\delta^{18}O$ signal pattern, although inconsistencies remain between oxygen isotope stages 15 and 13. Climate proxy records not exclusively linked to global ice volume are necessary to advance understanding of the MPT[15]. Here we present high-resolution Pleistocene magnetic susceptibility time series of twelve sediment cores from the subtropical South Atlantic essentially reflecting variations in carbonate accumulation. In addition to characteristics known from $\delta^{18}O$ records, they reveal three remarkable features intimately related to the MPT chronology, (1) a premature occurrence of a near-100 kyr cycle around 1150 ka, (2) a MPT interim state of reduced carbonate deposition bound by transitions from 1000 to 920 ka and 640 to 500 ka, and (3) a terminal MPT event at around 530 ka documented in various unusual lithologies.

The twelve pelagic gravity cores recovered with R.V. METEOR in the framework of a long-term paleoceanographic research program (SFB 261 at the University of Bremen) form an oceanwide transect spanning the subtropical South Atlantic between 22°S and 34°S (Fig. 1). Located on the flanks of major submarine elevations (Rio Grande Rise, Mid-Atlantic Ridge, Walvis Ridge) in the depth zone alternately influenced by North Atlantic Deep Water (NADW) and Circumpolar Deep Water (CDW), the sediments provide detailed records of carbonate dissolution cycles related to changes in deep water chemistry. Oligotrophic open ocean conditions result in low average sedimentation rates of 0.5 to 1 cm/kyr at these latitudes. In such environments, a close inverse correlation of magnetic susceptibility to carbonate content is typically observed[16]. The data were acquired on split core halves using a Bartington spot sensor at a 1 cm spacing allowing a signal definition and temporal resolution commonly not attained in $\delta^{18}O$ or $\%CaCO_3$ analyses.

The records were found particularly suitable to refine initial magnetostratigraphic age models by means of astronomical tuning[17] to orbital variations calculated by Berger and Loutre[18]. A phase lag applied (4.5 kyr to obliquity) was

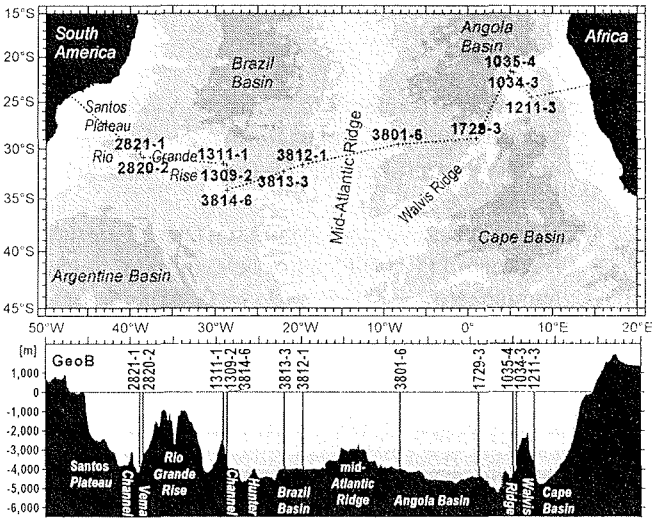

Figure 1 Locations of GeoB cores defining the SUSAS transect. The depth profile follows the dashed line in the map and is plotted against longitude to depict affinities to the major basins of the South Atlantic and their deep water bodies. It is not suitable to identify positions and depths of deep water passages.

determined by cross spectral analysis of $\delta^{18}O$ and magnetic susceptibility of one of the cores (GeoB 1211-1, $\delta^{18}O$ data from Bickert & Wefer[19]). The perfect overall correlation of all twelve individually tuned records (Fig. 2) led us to define the SUSAS (subtropical South Atlantic susceptibility) stack.

A prominent feature of this stack and all individual records is a baseline shift to 40% higher average susceptibilities during the MPT interim state (920 to 640 ka). Confined by transitional intervals lasting about 80 and 140 kyr at its onset and termination, this period exhibits the most distinct dissimilarities between individual core logs. The preceding and following climate states show similar mean susceptibilities modulated by clearly developed and coherent cyclicities of 41 and 100 kyr, respectively. An exception is a 'premature' near 100 kyr cycle around 1150 ka which was also identified in $\delta^{18}O$ records and has been interpreted by Mudelsee and Stattegger[7] as an 'unsuccessful attempt of the climate system to attain a non-linear Late Pleistocene ice age state'. The MPT susceptibility shift is notably mirrored in lowered average sedimentation rates (Fig. 2).

Evolutionary spectral analysis of the SUSAS stack exhibits a continuous Pleistocene decline of 41 kyr cyclicity, but a comparatively abrupt intensification of 100 kyr cyclicity after about 640 ka[17]. Oxygen isotope records document larger ice shields since the beginning of the MPT interim state at 920 ka. Why did 100 kyr cyclicity not start until 640 ka and hence lag the initial ice volume increase by approximately 280 kyr[8]? The observed baseline shift in the SUSAS records precisely fills this time lag and should shed light on this question.

The cause for the overall rise in magnetic susceptibility during the MPT interim state is revealed by a temporal analysis of west-east trends. Plotted against longitude, core mean susceptibilities for the postulated three climate states (Fig. 3 top) reflect the well-known west-east asymmetry of

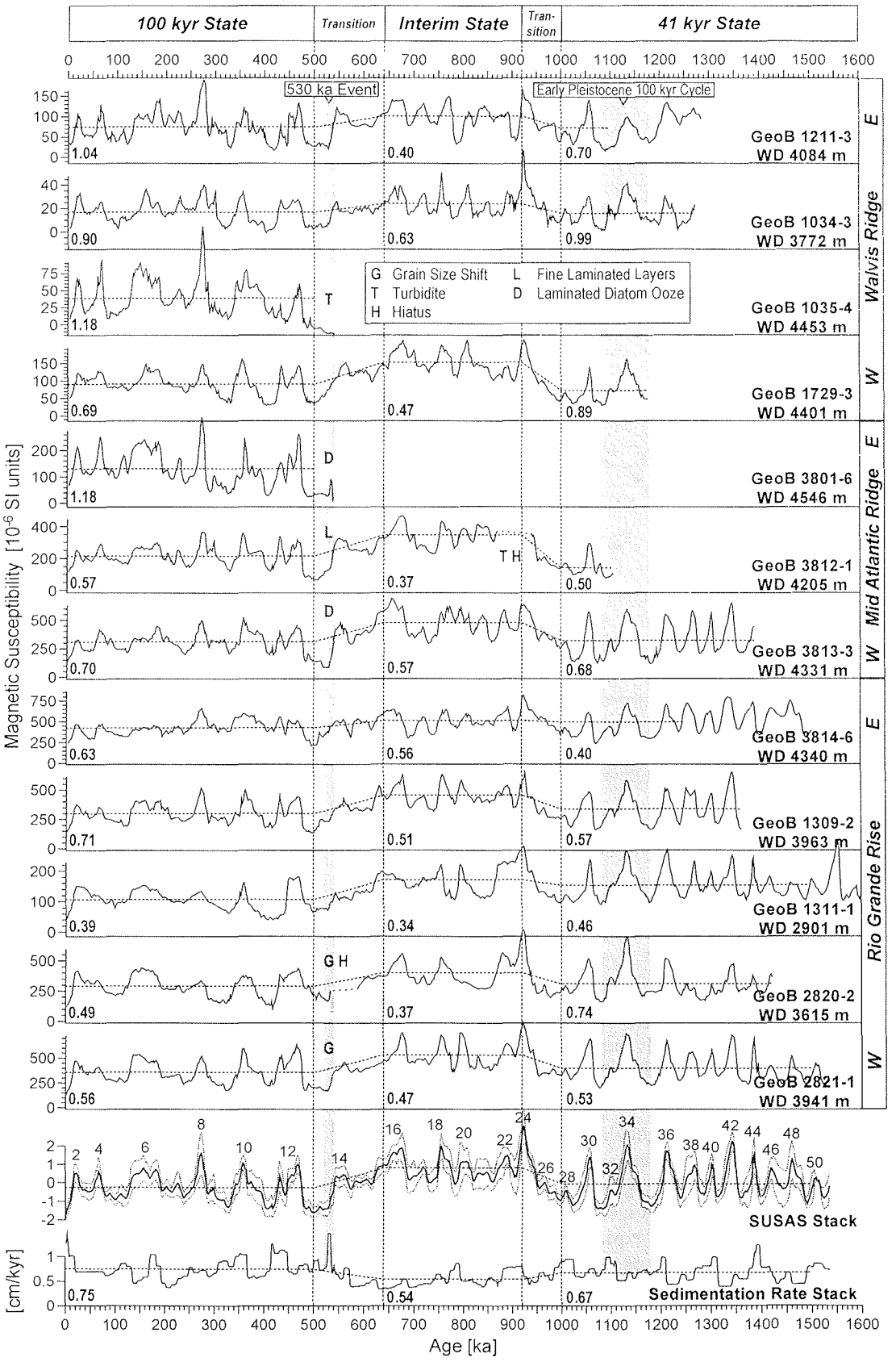

Figure 2 Individually tuned SUSAS records (WD = Water Depth) and resulting susceptibility (arithmetic mean with standard deviation band) and sedimentation rate stack. A diamagnetic susceptibility of -15·10^{-6} SI units representing pure carbonate sediment was chosen as axis minimum. To compensate for different signal levels in the stacking, each record was normalised by subtracting its mean and dividing by its standard deviation. Labels at the SUSAS stack indicate even oxygen isotope stages. Horizontal dotted lines mark baseline averages for pre-, syn- and post-MPT states excluding the bounding transitions. During the interim state, all cores display increased susceptibilities and reduced sedimentation rates. The timing of the three intervals approximately corresponds to the Laplace (1800-1200 ka), Croll (1200-600 ka) and Milankovitch chron (600-0 ka) defined by Berger and Wefer[5]. Numbers in each section denote mean sedimentation rates; grey vertical bars a premature 100 kyr cycle centred near 1150 ka and a terminal MPT event featuring unusual lithologies at about 530 ka.

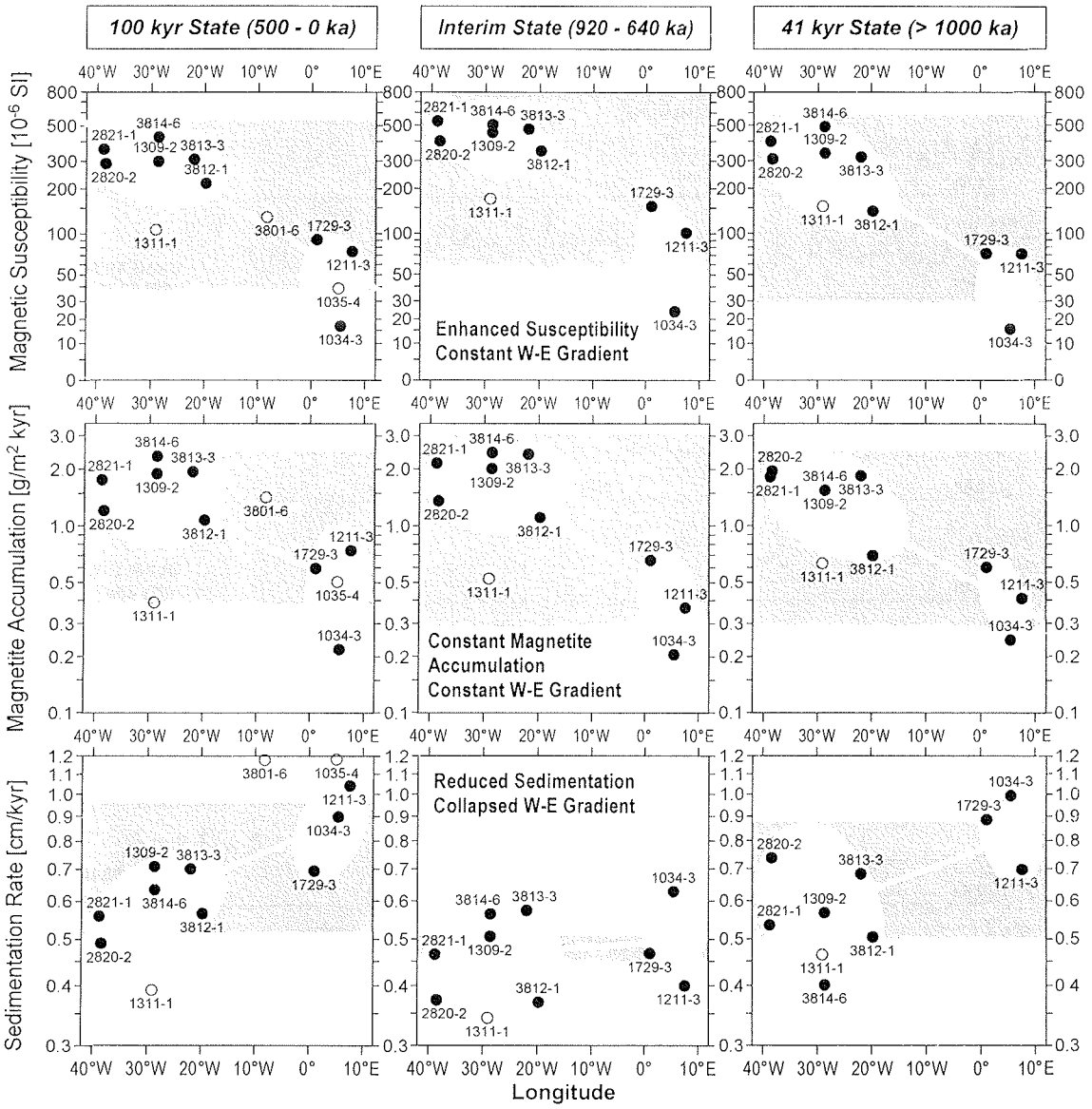

Figure 3 Combined spatial and temporal trend analyses of magnetic susceptibility, magnetite accumulation (calculated by splitting susceptibility into a diamagnetic background and ferrimagnetic, grain-size independent magnetite signal) and sedimentation rate. Major asymmetries and shifts are summarised by white regression lines, dark-grey shading delimits mean data range, light-grey shading western and eastern South Atlantic core sets. Three cores were excluded from the analysis: cores GeoB 1035-4 and 3801-6, as they do not reach beyond the 530 ka event, and core GeoB 1311-1 recovered from 2901 m water depth clearly above the CDW/NADW transition zone and therefore showing a somewhat different evolution.

terrigenous particle flux and accumulation in the South Atlantic[20]. While the gradients are almost identical throughout Pleistocene, a shift to higher susceptibilities is evident during the MPT interim state. This relative increase of magnetic mineral concentration cannot be explained in terms of temporal changes in magnetite accumulation (Fig. 3 centre), as its west-east decline from 2.5 to 0.3 g/m^{2}kyr remains fairly constant over time. A time-varying dilution of the terrigenous fraction by non-magnetic carbonate must therefore be responsible for the observed shift.

Mean sedimentation rates (Fig. 3 bottom) deduced from our age models are mainly controlled by carbonate accumulation. Even the westernmost core GeoB 2821-1 near the South American continent consists to 70 ± 9% of $CaCO_3$ (P. Mueller, pers. comm.). Both for the 41 and 100 kyr climate states, sedimentation rates vary from about 0.5 cm/kyr in the western to around 0.9 cm/kyr in the eastern South Atlantic. During MPT interim state sedimentation rates on either side of the mid-Atlantic Ridge are restricted to between 0.4 and 0.6 cm/kyr. The decline primarily affects the eastern part and brings the west-east asymmetry to collapse.

In the working area cyclic variations of the sediment $CaCO_3$ content at Milankovitch frequencies are mainly due to orbitally driven lysocline shifts resulting from an interplay of NADW and more corrosive CDW[19]. In the Angola Basin (cores GeoB 1034-3, 1035-4 and 1729-3) the glacial-interglacial contrast is particularly manifest as the surrounding bathymetric highs restrict the access of CDW during interglacials. The same reasoning should apply for long-term changes in carbonate accumulation. We therefore assume that the influence of southern-source deep water

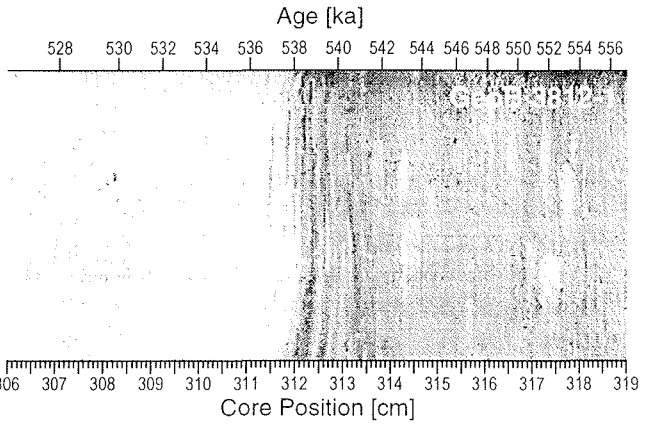

Figure 4 Terminal MPT event documented in a sharp colour transition at unbioturbated finely laminated layers in core GeoB 3812-1.

conclusion is supported by a simultaneous decrease of glacial and interglacial kaolinite/chlorite ratios in core GeoB 2821-1[21], interpreted to be induced by chlorite-enriched deep southern waters. Consequently, NADW should have been reduced during that interval. Indeed, $\delta^{13}C$ records from Atlantic and Pacific ODP sites indicate significantly weaker NADW between 900 and 400 ka[15]. In view of this global evidence we suggest, that the MPT should not be regarded as a gradual transition from a '41 kyr world' to a '100 kyr world', but rather as a third, contrasting climate state.

A conspicuous finding in several of our cores is the coincident occurrence of unusual sediment facies at around 530 ka close to the end of the terminal MPT transition. Granulometric analyses of cores GeoB 2820-2 and 2821-1 show a sharp grain-size shift with an almost total loss of the > 63 µm fraction[22], possibly related to the mid-Brunhes dissolution cycle[23]. In core GeoB 2820-2 this episode corresponds to a short hiatus. The continuous Late Pleistocene record of core GeoB 1035-4 is interrupted by a thick turbidite dating to the same age. Core GeoB 3812-1 displays a sharp colour change at a delicately laminated horizon (Fig. 4). Most impressive are thick intercalated laminated diatom ooze layers in cores GeoB 3801-6 (124 cm) and 3813-3 (38 cm). Omitting these intervals in the susceptibility time series results in continuous Milankovitch signal sequences. Hence, the laminations must have been deposited in a very short time and should reflect an extremely short-term climate variability. Very high sedimentation rates in the overlying carbonate sediments may have contributed to preserve the siliceous sections in both cores. The almost monospecific layers consist of the giant diatom *Ethmodiscus rex* (Rattray) Wiseman & Hendey (C.B. Lange, pers. comm.) and are entirely uncommon at these latitudes. Thick ooze deposits of this diatom were mainly reported from equatorial regions of the world oceans[24-26]. Even there, their occurrence is puzzling, because *Ethmodiscus rex* very rarely occurs in plankton samples. However, enigmatic deep populations have been observed in the Pacific Ocean[27]. Several hypothesis have been proposed to clarify the paradoxical '*Ethmodiscus rex* problem'[26], including differential dissolution, focusing by bottom currents and intense productivity blooms. Results from the Joint Global Ocean Flux Study (JGOFS), based on photographs and measurements from satellites, aircraft, ships, and the Space Shuttle ATLANTIS, emphasise the potentially important role of oceanic frontal zones for the rapid accumulation of diatom biomass[28]. They indicate dramatic biological responses to circulation and mixing processes associated with open-ocean frontal systems separating cold from warm waters and gave rise to the idea that thick diatom layers may be deposited in such environments.

The diversified terminal MPT events at around 530 ka documented in South Atlantic Ocean sediments might well be related to other paleoclimatic 'puzzles' like unusually high and low $\delta^{18}O$ values during isotope stages 13.2 and 13.3, respectively, found in the equatorial Indian Ocean[29], an anomalous sapropel layer in the Mediterranean Sea dated 528-525 ka[30] and highest magnetic susceptibilities of the past 2500 kyr at about 500 ka in Chinese loess deposits[31], implying an extremely warm and humid climate.

The South Atlantic plays a key role for the global thermohaline circulation. We have reasons, therefore, to assume that the MPT phenomena documented in the SUSAS cores respond to major global paleoceanographic shifts and substantially extend constraints on mid-Pleistocene climate reconstructions.

Acknowledgements. We are grateful to W.H. Berger for helpful suggestions. This study was funded by the Deutsche Forschungsgemeinschaft (Sonderforschungsbereich 261 at Bremen University, contribution No. XXX). F.S. was supported by the Deutsche Forschungsgemeinschaft in the framework of Graduiertenkolleg 221.

1. Pisias, N.G. & Moore, T.C. The evolution of Pleistocene climate: a time series approach. *Earth Planet. Sci. Lett.* **52**, 450-458 (1981).
2. Prell, W.L. Oxygen and carbon isotope stratigraphy for the Quaternary of hole 502B: evidence for two modes of isotopic variability. *Init. Rep. DSDP* **68**, 455-464 (1982).
3. Maasch, K.A. Statistical detection of the mid-Pleistocene transition. *Clim. Dyn.* **2**, 133-143 (1988).
4. Ruddiman, W.F., Raymo, M.E., Martinson, D.G., Clement, B.M. & Backman, J. Pleistocene evolution: northern hemisphere ice sheets and North Atlantic ocean. *Paleoceanography* **4**, 353-412 (1989).
5. Berger, W.H. & Wefer, G. Klimageschichte aus Tiefseesedimenten. *Naturwissenschaften* **79**, 541-550 (1992).
6. Berger, W.H., Yasuda, M.K., Bickert, T., Wefer & G., Takayama, T. Quaternary time scale for the Ontong Java Plateau: Milankovitch template for Ocean Drilling Program Site 806. *Geology* **22**, 463-467 (1994).
7. Mudelsee, M. & Stattegger, K. Exploring the structure of the mid-Pleistocene revolution with advanced methods of time-series analysis. *Geol. Rundschau* **86**, 499-511 (1997).
8. Mudelsee, M. & Schulz, M. The mid-Pleistocene climate transition: onset of 100 ka cycle lags ice volume build-up by 280 ka. *Earth Planet. Sci. Lett.* **151**, 117-123 (1997).

9. Imbrie *et al.* On the structure and origin of major glaciation cycles: 2. The 100,000 year cycle. *Paleoceanography* **8**, 699-735 (1993).
10. Saltzman, B. & Verbitsky, M.Y. Multiple instabilities and modes of glacial rhythmicity in the Plio-Pleistocene: a general theory of late Cenozoic climatic change. *Clim. Dyn.* **9**, 1-15 (1993).
11. Berger, W.H. & Jansen, E. Mid-Pleistocene climate shift - the Nansen connection. In *The Polar Oceans and Their Role in Shaping the Global Environment* (eds. Johannessen, M., Muench, R.D. & Overland, J.E.) 295-311 (Geophys. Monogr. **85**, AGU, Washington, 1994)
12. Raymo, M.E. The timing of major climate transitions. *Paleoceanography* **12**, 577-585 (1997).
13. Paillard, D. The timing of Pleistocene glaciations from a simple multiple-state climate model. *Nature* **391**, 378-381 (1998).
14. Raymo, M.E. Glacial puzzles. *Science* **281**, 1467-1468 (1998).
15. Raymo, M.E., Oppo, D.W. & Curry, W. The mid-Pleistocene climate transition: a deep sea carbon isotopic perspective. *Paleoceanography* **12**, 546-559 (1997).
16. Robinson, S.G. Applications for whole-core magnetic susceptibility measurements of deep-sea sediments: Leg 115 results. *Proc. ODP, Sci. Res.* **115**, 737-771 (1990).
17. von Dobeneck, T. & Schmieder, F. Using rock magnetic proxy records for orbital tuning and extended time series analyses into the super- and sub-Milankovitch bands. In *Use of proxies in Paleoceanography: Examples from the South Atlantic* (eds. Fischer, G. & Wefer, G.), 601-633 (Springer Verlag, Berlin, 1999).
18. Berger, A. & Loutre, M.F. Insolation values for the climate of the last 10 million years. *Quat. Sci. Rev.* **10**, 297-317 (1991).
19. Bickert, T. & Wefer, G. Late Quaternary deep water circulation in the South Atlantic: reconstructions from carbonate dissolution and benthis stable isotopes. In *The South Atlantic: present and past circulation* (eds. Wefer, G., Berger, W.H., Siedler G. & Webb, D.J.), 599-620 (Springer Verlag, Berlin, 1996).
20. Lisitzin, A.P. Oceanic sedimentation: lithology and geochemistry. AGU, Washington D.C., 400 pp (1996).
21. Gingele, F.X., Schmieder, F., von Dobeneck, T., Petschick, R. & Rühlemann, C. Terrigenous flux in the Rio Grande Rise area during the last 1500 ka: evidence of deepwater advection or rapid response to continental rainfall patterns? *Paleoceanography*, **14**, 84-95.
22. Breitzke, M. Elastische Wellenausbreitung in marinen Sedimenten - neue Entwicklungen der Ultraschall Sedimentphysik und Sedimentechographie. *Berichte, Fachbereich Geowissenschaften, Univ. Bremen*, **104**, 298 pp (1997).
23. Adelseck, C.G. Jr. Recent and late Pleistocene sediments from the eastern equatorial Pacific Ocean: Sedimentation and dissolution. Ph.D. thesis, 192 pp, Univ. of Calif., San Diego (1977).
24. Mikkelsen, N. On the origin of *Ethmodiscus* ooze. *Mar. Micropaleontol.* **2**, 35-46 (1977).
25. Stabell, B. Variations of diatom flux in the eastern equatorial Atlantic during the last 400,000 years („METEOR" cores 13519 and 13521). *Marine Geol.* **72**, 305-323 (1986).
26. Gardner, J.V. & Burckle, L.H. Upper Pleistocene *Ethmodiscus rex* oozes from the eastern equatorial Atlantic. *Micropaleontol.* **21**, 236-242 (1975).
27. Villareal, T.A. Abundance of the giant diatom *Ethmodiscus* in the Southern Atlantic Ocean and the central Pacific gyre. *Diatom Res.* **8**, 171-177 (1993).
28. Yoder , J.A., Ackleson, S.G., Barber, R.T., Flament, P. & Balch, W.M. A line in the sea. *Nature* **371**, 689-692 (1994).
29. Bassinot, F.C., Labeyrie, L.D., Vincent, E., Quidelleur, X., Shackleton, N.J. & Lancelot, Y. The astronomical theory of climate and the age of the Brunhes-Matuyama magnetic reversal. *Earth Planet. Sci. Lett.* **126**, 91-108 (1994).
30. Rossignol-Strick, M., Paterne, M., Bassinot, F.C., Emeis, K.-C. & DeLange, G.J. An unusual mid-Pleistocene monsoon period over Africa and Asia. *Nature* **392**, 269-272 (1998).
31. Bloemendal, J., Liu, X.M. & Rolph, T.C. Correlation of the magnetic susceptibility stratigraphy of Chinese loess and the marine oxygen isotope record: chronological and palaeoclimatic implications. *Earth Planet. Sci. Lett.* **131**, 371-380 (1995).

Cycles, trends and events of Pleistocene sedimentation in the oligotrophic subtropical South Atlantic Ocean

(to be submitted to Paleoceanography)

Frank Schmieder, Tilo von Dobeneck and Ulrich Bleil

Fachbereich Geowissenschaften, Universität Bremen, 28334 Bremen, Germany

Abstract. Most investigations of the mid-Pleistocene climate transition (MPT) were based on the ice volume proxy $\delta^{18}O$. This study develops new aspects of this enigmatic period of Quaternary climate evolution from twelve subtropical South Atlantic susceptibility records reflecting carbonate dissolution cycles and hence changes in deep water chemistry. Comparative evolutionary spectra of these rock magnetic proxy records and orbital forcing imply reciprocal exchange of spectral energy between the 41 and 100 kyr bands. A MPT interim state of reduced carbonate deposition is defined from a temporal analysis of west-east-asymmetry. Presumably resulting from enhanced influence of southern source waters, this interval exactly fills the time lag between the first occurrence of larger glacial ice shields (~920 ka) and the onset of 100 kyr ice age cyclicity (~650 ka). It ends with an unusual, probably global scale paleoclimatic episode at about 530 ka, which is documented in several uncommon lithologies and interpreted as terminal MPT event.

Introduction

The South Atlantic Ocean plays a major role in the framework of global thermohaline circulation. 'North Atlantic heat piracy' (Berger and Wefer, 1996), the interglacial exchange of cold North Atlantic Deep Water (NADW) for warm surface waters from the south, is essential for today's warm climate in northern Europe. Switching on and off the Atlantic Heat Conveyor in the global ice age rhythm also modifies conditions in the deep ocean. Glacial reduction of NADW gives way for a thicker layer of Lower Circumpolar Deep Water (LCDW) in the Atlantic Ocean and lifts the NADW/LCDW boundary. Beside contrasting in temperature, salinity and nutrient concentration these two deep water masses differ in corrosiveness with respect to calcium carbonate and hence in the preservation of calcareous shells. The fluctuating NADW/LCDW lysocline leaves carbonate dissolution cycles in transition zone sediments as documentation of paleoclimatic history.

The three major submarine ridges dividing the subtropical South Atlantic into four pelagic basins are by far the best locations to find recordings of this history as they intersect the transition zone during glacial as well as interglacial times. Permanent oligotrophic conditions in this 'open ocean desert' keep the sedimentation rates as low as 0.5-1 cm/kyr. On one hand, this makes it rather difficult to build precise age models. On the other hand, gravity coring of the top 10 m of the sediment column yields continuous, nearly undisturbed records of the whole Quaternary. These sequences offer the opportunity to study not only cyclic changes but also long-term trends of Pleistocene climate evolution.

Still enigmatic within this epoch is the mid-Pleistocene transition (MPT) of the global climate system (e.g., Pisias and Moore, 1981; Prell, 1982; Ruddiman et al., 1989). In the course of the MPT, the response to orbitally driven changes in insolation received on Earth changed fundamentally. While late Pliocene to early Pleistocene paleoclimate re-

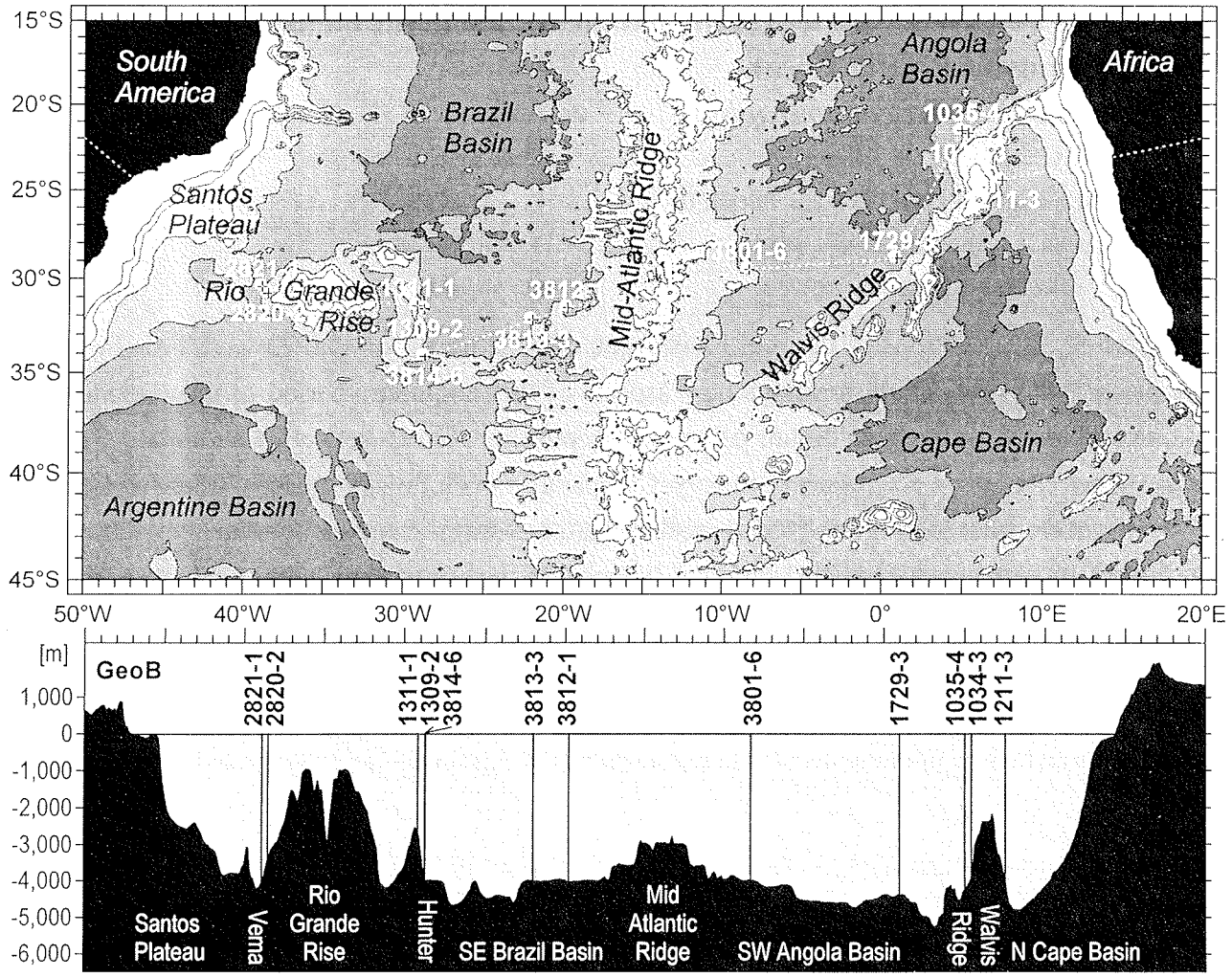

Figure 1. GeoB core locations defining the SUSAS transect. The depth profile follows the white dashed line in the map and is plotted against longitude to depict the cores' affinities to the four major pelagic basins and their deep water bodies. It is not suitable to identify the positions and depths of deep water passages.

cords exhibit mainly obliquity and precession related variance (e.g., Raymo et al., 1989; Ruddiman et al., 1989; Bloemendal and de Menocal, 1989), which can be explained as linear responses (e.g., Imbrie et al., 1992), the primary rhythm of late Pleistocene climatic change with a period near 100 kyr calls for more difficult explanations (for a summary of research and proposed models see Imbrie et al., 1993). The exact timing of the MPT and the question whether it was a gradual ('mid-Pleistocene evolution', Ruddiman et al., 1989) or a sudden change ('mid-Pleistocene revolution', Berger et al., 1994) were subject to many studies, which attempted to model or characterize the transition with different statistical techniques (e.g., Maasch, 1988; DeBlonde and Peltier, 1991; Park and Maasch, 1993; Mudelsee and Schulz, 1997; Mudelsee and Stattegger, 1997; Clark and Pollard, 1998). With few exceptions (e.g., Raymo et al., 1997) all of these investigations were based on oxygen isotope records. In our view, climate proxy records not exclusively linked to global ice volume are necessary to advance understanding of the MPT. Records of carbonate dissolution cycles in the deep South Atlantic should provide an decisive complementary perspective of this phenomenon.

In many marine environments, variations in carbonate accumulation can be precisely traced by rock magnetic methods. Here we present twelve high-resolution magnetic susceptibility time series of

Core	METEOR expedition	Water depth (m)	Position		Core length (m)	Cruise report
			Latitude	Longitude		
GeoB 1034-3	M6/6	3772	21°44.1'S	05°25.3'E	10.65	Wefer et al. (1988)
GeoB 1035-4	M6/6	4453	21°35.2'S	05°01.7'E	10.61	Wefer et al. (1988)
GeoB 1211-3	M12/1	4084	24°28.5'S	07°32.0'E	8.61	Wefer et al. (1990)
GeoB 1309-2	M15/2	3963	31°40.0'S	28°40.0'W	9.48	Pätzold et al. (1993)
GeoB 1311-1	M15/2	2901	31°30.7'S	29°05.9'W	7.42	Pätzold et al. (1993)
GeoB 1729-3	M20/2	4401	28°53.6'S	01°00.1'E	7.45	Schulz et al. (1992)
GeoB 2820-2	M29/2	3615	30°49.4'S	38°26.4'W	7.67	Bleil et al. (1994)
GeoB 2821-1	M29/2	3941	30°27.1'S	38°48.9'W	8.19	Bleil et al. (1994)
GeoB 3801-6	M34/3	4546	29°30.7'S	08°18.3'W	9.37	Wefer et al. (1996)
GeoB 3812-1	M34/3	4205	31°36.9'S	19°45.5'W	5.32	Wefer et al. (1996)
GeoB 3813-3	M34/3	4331	32°16.1'S	21°58.0'W	9.83	Wefer et al. (1996)
GeoB 3814-6	M34/3	4340	34°11.0'S	28°38.0'W	7.95	Wefer et al. (1996)

Table 1. Water depths, positions and core lengths of the GeoB gravity cores presented in this paper.

Pleistocene sediment cores from the subtropical South Atlantic.

Material and Methods

The cores were chosen from material recovered during six expeditions with R.V. METEOR in the framework of a long-term paleoceanographic research program (SFB 261 at the University of Bremen). This core selection covers the time range of the MPT and forms a transect across the entire deep South Atlantic Ocean between 20°S and 35°S (Figure 1). Table 1 summarizes positions, water depths and core lengths. With the exception of GeoB 1311-1, which was recovered from 2901 m, all cores are located within the broad transition zone between NADW and LCDW during glacial as well as interglacial times.

The westernmost cores GeoB 2820-2 and 2821-1 are located on the east side of the Vema Channel, the predominant of two LCDW deep water passages. Cores GeoB 1309-2, 1311-1 and 3814-6 lay on the eastern flank of the Rio Grande Rise in the vicinity of the Hunter Channel, GeoB 3812-1 and 3813-3 on the western slope of the Mid-Atlantic Ridge. As the flow of corrosive LCDW into the Angola basin is to some extent restricted by surrounding ridges, especially during interglacials (e.g., Bickert and Wefer, 1996), sedimentation there is less affected by dissolution and sedimentation rates are somewhat higher. While GeoB 1034-3 and 1729-3 from the northern and 1211-1 from the southern flank of the Walvis Ridge reach back to 1200 ka, GeoB 1035-4 and 3801-6 do not reach the Brunhes/Matuyama boundary. They were selected for this study as they contribute detailed records of the last about 500 kyr and additionally document a paleoceanographic event discussed later.

The pelagic carbonate sediments mainly consist of nannofossil ooze with varying amounts of foraminifera. Five cores were disturbed by one or two, GeoB 3801-6 by five thin turbidites. Susceptibility signal correlations showed that simply removing the turbidites from the sequence results in complete time series, only in GeoB 3812-1 a record section was lost. Siliceous fossils are generally negligible in the sediments, but two cores contain an enormous diatom ooze layer. In GeoB 3813-3 this layer is 38 cm thick, in GeoB 3801-6 even 124 cm. As in the case of the turbidites, removal of the diatom layers results in complete, correlatable susceptibility records. Obviously, these layers have been deposited in relatively short time.

Paleomagnetic analyses were performed at 5-10 cm sampling intervals. Natural remanent mag-

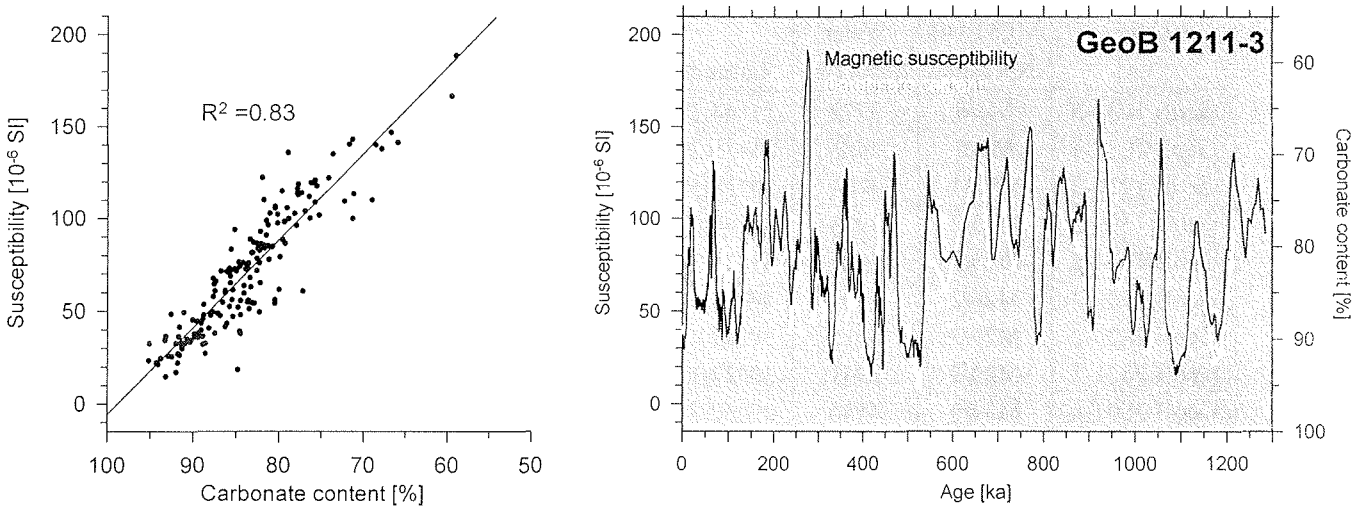

Figure 2. Comparision of magnetic susceptibility and carbonate content (T.Bickert, 1992) for core GeoB 1211-3. For the cross-plot on the left side susceptibility data were reduced to the 5 cm sampling intervall of the carbonte data. The inverse correlation is very close in all period ranges, long-term trends and Milankovitch cycles are well reproduced. Due to higher resolution, high-frequent signal features are expressed in more detail in magnetic susceptiblity.

netization was measured using a three-axis cryogenic magnetometer (Cryogenic Consultants GM 400) and statically AF demagnetized in ten steps up to 100 mT (2G demagnetizer). The direction of the characteristic remanent magnetization (ChRM) was calculated by averaging over at least three successive demagnetization steps.

Magnetic volume susceptibility κ was measured on the archive halves of the cores at a 1-cm spacing using a Bartington Instruments M.S.2.F spot sensor. The suceptometer was operated in the sensitive range and each measurement corrected with a separate background reading.

In most marine sediments susceptibility primarily quantifies magnetite content (Thompson and Oldfield, 1986), which is generally part of the terrigenous input, although it may occasionally be supplemented by bacterial magnetite (Petersen et al., 1986, Vali et al., 1987). The susceptibility signal of marine sediment series frequently reflects the ratio of biogenic and lithogenic components (Robinson, 1990), which may vary due to changes in terrigenous input, carbonate production and dissolution, or a combination of these often climatically controlled mechanisms. Susceptibility records have been regionally established as excellent paleoclimatic proxies (e.g., Mead et al., 1986; Bloemendal et al., 1988; Bloemendal and de Menocal, 1989; Park et al., 1993; Robinson et al., 1995; Chi and Mienert, 1996).

If magnetic susceptibility is interpreted as inverse carbonate proxy, all potential exceptions like sand and ash layers or sections affected by reductive diagenesis must be excluded (e.g., Bloemendal et al., 1989; Frederichs et al., 1999a). Except for the earlier mentioned turbidites, there is no indication of such effects in any of the twelve cores. Their magnetic susceptibility records reflect variations in carbonate content as the comparison of magnetic susceptibility and $\%CaCO_3$ (Bickert, 1992) records of GeoB 1211-3 show (Figure 2). The inverse correlation of susceptibility and carbonate content is very close in all period ranges. Long-term trends, Milankovitch cycles and high-frequent signal features are well reproduced, although comparison of the latter is restricted due to the much lower resolution of the $\%CaCO_3$ record (5 cm spacing). Only in isotope stage 14 at about 550 ka considerable differences appear. The extrapolated end-member values for 100% and 0% carbonate are $-5.6 \cdot 10^{-6}$ SI units

and 464.1·10^{-6} SI units, respectively. The susceptibility of pure diamagnetic calcite, -15·10^{-6} SI units (Thompson and Oldfield, 1986), is the theoretical absolute minimum and logical origin of the susceptibility axis.

As mentioned above, the three factors governing the carbonate content of marine sediments are productivity fluctuations of calcareous organisms, dilution by terrigenous material, and calcium carbonate dissolution. Volat et al. (1980) analyzed Pleistocene sediments in the Pacific, Indian, and Atlantic Ocean and concluded that dissolution is the most important factor influencing carbonate content in all three oceans. Johnson et al. (1977) found carbonate cycles in late Pleistocene sediments recovered in the Vema Channel and on the lower flanks of the Rio Grande Rise at water depths between 2900 and 4000 m. They evaluated the extent to which these cycles may be dissolution controlled by comparing carbonate content data and a semi-quantitative measure of dissolution. Finding a strong correlation between low carbonate content and a high dissolution index they interpret the variations in carbonate content as dissolution cycles.

While in the South Atlantic carbonate dilution by varying terrigenous sedimentation is important near coasts and in regions of enhanced fluvial and eolian sedimentation, it diminishes with distance from the continents (Schmidt et al., submitted). In spite of the fact, that terrigenous input is much greater in the western than in the eastern South Atlantic (Lisitzin, 1996), even our westernmost core GeoB 2821-1 consists primarily (70±9 %) of $CaCO_3$ (P. Müller, unpublished data). Varying terrigenous input certainly effects the susceptibility signals to some extent, but carbonate dissolution by alternating influence of NADW and more corrosive LCDW is believed to be the main cause of signal variance in the records presented here.

Chronostratigraphy

Magnetostratigraphies of GeoB 1034-3 and 1211-3 were established by Thiessen (1993) and for all other cores by von Dobeneck and Schmieder (1999). Except for GeoB 1035-4 and 3801-6 all cores reach the Brunhes/Matuyama boundary (780 ka) and the Jaramillo Event (990-1070 ka). In three cases the short Cobb Mountain Event (1190 ka) was detected despite low sedimentation rates. Oxygen isotope records exist for GeoB 1034-3, 1035-4, 1211-3 (Bickert, 1992; Bickert and Wefer, 1996) and 1309-2 (W. Hale, personal communication). Their stratigraphic interpretability is limited by very low sedimentation rates, particularly in the deeper, obliquity-dominated sections. By interpolating between the magnetostratigraphic tie points, spectral characteristics of Milankovitch cyclicity become apparent in the susceptibility logs. These initial spectra display significant maxima at around 100 and 40 kyr, but show little or no indications of a precessional signal component (von Dobeneck and Schmieder, 1999).

A pattern matching to standard $\delta^{18}O$ records, e.g. from equatorial Pacific ODP Site 677 (Shackleton et al., 1990) was feasible over most signal sections, but remained ambiguous between oxygen isotope stages 16 and 13 between about 650 and 500 ka. Continuously high similarities, including long-term fluctuations of about 500 kyr duration, exist between all susceptibility signals and the benthic $\delta^{13}C$ record at Pacific ODP site 806 (T. Bickert, unpublished data) based on an orbitally tuned $\delta^{18}O$ stratigraphy (Berger et al., 1994). The complete and undisturbed susceptibility record of core GeoB 3814-6 (Figure 3b) correlates particularly well and helped to substantiate the other eleven matches.

The most widely used orbital tuning procedure assumes a phase lock between climate and metronome record (Martinson et al., 1987). In order to assess the absolute lag of any proxy record with

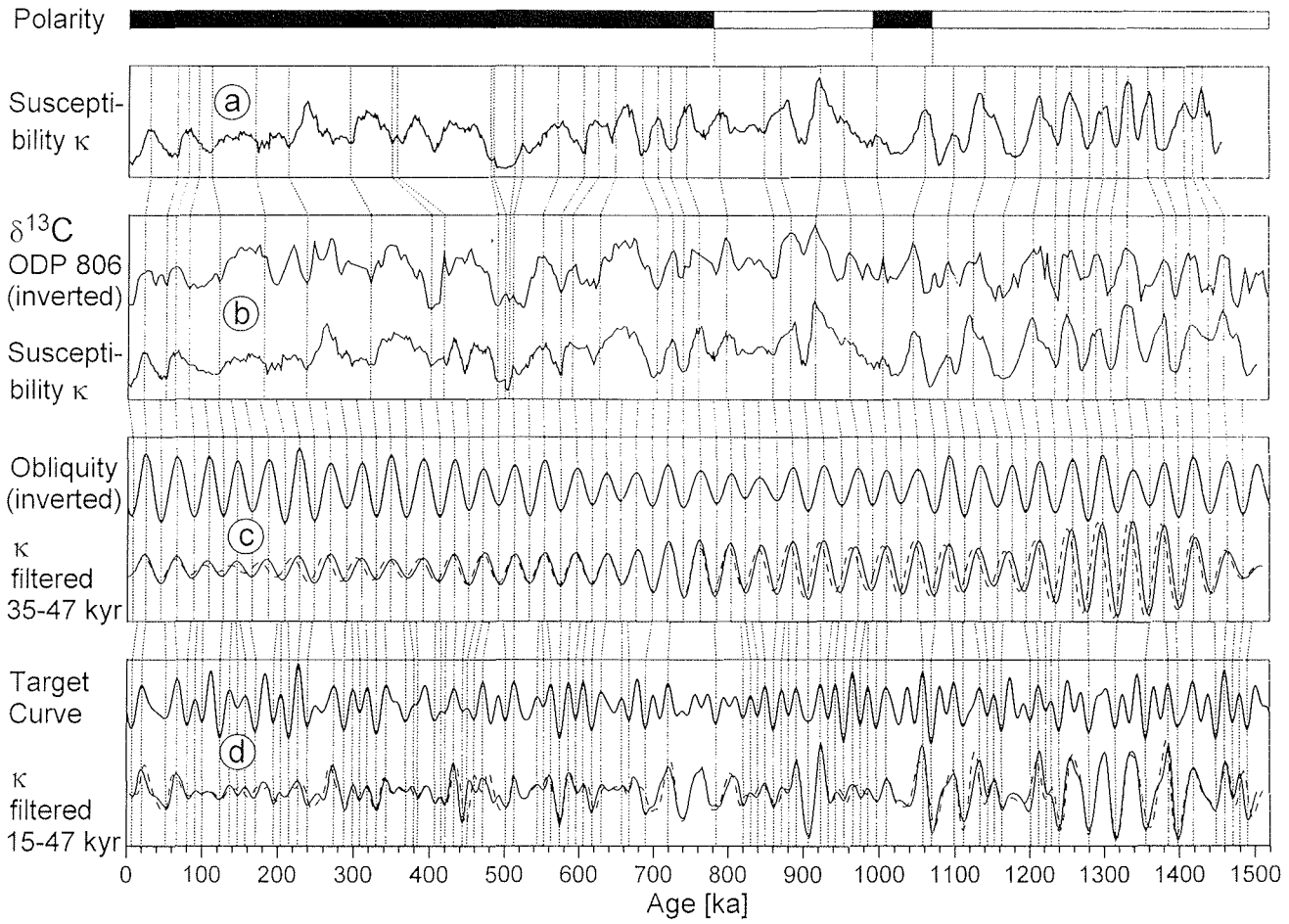

Figure 3. Four step refinement of the age model for core GeoB 3814-6. **(a)** Susceptibility record dated by magnetostratigraphy (3 tie points). **(b)** Signal pattern correlation to the tuned $\delta^{13}C$ record of ODP Site 806 (T. Bickert, unpubl. data, 44 tie points). In critical intervals other SUSAS records were inspected for supplementary information **(c)** Susceptibility filtered (35-47 kyr) in the obliquity range (dashed line) and tuned (solid line) to an astronomical obliquity signal shifted by -4.5 kyr (73 tie points). **(d)** Susceptibility filtered (15-47 kyr) and tuned to an astronomical (obliquity and precession) target curve (95 tie points).

respect to astronomical obliquity and precession, an independent and precise absolute chronology is required. $\delta^{18}O$ phase lags have been determined on basis of radiometric ages (Hays et al., 1976: 9 kyr for obliquity, 3 kyr for precession) and assumptions on the coupling of insolation and ice mass (Imbrie et al., 1984: 7.9 (7.4-8.2) kyr for obliquity, 5.0 (4.8-5.1) kyr and 4.2 (4.1-4.3) kyr for precession). To estimate orbital phase lags for regional proxy parameters such as susceptibility it is therefore sufficient to know the phase lags relative to a $\delta^{18}O$ curve from the same core.

Here we use a revised $\delta^{18}O$ time scale of core GeoB 1211-3 (Bickert, 1992) based on a correlation to the SPECMAP stack (Imbrie et al., 1984). Cross spectral analysis of $\delta^{18}O$ and κ yields a coherence of 0.99 and 0.96 for the 100 kyr and 41 kyr cycles and reasonable phase angles of -41° and -30°. This implies that susceptibility leads $\delta^{18}O$ by 3.4 kyr in the obliquity band and therefore lags the obliquity forcing function by 7.9 kyr-3.4 kyr=4.5 kyr and is in good agreement with Imbrie et al.'s (1993) values calculated for early proxy responses in the southern hemisphere. The temporal resolution of the $\delta^{18}O$ record was too low to determine the precessional phase lags within acceptable error margins.

The subsequent orbital tuning process was performed in two stages. At first the obliquity-related signal component was extracted applying a 1st order butterworth bandpass (35-47 kyr) filter in forward and reverse direction. Each maximum and minimum in the filtered signal was assigned the age (+4.5 kyr)

of its postulated equivalent in the astronomical record (Berger and Loutre, 1991), starting from the most uncritical sections near magnetostratigraphic or other reliable tie points. As illustrated in Figure 3c, changes in the correlation age model are small, typically less than a half-cycle of obliquity. The second tuning step proceeds from the observation that faintly visible precessional peaks in the spectra gradually sharpened at both refinements of the age model (von Dobeneck and Schmieder, 1999). To benefit from this precessional signal component, a target curve of normalized obliquity and precession index (mixing ratio of 2:3 chosen by visual evaluation) and 4.5 kyr lag was calculated, comprising not just more, but also more prominent signal features than either single orbital parameter. The obliquity-tuned primary susceptibility record was filtered using a wide bandpass (15-47 kyr) to include obliquity and precession cycles. As many extrema as possible were matched (Figure 3d), admittedly at the resolution limit of these records. The resulting final age models are again just slight modifications of the previous models and possibly not even more precise in absolute ages as the precession time lag is undetermined. Nevertheless, this higher-frequency tuning leads to a better mutual signal correlation of the twelve records.

Results and Discussion

Figures 4 and 5 summarize the combined results of magnetic age modeling for the complete transect. Resulting sedimentation rates are fairly constant over time. A few question marks remain in core sections, where individual signal features seem to be missing or incomplete (e.g., GeoB 1311-1 at 420 ka, GeoB 2820-2 at 800 ka). The high conformity of all records led us to compute the SUSAS (Subtropical South Atlantic Susceptibility) stack, which is free of local effects and therefore representative for the whole Quaternary oligotrophic

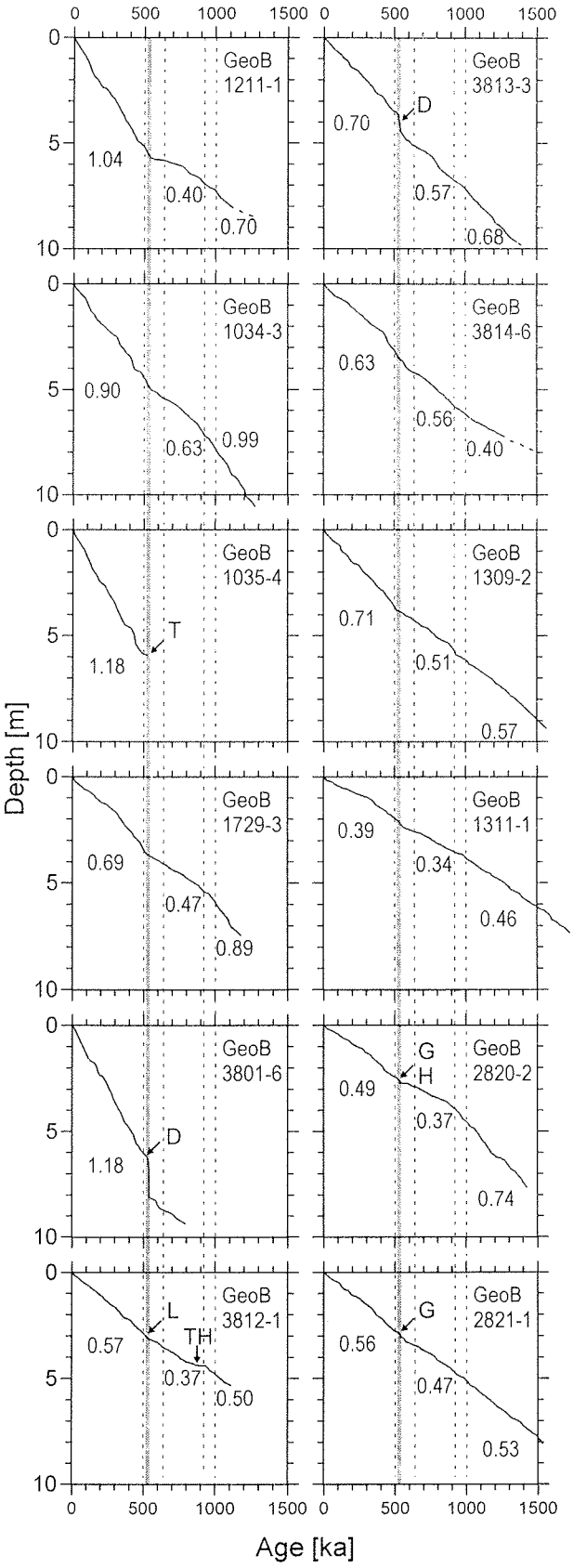

Figure 4. Age depth relation of all SUSAS cores. Sedimentation rates are generally fairly constant. Dashed lines mark the MPT interim state, bounded by two transitions. During this interval sedimentation decreased. The grey vertical bar denotes the time of a terminal MPT event indicated by unusual lithologies in several SUSAS cores (for abreviations see Figure 5).

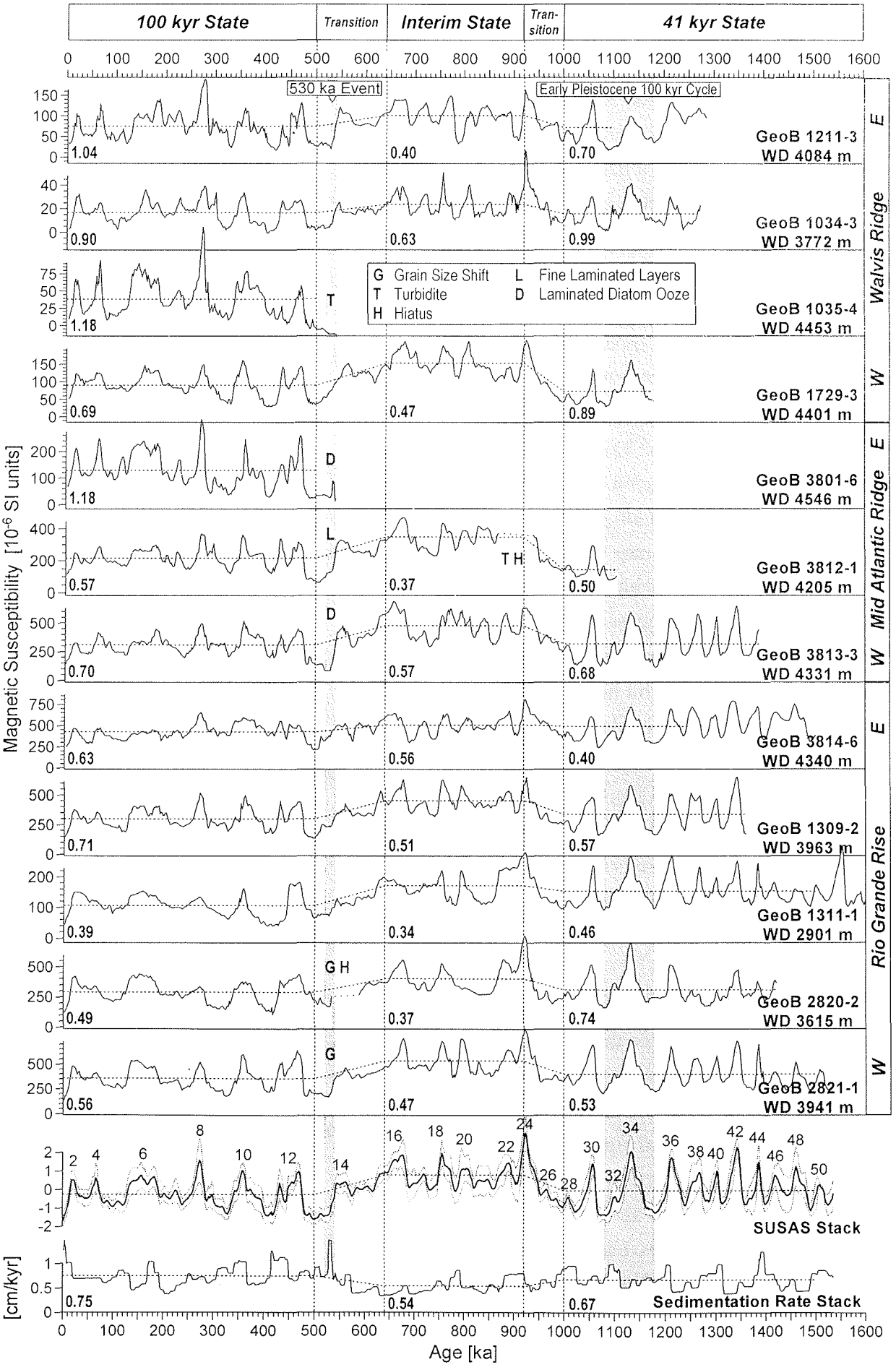
100 kyr State
Transition
Interim State
Tran-sition
41 kyr State
530 ka Event
Early Pleistocene 100 kyr Cycle
G Grain Size Shift
T Turbidite
H Hiatus
L Fine Laminated Layers
D Laminated Diatom Ooze
GeoB 1211-3 WD 4084 m
GeoB 1034-3 WD 3772 m
GeoB 1035-4 WD 4453 m
GeoB 1729-3 WD 4401 m
GeoB 3801-6 WD 4546 m
GeoB 3812-1 WD 4205 m
GeoB 3813-3 WD 4331 m
GeoB 3814-6 WD 4340 m
GeoB 1309-2 WD 3963 m
GeoB 1311-1 WD 2901 m
GeoB 2820-2 WD 3615 m
GeoB 2821-1 WD 3941 m
Walvis Ridge
Mid Atlantic Ridge
Rio Grande Rise
E
W
Magnetic Susceptibility [10-6 SI units]
SUSAS Stack
Sedimentation Rate Stack
[cm/kyr]
Age [ka]

deep South Atlantic Ocean. Because of different amplitude ranges, the stack was determined as an arithmetic mean of normalized (subtraction of core mean and division by standard deviation), interpolated (Δt = 2 kyr) records.

Some important features of the SUSAS series discussed in the following are visible by closer visual inspection of Figure 4:

- an east-west trend of increasing average magnetic susceptibilities,
- changing signal cyclicities during the Pleistocene with particularly uniform patterns during the early (41 kyr state) and late Pleistocene (100 kyr state),
- a shift towards enhanced magnetic susceptibilities and reduced sedimentation rates during the intermediate time interval,
- the premature occurrence of a near-100 kyr cycle at about 1150 ka,
- a paleoceanographic event at about 530 ka documented in unusual lithologies in several SUSAS cores.

Adapted statistical analysis must be applied to gain insight into these phenomena and their interrelations.

Figure 5. (opposite) Individually tuned SUSAS records (WD = Water Depth) and resulting susceptibility (arithmetic mean with standard deviation band) and sedimentation rate stack. A diamagnetic susceptibility of -15×10^{-6} SI units representing pure carbonate sediment was chosen as axis minimum. To compensate for different signal levels in the stacking, each record was normalized by subtracting its mean and dividing by its standard deviation. Labels at the SUSAS stack indicate even oxygen isotope stages. Horizontal dotted lines mark baseline averages for pre-, syn- and post-MPT states excluding the bounding transitions. During the interim state, all cores display increased susceptibilities and reduced sedimentation rates. The timing of the three intervals approximately corresponds to the Laplace (1800-1200 ka), Croll (1200-600 ka) and Milankovitch chron (600-0 ka) defined by Berger and Wefer (1992). Numbers in each section denote mean sedimentation rates; grey vertical bars a premature 100 kyr cycle centred near 1150 ka and a terminal MPT event featuring unusual lithologies at about 530 ka.

Cycles

Evolutionary spectral analysis is an excellent method to visualize the variability of cyclic climate characteristics in a record through time, either presented as a sectionalized analysis (e.g., Pestiaux and Berger, 1984; Bloemendal and deMenocal, 1989; Mwenifumbo and Blangy, 1991; Tiedemann et al., 1994; Berger and Jansen, 1994) or in the form of 'spectrograms' (e.g., Joyce et al., 1990; Yiou et al., 1991; Birchfield and Ghil, 1993; Grützner et al., 1997; Harris et al., 1997; Paillard, 1998). These three-dimensional diagrams result from spectra generated within a moving window and thus combine frequency and time domain. The SPECGRAM algorithm embedded in the MATLAB Signal Processing Toolbox was used to calculate the spectrograms in Figure 6. For all time series analyzed a 500 kyr frame was advanced at 10 kyr steps and, in order to minimize cut-off effects, tapered with a Hanning window, thereby focusing to the central section at each step. Long-term trends (periods >350 kyr) were previously removed by highpass filtering to minimize disturbance by this signal component. The resulting data matrix was normalized to an average spectral density of 1 by dividing all values by the total matrix mean. This procedure merely scales all spectrograms uniformly and enables their comparison, but does not alter relative variations in the time or frequency domain. As a consequence of the window length used no spectra could be calculated for the first and the last 250 kyr of the record. In order to avoid loss of information on the early Pleistocene the SUSAS stack was extended beyond the age of 1530 ka by the normalized signal of GeoB 1311-1 which reaches back to 1730 ka (Figure 4).

In the resulting spectrogram (Figure 6c) the precession related signal is poorly documented due to bioturbation damping with the exception of sections of relatively higher sedimentation rates and

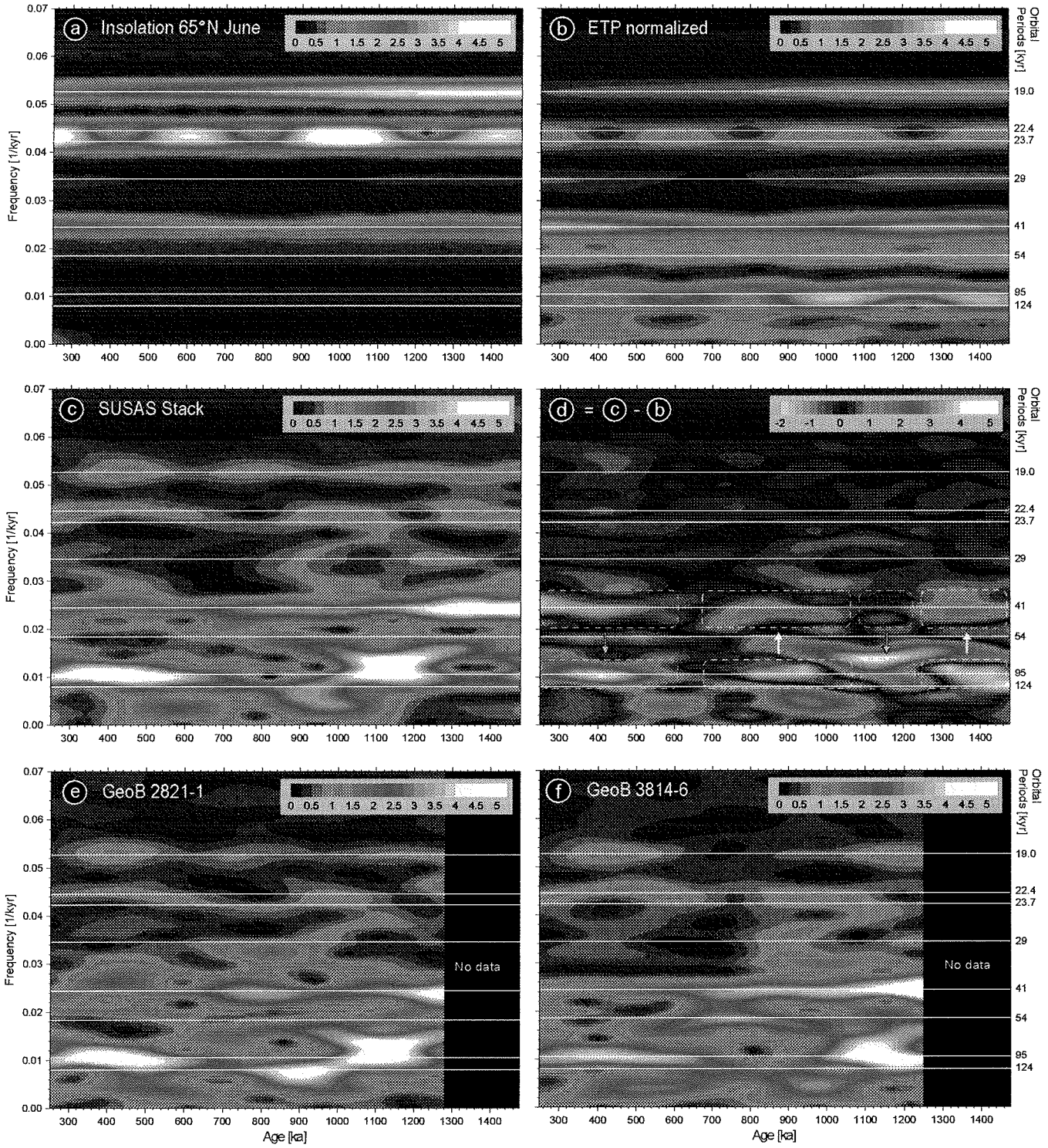

Figure 6. Evolutionary spectral analysis of driving and responding climate variables. The spectrograms were calculated by advancing a tapered (Hanning window) 500 kyr frame at 10 kyr steps. All records were previously highpass filtered (< 350 kyr) to minimize disturbance by low-frequency signal components. **(a)** Mid-month insolation at 65°N for July (Berger and Loutre, 1991), **(b)** ETP curve, calculated from eccentricity, obliquity and precession by calibrating the cumulative spectral intensity in each band to equal that of **(c),** the SUSAS spectrogram. **(d)** For a comparison of forcing and response the numerical difference of (c) and (b) was calculated. In general, spectrograms of core GeoB 2821-1**(e)** and GeoB 3814-6 **(f)** display a good overall correlation to each other and the SUSAS stack (c), slight deviations occur during the MPT interim state.

enhanced forcing (e.g., prior to 900 ka). The influence of obliquity on the SUSAS stack diminishes continuously with a major decrease near 1200 ka and a second, somewhat less enhanced reduction at about 700 ka. Near 100 kyr periods clearly dominate the signal in late Pleistocene since 650 ka, but also give important contributions to older sections, particularly expressed between 1250 and 1050 ka. In this time range strong spectral components between the obliquity and the eccentricity band emerge. At about 1150 ka they fuse with near 100 kyr cyclicity into a broad maximum. This merging is a result of the compromise between time and frequency resolution. A conventional sectionalized spectral analysis with a longer time window (1530-920 ka) separates a component with a period of about 70 kyr (Figure 7, top). Anomalous spectral peaks near 70 kyr have been reported from Pleistocene paleoclimate records of the North Atlantic (e.g., Ruddiman et al., 1989), the Indian (e.g., Robinson, 1990), and the Pacific Ocean (e.g., Bassinot et al., 1994a), but few attempts have been made to explain their origin. Considering the simultaneous presence of strong variance in the 100 and the 41 kyr band in the SUSAS record (Figure 5, top and 7c), a nonlinear interference of these two frequencies (1/41-1/100=1/69), previously discussed by Robinson (1990) and Muller and Mac Donald (1997), is a plausible explanation. A simple nonlinear model of sea-level change produces a spectral peak near 72 kyr beside moving energy from the orbital forcing bands into the approximately 100 kyr band (Berger et al., 1996). Similar to our results Mudelsee and Stattegger (1997) identified high 100 and 41 kyr amplitudes in the benthic oxygen isotope records of ODP sites 607 and 659 in the time period around 1200 ka. They hypothesize that this interval of generally stronger climate fluctuations was 'a first but unsuccessful "attempt" of the climate system to attain a nonlinear "late Pleistocene ice ages" state'. Our spectrogram analysis strongly supports this assumption.

The evolution of the 100 and 41 kyr cycle documented in the SUSAS spectrogram matches in great detail the results of statistical analysis of benthic oxygen isotopes of DSDP site 607 and ODP sites 659 and 677 (Park and Maasch, 1993; Mudelsee and Stattegger, 1997): strongest Pleistocene 41 kyr amplitudes between 1400-1200 ka and nearly constant values since about 1100 ka as well as increasing 100 kyr cycles at about 650 ka and enhanced values between 1200 and 1000 ka. Despite some deviations the impressive correlation of our analysis and the calculations made for benthic $\delta^{18}O$ time series from the midlatitude North Atlantic (DSDP 607, ODP 659), and the equatorial Pacific (ODP 677) suggests a global character of the change from 41 to 100 kyr cyclicity. Evidently the cyclic variations of the SUSAS stack are closely linked to global ice volume via changes in deep water chemistry.

How is the observed evolution of the cyclicity related to the driving orbital fluctuations? In Figure 6a-d spectrograms of forcing and responding variables are compared. The mid-summer insolation signal at 65°N (Figure 6a, Berger and Loutre, 1991) and a normalized ETP curve (Figure 6b) are shown as reference. ETP curves are artificial, but often employed target records composed by calibrating and adding the time series of Eccentricity, Tilt (obliquity) and Precession (Imbrie et al., 1984). Here, the cumulative spectral intensity in each band of the ETP spectrogram was calibrated to equal that of the SUSAS spectrogram. Being based on the same orbital variations, both reference signals exhibit identical amplitude modulation patterns, but very different spectral power in each band. In the eccentricity band this difference amounts to several orders of magnitude - an expression of the 100 kyr cycle problem (Imbrie et al., 1993).

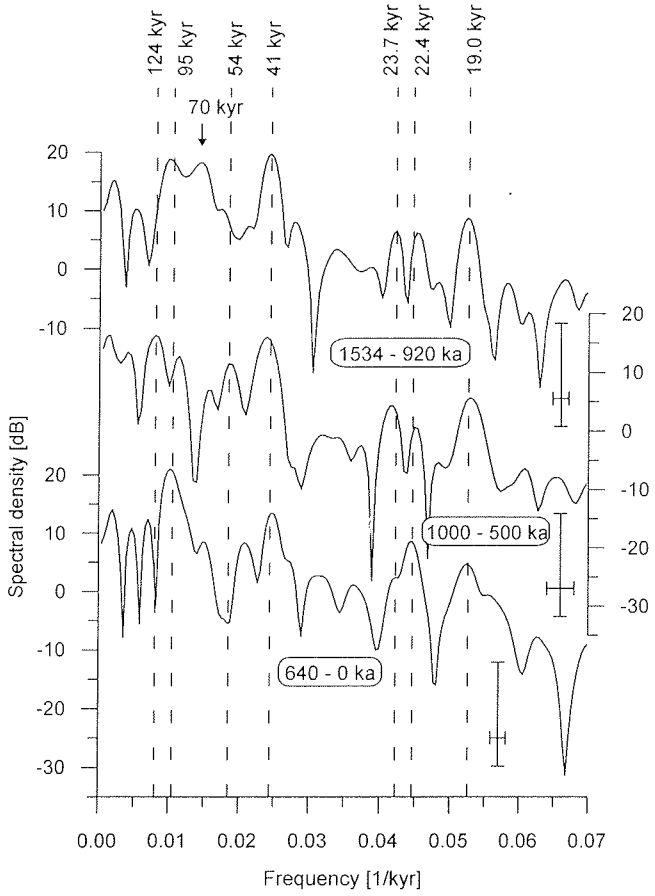

Figure 7. Spectral analysis of the SUSAS stack for the three Pleistocene states defined in Figure 5.

The numerical difference between the spectrograms of the SUSAS stack and the ETP curve is displayed in Figure 6d. With restrictions due to the overall low variability in the 19 and 23 kyr bands, the assumption of a constant proxy response appears justified for precession, as both records largely compensate throughout the whole record. This hypothesis can also be drawn from simple visual comparison of Figures 6a and c. The reduced 23 kyr maximum centered at 600 ka and enhanced values in the 19 kyr band near 400 ka may result from the influence of different sedimentation rates (Figure 4) on the definition of these high-frequency cycles.

41 kyr cyclicity is less affected by bioturbation damping (von Dobeneck and Schmieder, 1999). Yet, residues in the obliquity band show a more variable, non-stationary response to forcing (Figure 6d). The spectral intensity decline at 1200 to 1100 ka (Figure 6c) may result from the simultaneous decrease in obliquity although the gradient is steeper as in Figures 6a, b. The reduction near 700 to 600 ka and the subsequently low amplitudes during the entire late Quaternary however do not mirror the evolution of the forcing signal. Quite the reverse, obliquity amplitudes increase again during the late Pleistocene (Figure 6a, b) and thus produce negative residues (Figure 6d). Obviously the ability of obliquity to drive the observed carbonate dissolution cycles decreased during Pleistocene times and remained low since the onset of 100 kyr cyclicity at about 650 ka. This finding is in accordance with the suggestion of Ruddiman et al. (1989) and Joyce et al. (1990) that the climatic system was less sensitive to obliquity forcing during the late Pleistocene and as well with the results of Imbrie (1992) who found, that response in the obliquity band was fairly constant over the past half-million years.

The coincidence of target and proxy records in the 100 kyr band is even lower, as indicated by larger residues and steeper gradients. While the ETP model looses 100 kyr power in the late Pleistocene (Figure 6b), the SUSAS stack, like most climate records, documents an intensification resulting in a positive residue. The preceding residue maximum originates from the early Pleistocene 100 kyr cycle near 1150 ka. Two low-frequency positive maxima centered at 950 and 600 ka in the SUSAS and the residual spectrogram (Figure 6c, d) result from remainders of the earlier mentioned base line transitions of the long-term susceptibility trend (Figure 5).

The most striking result of the residual spectrogram is the reciprocity of spectral intensities in the 41 and 100 kyr bands (dashed outlines in Figure 6d). In relation to the ETP model, the SUSAS 100 kyr cyclicity develops over-proportionally in sections with reduced response to obliquity (blue outline) and retreats, where the response to obliquity is strong (yellow outline). These findings imply an exchange of spectral energy between the obliquity

and eccentricity band. A possible explanation is provided by climate models invoking a changing insolation threshold (e.g., Saltzman and Verbitsky, 1993; Raymo, 1997; Paillard, 1998). Intensified northern hemisphere summer insolation capable of triggering major deglaciations hence should result from an interference of obliquity maxima with precession index minima. At times, when the insolation threshold is relatively low, obliquity maxima alone will trigger the withdrawal of continental ice shields and 41 kyr cyclicity prevails. When the insolation threshold is higher, the required peak insolation is only reached by optimum interaction of obliquity and precession. As the precession amplitude is modulated by eccentricity, sufficiently large precessional peaks occur only during 100 kyr eccentricity maxima suppressing obliquity and causing the observed 100 kyr climate cycles. While a linearly increasing threshold (e.g., Raymo, 1997; Paillard, 1998; Raymo, 1998) results in a single transition from 41 to 100 kyr predominance, a slightly fluctuating threshold should also be capable to explain the 100 kyr excursion near 1150 ka.

The good overall correlation of all records discussed in the time domain is also visible in the synchronous time-frequency view of individual spectrograms. Slight deviations in the spectrograms of cores GeoB 2821-1 and 3814-6 possibly relate to local effects (Figure 6e, f) and are concentrated in the MPT interim state, where both records exhibit higher variance in the obliquity band than the stack. In GeoB 3814-6 this response includes a strong 54 kyr component, which is also visible in GeoB 1211-3 (not shown) and in the spectrum of the corresponding SUSAS stack section (Figure 7, center). In both cores this subordinate obliquity cycle amplitude reaches values comparable to the 41 kyr cycle although the latter, summarizing four major terms, contributes six times as much to astronomical obliquity variation (e.g., Berger and Loutre, 1992). The mid-Pleistocene increase in response to obliquity is even more puzzling as it precisely coincides with a time of reduced amplitudes in the forcing function (Figure 6a, b). The three diverging cores were recovered from southern ridge slopes or deep water passages (Figure 1) and are thus more intensely influenced by southern source waters. The influence of obliquity-dominated high latitude climate forcing was possibly intensified during the MPT interim state.

The evolutionary spectral analysis of the SUSAS stack documents a continuous Pleistocene decline of 41 kyr cyclicity, but a comparatively abrupt intensification of 100 kyr cyclicity after about 650 ka. Oxygen isotope records indicate larger ice shields since the beginning of the MPT interim state at 920 ka (e.g., Berger and Jansen, 1994). Why did 100 kyr cyclicity lag the initial ice volume increase by approximately 280 kyr (Mudelsee and Schulz, 1997)? The observed baseline shift in the SUSAS records (Figure 5) precisely fills this time lag and should shed light on this question.

Trends

A prominent feature of the SUSAS stack and all individual records summarized in Figure 5 is a baseline shift towards 40% higher average susceptibilities during the MPT interim state (920 to 640 ka). Confined by transitional intervals lasting about 80 and 140 kyr at its onset and termination, this period exhibits the most distinct dissimilarities between individual core logs. The preceding and following climate states show similar mean susceptibilities modulated by clearly developed and coherent 41 and 100 kyr cycles, respectively. An exception is the 'premature' near-100 kyr cycle at around 1150 ka discussed above. The MPT susceptibility shift is notably mirrored in lowered average sedimentation rates (Figure 5, bottom).

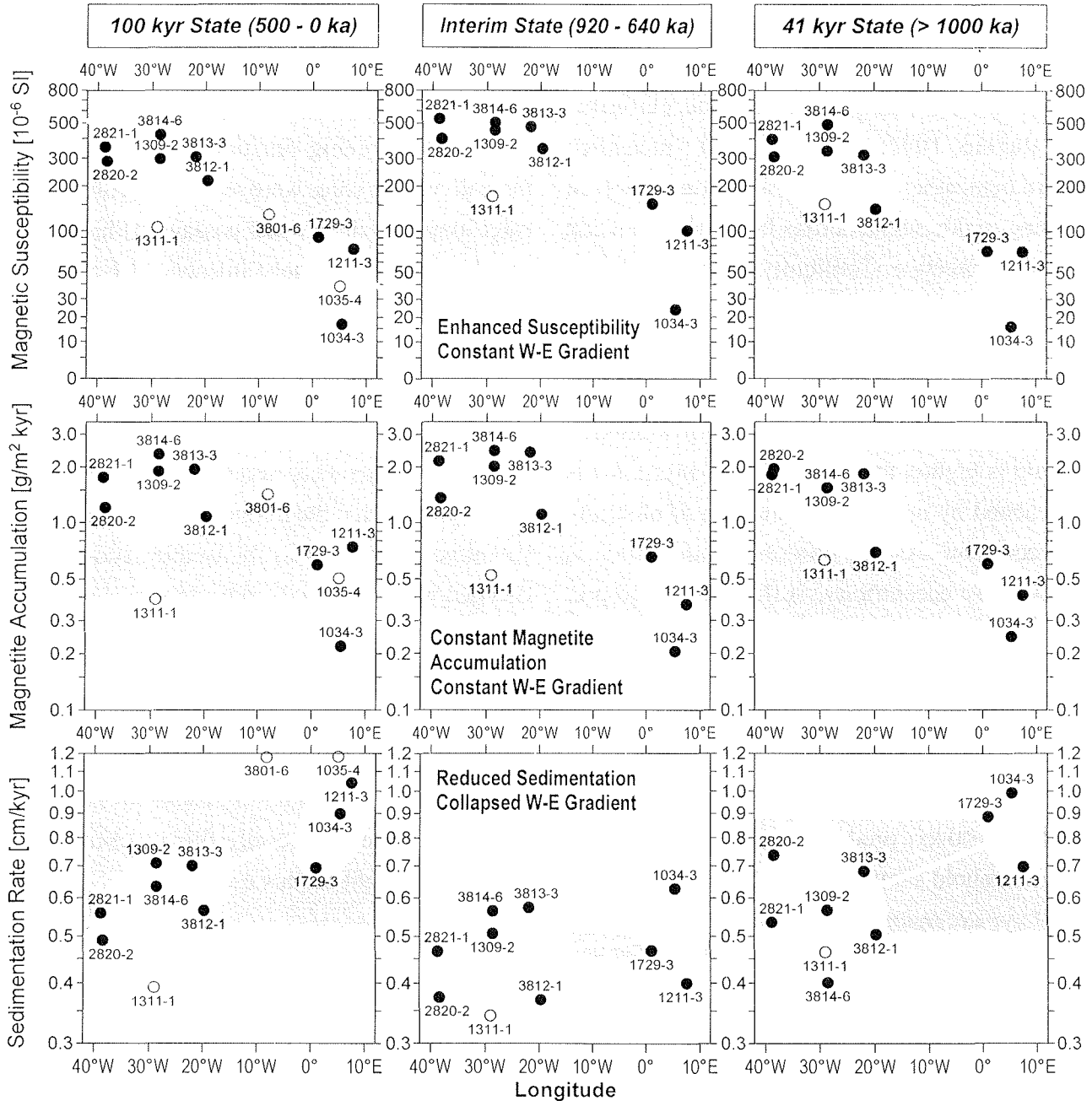

Figure 8. Combined spatial and temporal trend analyses of magnetic susceptibility, magnetite accumulation (calculated by splitting susceptibility into a diamagnetic background and ferrimagnetic, grain-size independent magnetite signal) and sedimentation rate. Major asymmetries and shifts are summarized by white regression lines, dark-gray shading delimits mean data range, light-gray shading western and eastern South Atlantic core sets. Three cores were excluded from the analysis: cores GeoB 1035-4 and 3801-6, as they do not reach beyond the 530 ka event, and core GeoB 1311-1 recovered from 2901 m water depth clearly above the LCDW/NADW transition zone and therefore showing a somewhat different evolution.

The cause for the overall rise in magnetic susceptibility during the MPT interim state is revealed by a temporal analysis of west-east trends. Plotted against longitude, core mean susceptibilities for the postulated three climate states (Figure 8 top) reflect the well-known west-east asymmetry of terrigenous particle flux and accumulation in the South Atlantic (e.g., Balsam and McCoy, 1987; Lisitzin, 1996). While the gradients are almost identical throughout Pleistocene, a shift to higher susceptibilities is evident during the MPT interim state. This relative increase of magnetic mineral concentration cannot be explained in terms of temporal changes in magnetite accumulation (Figure 8 center), as its west-east decline from 2.5 to 0.3 g/m²kyr remains fairly constant over time. A time-varying dilution of the terrigenous

fraction by non-magnetic carbonate must therefore be responsible for the observed shift.

Mean sedimentation rates (Figure 8 bottom) deduced from our age models are mainly controlled by carbonate accumulation. Both for the 41 and 100 kyr climate states, sedimentation rates vary from about 0.5 cm/kyr in the western to around 0.9 cm/kyr in the eastern South Atlantic. During MPT interim state sedimentation rates on either side of the mid-Atlantic Ridge are restricted to between 0.4 and 0.6 cm/kyr. The decline primarily affects the eastern part and brings the west-east asymmetry to collapse.

In the working area cyclic variations of the sediment $CaCO_3$ content at Milankovitch frequencies are mainly due to orbitally driven lysocline shifts resulting from an interplay of NADW and more corrosive LCDW (Bickert and Wefer, 1996). In the Angola Basin (cores GeoB 1034-3, 1035-4,1729-3 and 3801-6) the glacial-interglacial contrast is particularly manifest as the surrounding bathymetric highs restrict the access of LCDW during interglacials. The same reasoning should apply for long-term changes in carbonate accumulation. We therefore assume that the influence of southern-source deep water was greatly enhanced during the MPT interim state. This conclusion is supported by a simultaneous decrease of glacial and interglacial kaolinite/chlorite ratios in core GeoB 2821-1 (Gingele et al., 1999), interpreted to be induced by chlorite-enriched deep southern waters. Consequently, NADW should have been reduced during that interval. Indeed, $\delta^{13}C$ records from Atlantic and Pacific ODP sites indicate significantly weaker NADW between 900 and 400 ka (Raymo et al., 1997). In view of this global evidence we suggest, that the MPT should not be regarded as a gradual transition from a '41 kyr world' to a '100 kyr world', but rather as a third, contrasting climate state.

Terminal MPT event

In several of the SUSAS cores unusual sediment facies occur coincidentally at around 530 ka, close to the end of the terminal MPT transition. Granulometric analyses of cores GeoB 2820-2 and 2821-1 show a sharp grain-size shift with an almost total loss of the > 63 μm fraction (Breitzke, 1997), possibly related to the mid-Brunhes dissolution cycle (e.g, Adelseck, 1977). In core GeoB 2820-2 this episode corresponds to a short hiatus. The continuous late Pleistocene record of core GeoB 1035-4 is interrupted by a thick turbidite dating to the same age. Core GeoB 3812-1 displays a sharp color change at a delicately laminated horizon (Figure 9).

Most impressive are thick intercalated laminated diatom ooze layers in cores GeoB 3801-6 (124 cm) and 3813-3 (38 cm). As discussed above, the laminations must have been deposited in a very short time and should reflect an extremely short-term climate variability. Very high sedimentation rates in the overlying carbonate sediments may have contributed to preserve the siliceous sections in both cores. The almost monospecific layers consist of the giant diatom *Ethmodiscus rex* (Rattray) Wiseman and Hendey (C.B. Lange, pers. comm.), the largest solitary (not chain-forming) diatom known, reaching diameters of 2-3 mm (Wiseman and Hendey, 1953; Round et al., 1990). They are entirely uncommon at these latitudes as *Ethmodiscus rex* is found in plankton primarily in equatorial regions in a range of temperature from 19° to 29.5°C (Lisitzin, 1996). Recently an unusual diatom ooze layer was detected in core GeoB 5112-4 recovered on R.V. METEOR cruise M41/3 at 23°49,5'S 16°15,5' W from a water depth of 3842 m (Pätzold et al., 1999). Correlating the magnetic susceptibility record of this core to the SUSAS stack proves that the diatoms were deposited at the same time as in the two SUSAS cores (Frederichs et al., 1999b).

Thick ooze deposits of this diatom were mainly

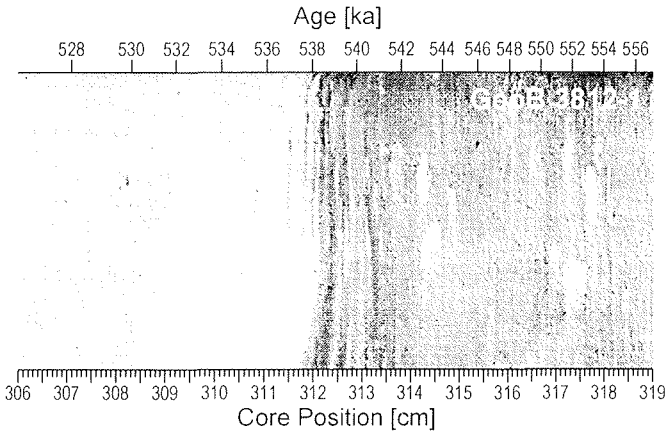

Figure 9. Terminal MPT event documented in a sharp colour transition at unbioturbated finely laminated layers in core GeoB 3812-1.

reported from equatorial regions of the world oceans (e.g., Gardner and Burckle, 1975; Mikkelsen, 1977; Stabell, 1986; Lisitzin, 1996). Even there, their occurrence is puzzling, because *Ethmodiscus rex* very rarely occurs in plankton samples (not more than 0.5 cells/m^3; Lisitzin (1996)). However, enigmatic deep populations have been observed in the Pacific Ocean (Villareal, 1993). Several hypothesis have been proposed to clarify the paradoxical '*Ethmodiscus rex* problem' (Gardner and Burckle, 1975), including differential dissolution, focusing by bottom currents and intense productivity blooms. Results from the Joint Global Ocean Flux Study (JGOFS), emphasize the potentially important role of oceanic frontal zones for the rapid accumulation of diatom biomass (Yoder et al., 1994). They indicate dramatic biological responses to circulation and mixing processes associated with open-ocean frontal systems separating cold from warm waters and gave rise to the idea that thick diatom layers may be deposited in such environments.

Picking up this suggestion and taking into account the occurrence of the terminal event at the end of the MPT interim state of strongly reduced NADW flux we believe it to result from elemental changes in the global ocean circulation system. Possibly an oceanic frontal zone shifted into the subtropical South Atlantic for a short time and thus initiated the massive diatom growth. The diversified terminal MPT events at around 530 ka documented in South Atlantic Ocean sediments might well be related to other paleoclimatic 'puzzles'. Recently, Rossignol-Strick et al. (1998) found an anomalous sapropel layer in the Mediterranean Sea dated 528-525 ka and interpreted it to result from a 'massive odd monsoon'. Previously Bassinot et al. (1994b) reported extremely high and low $\delta^{18}O$ values during isotope stages 13.2 and 13.3, respectively, in a giant piston core from the equatorial Indian Ocean. Analogously to the sapropel layer the unusually depleted value at stage 13.3 can be interpreted as a regional effect resulting from low surface-water salinity due to heavy monsoonal fluvial discharge (Rossignol-Strick et al., 1998). But insolation conditions would not predict heavy monsoon rainfall over Africa and Asia during that time. However, also a terrestrial climate proxy indicates an extraordinary warm climate. Chinese loess sequences and interbedded paleosols are known to record paleoclimate, as loess was deposited in a cold, dry climate, while soils formed during wet and mild episodes. Paleosol S5, which can be related to oxygen isotope stages 15-13, is by far the thickest and most weathered of the whole sequence (An and Wei, 1980). At its top, near stage 13, the highest magnetic susceptibilities of the past 2500 kyr (Kukla et al., 1988; Heller et al., 1991; Bloemendal et al., 1995) imply an extremely warm and humid climate in Asia, although oxygen isotope records identify this stage as one of the least expressed interglacials during the late Pleistocene.

Similarly as the MPT interim state, the terminal event can not be explained by astronomical forcing nor is it documented in global ice-volume records.

Conclusions

The rock magnetic view at sediment sequences from the oligotrophic subtropical South Atlantic uncovers several new and decisive aspects of the mid-

Pleistocene climate transition (MPT). The analyses are based on high-resolution magnetic age models which were built despite very low sedimentation rates for a series of twelve sediment cores by orbital tuning of their magnetic susceptibility records. Located on the submarine ridges in water depths affected alternately by NADW and LCDW these sediment sequences have recorded ocean history over the past 1500 kyr in a region very important in the framework of the global thermohaline circulation. The good overall correlation of all records let us to compute the SUSAS stack.

Cyclic patterns, which partly were used for the magnetic cyclostratigraphy, essentially reflect orbitally forced changes in deep water chemistry. In the course of the MPT they document the well-known change from variations with a period of 41 kyr to the late Pleistocene 100 kyr ice age rhythm. Compared to the driving functions in an evolutionary spectral analysis an alternating exchange of spectral energy between the 41 and 100 kyr bands is implied. In accordance with the suggestions of Ruddiman et al. (1989) and Joyce et al. (1990) residues between the SUSAS stack and an adapted ETP record characterize the climate system as less sensitive to obliquity changes during the late Pleistocene. According to our analysis the shift towards strongly reduced response to obliquity forcing takes place at about 650 ka and is synchronous with the onset of 100 kyr cyclicity in our data and as well in global ice volume (e.g., Ruddiman et al., 1989; Mudelsee and Schulz, 1997). This result substantiates threshold models, which mimic the occurrence of near-100 kyr cycles in the late Quaternary by introducing a decreasing atmospheric pCO_2 level (e.g., Raymo, 1997; Paillard, 1998). The residual analysis also documents reduced response in the 41 kyr band coinciding with the premature occurrence of a near-100 kyr cycle at about 1150 ka. Being previously reported from several $\delta^{18}O$ records (e.g., Mudelsee and Stattegger, 1997), this incident involves global ice volume.

In addition to features which mimic oxygen isotopes, the rock magnetic proxy unveils a MPT interim state of reduced carbonate deposition obviously not directly linked to changes in global ice volume. Bounded by transitions lasting from 1000 to 920 ka and from 640 to 500 ka this interval precisely fills the time lag between the first occurrence of larger glacial ice shields and the onset of near-100 kyr cyclicity (e.g., Mudelsee and Schulz, 1997). Our trend analyses implies that the outstanding feature of this episode is enhanced influence of southern source deep waters. Support for this hypothesis comes from analyses of $\delta^{13}C$ records implying a consistent reduced influence of NADW during this time interval (Raymo et al., 1997).

At the end of the MPT interim state a terminal event is documented in several SUSAS cores. It is believed to be due to strong changes in the ocean circulation system linked to the end of the MPT interim state and the beginning of the late Pleistocene 100 kyr state. A global character of this event is suggested as it occurs coincidentally with other unusual climate excursions which point towards extremely warm and humid climates in Asia and Africa (e.g., Kukla et al., 1988; Bassinot et al., 1994b; Rossignol-Strick et al., 1998).

Acknowledgements

We thank T. Bickert for kindly providing $CaCO_3$ data of GeoB 1211-1 and the unpublished $\delta^{13}C$ record of ODP Site 806. This study was funded by the Deutsche Forschungsgemeinschaft (Sonderforschungsbereich 261 at Bremen University, contribution No. XXX). F.S. was supported by the Deutsche Forschungsgemeinschaft in the framework of Graduiertenkolleg 221.

References

Adelseck, C.G. Jr., Recent and late Pleistocene sediments from the eastern equatorial Pacific Ocean: sedimentation and dissolution, Ph.D. thesis, Univ. of Calif., San Diego, 192 pp, 1977.

An, Z.S. and L.Y. Wei, The fifth layer paleosol in the Lishi Loess and their paleoclimatic significance, *Acta Pedologica Sinica*, 17, 1-10, 1980.

Balsam, W.L. and F.W. McCoy, Jr., Atlantic sediments: glacial/interglacial comparisons, *Paleoceanography*, 2, 531-542, 1987.

Bassinot, F.C., L. Beaufort L, E. Vincent, L.D. Labeyrie, F. Rostek, P.J. Müller, X. Quidelleur and Y. Lancelot, Coarse fraction fluctuations in pelagic carbonate sediments from the tropical Indian Ocean: a 1500-kyr record of carbonate dissolution, *Paleoceanography*, 9, 579-600, 1994a.

Bassinot, F.C., L.D. Labeyrie, E. Vincent, X. Quidelleur, N.J. Shackleton and Y. Lancelot, The astronomical theory of climate and the age of the Brunhes-Matuyama magnetic reversal, *Earth Planet. Sci. Lett.*, 126, 91-108, 1994b.

Berger, A. and M.F. Loutre, Insolation values for the climate of the last 10 million years, *Quat. Sci. Rev.*, 10, 297-317, 1991.

Berger, A. and M.F. Loutre, Astronomical solutions for paleoclimate studies over the last 3 million years, *Earth Planet. Sci. Lett.*, 111, 369-382, 1992.

Berger, W.H. and G. Wefer, Klimageschichte aus Tiefseesedimenten, *Naturwissenschaften*, 79, 541-550, 1992.

Berger, W.H. and E. Jansen, Mid-Pleistocene climate shift – the Nansen connection, in *The Polar Oceans and their Role in Shaping the Global Environment*, Geophys. Monogr., 84, 295-311, AGU, Washington, 1994.

Berger, W.H., M.K. Yasuda, T. Bickert, G. Wefer and T. Takayama, Quaternary time scale for the Ontong Java plateau: Milankovitch template for Ocean Drilling Program Site 806, *Geology*, 22, 463-467, 1994.

Berger, W.H. and G. Wefer, Expeditions into the past: paleoceanographic studies in the South Atlantic, in *The South Atlantic: Present and Past Circulation* edited by G. Wefer, W.H. Berger, G. Siedler and D.J. Webb, Springer Verlag, Berlin, pp 363-410, 1996.

Berger, W.H., T. Bickert, M.K. Yasuda and G. Wefer, Reconstruction of atmospheric CO_2 from ice-core data and the deep-sea record of Ontong Java plateau: the Milankovitch chron, *Geol. Rundschau*, 85, 466-495, 1996.

Bickert, T., Rekonstruktion der spätquartären Bodenwasserzirkulation im östlichen Südatlantik über stabile Isotope benthischer Foraminiferen, Ph.D. thesis, *Ber. FB Geow. Univ. Bremen*, 27, 205 pp, 1992.

Bickert, T. and G. Wefer, Late Quaternary deep water circulation in the South Atlantic: reconstruction from carbonate dissolution and benthic stable isotopes, in *The South Atlantic: Present and Past Circulation* edited by G. Wefer, W.H. Berger, G. Siedler and D.J. Webb, Springer Verlag, Berlin, pp 599-620, 1996.

Birchfield, G.E. and M. Ghil, Climate evolution in the Pliocene and Pleistocene from marine-sediment records and simulations: internal variability versus orbital forcing, *J. Geophys. Res.*, 98, 10385-10399, 1993.

Bleil, U. and cruise participants, Report and preliminary results of METEOR cruise 29/2, Montevideo – Rio de Janeiro, 15.7.1994 – 8.8.1994, *Ber. FB Geow. Univ. Bremen*, 59, 153 pp, 1994.

Bloemendal, J., B. Lamb and J. King, Paleoenvironmental implications of rock-magnetic properties of Late Quaternary sediment cores from the eastern equatorial Atlantic, *Paleoceanography*, 3, 61-87, 1988.

Bloemendal, J. and P. deMenocal, Evidence for a change in the periodicity of tropical climate cycles at 2.4 Myr from whole-core magnetic susceptibility measurements, *Nature*, 342, 897-900, 1989.

Bloemendal, J., J.W. King, L. Tauxe and J.-P. Valet, Rock magnetic stratigraphy of leg 108 sites 658, 659, 661, and 665, eastern tropical Atlantic, *Proc., ODP, Sci. Results*, 108, 415-428, 1989.

Bloemendal, J., X.M. Liu and T.C. Rolph, Correlation of the magnetic susceptibility stratigraphy of Chinese loess and the marine oxygen isotope record: chronological and palaeoclimatic implications, *Earth Planet. Sci. Lett.*, 131, 371-380, 1995.

Breitzke, M. Elastische Wellenausbreitung in marinen Sedimenten - neue Entwicklungen der Ultraschall Sedimentphysik und Sedimentechographie. *Ber. FB Geow. Univ. Bremen*, 104, 298 pp, 1997.

Chi, J. and J. Mienert, Linking physical property records of Quaternary sediments to Heinrich events, *Mar. Geology*, 131, 57-73, 1996.

Clark, P.U. and D. Pollard, Origin of the middle Pleistocene transition by ice sheet erosion of regolith, *Paleoceanography*, 13, 1-9, 1998.

DeBlonde, G. and W.R. Peltier, A one-dimensional model of continental ice volume fluctuations through the Pleistocene: implications for the origin of the Mid-Pleistocene climate transition, *J. Clim.*, 4, 318-344, 1991.

Frederichs, Th., U. Bleil, K. Däumler, T. von Dobeneck and A. Schmidt, The magnetic view on the marine paleoenvironment: parameters, techniques and potentials of rock magnetic studies as a key to plaeoclimatic and paleoceanographic changes, in *Use of Proxies in Paleoceanography: Examples from the South Atlantic* edited by Fischer, G. and G. Wefer, Springer-Verlag Berlin Heidelberg, in press, 1999a.

Frederichs, Th., K. Fabian and J. Funk, Physical properties studies, in *Report and preliminary results of METEOR cruise M41/3, Vitória – Salvador de Bahia, 18.4.1998 –*

15.5.1998, Ber. FB Geow. Univ. Bremen, in press, 1999b.

Gardner, J.V. and L.H. Burckle, Upper Pleistocene *Ethmodiscus rex* oozes from the eastern equatorial Atlantic, *Micropaleontol.* 21, 236-242, 1975.

Gingele, F.X., F. Schmieder, T. von Dobeneck, R. Petschick and C. Rühlemann, Terrigenous flux in the Rio Grande Rise area during the last 1500 ka: evidence of deepwater advection or rapid response to continental rainfall patterns?, *Paleoceanography*, in press, 1999.

Grützner, J., F.C. Bassinot and J. Mienert, High-resolution compressional-wave velocity measurements in Pleistocene sediments of the Ceará Rise (western equatorial Atlantic): implications for orbital driven sedimentary cycles, *Proc. ODP, Sci. Results*, 154, 135-149, 1997.

Hays, J.D., J. Imbrie and N.J. Shackleton, Variations in Earth's orbit: pace-maker of the ice ages, *Science*, 194, 1121-1132, 1976.

Harris, S.E., A.C. Mix and T. King, Biogenic and terrigenous sedimentation at Ceará Rise, western tropical Atlantic, supports Pliocene-Pleistocene deep-water linkage between hemispheres. *Proc. ODP, Sci. Results*, 154, 331-345, 1997.

Heller, F., X. Liu, T. Liu and T. Xu, Magnetic susceptibility of loess in China, *Earth Planet. Sci. Lett.*, 103, 301-310, 1991.

Imbrie, J., Measuring the gain of the climate system's response to Milankovitch forcing in the precession and obliquity bands, in *Long-term climatic variations – data and modelling*, Springer, Berlin, pp 403-410, 1992.

Imbrie, J., J.D. Hays, D.G. Martinson, A. McIntyre, A.C. Mix, The orbital theory of Pleistocene climate: support from a revised chronology of the marine $\delta^{18}O$ record, in *Milankovitch and Climate Part 1*, edited by A. Berger, J. Imbrie, J. Hays, G. Kukla, B. Saltzman, Reidel, Dordrecht, pp 269-305, 1984.

Imbrie, J., A. Berger, E.A. Boyle, S.C. Clemens, A. Duffy, W.R. Howard, G. Kukla, J. Kutzbach, D.G. Martinson, A. McIntyre, A.C. Mix, B. Molfino, J.J. Morley, L.C. Peterson, N.G. Pisias, W.L. Prell, M.E. Raymo, N.J. Shackleton and J.R. Toggweiler, On the structure and origin of major glaciation cycles 1. Linear responses to Milankovitch forcing, *Paleoceanography*, 7, 701-738, 1992.

Imbrie, J., A. Berger, E.A. Boyle, S.C. Clemens, A. Duffy, W.R. Howard, G. Kukla, J. Kutzbach, D.G. Martinson, A. McIntyre, A.C. Mix, B. Molfino, J.J. Morley, L.C. Peterson, N.G. Pisias, W.L. Prell, M.E. Raymo, N.J. Shackleton and J.R. Toggweiler, On the structure and origin of major glaciation cycles 2. The 100,000-year cycle, *Paleoceanography*, 8, 699-735, 1993.

Johnson, D.A., M. Ledbetter and L. Burckle, Vema Channel paleo-oceanography: Pleistocene dissolution cycles and episodic bottom water flow, *Mar. Geology*, 23, 1-33, 1977.

Joyce, J.E., L.R.C. Tjalsma, J.M. Prutzman, High resolution planktic stable isotope record and spectral analysis for the last 5.35 m.y.: Ocean Drilling Program Site 625, northeast gulf of Mexico, *Paleoceanography*, 5, 507-529, 1990.

Kukla, G., F. Heller, X.M. Liu, T.C. Xu, T.S. Liu and Z.S. An, Pleistocene climates in China dated by magnetic susceptibility, *Geology*, 16, 811-814, 1988.

Lisitzin, A.P., Oceanic sedimentation: lithology and geochemistry, AGU, Washington D.C., 400 pp, 1996.

Maasch, K.A., Statistical detection of the mid-Pleistocene transition, *Clim. Dyn.*, 2, 133-143, 1988.

Martinson, D.G., N.G. Pisias, J.D. Hays, J. Imbrie, T.C. Moore, N.J. Shackleton, Age dating and the orbital theory of the ice ages: development of a high-resolution 0 to 300,000-year chronostratigraphy, *Quat. Res.*, 27, 1-29, 1987.

Mead, G.A. and L. Tauxe, Oligocene paleoceanography of the South Atlantic: paleoclimatic implications of sediment accumulation rates and magnetic susceptibility measurements, *Paleoceanography*, 1, 273-284, 1986.

Mikkelsen, N., On the origin of Ethmodiscus ooze. *Mar. Micropaleontol.*, 2, 35-46, 1977.

Mudelsee, M. and M. Schulz, The Mid-Pleistocene climate transition: onset of 100 ka cycle lags ice volume build-up by 280 ka, *Earth Planet. Sci. Lett.*, 151, 117-123, 1997.

Mudelsee, M. and K. Stattegger, Exploring the structure of the mid-Pleistocene revolution with advanced methods of time-series analysis, *Geol. Rundschau*, 86, 499-511, 1997.

Muller, R.A. and G.J. MacDonald, Simultaneous presence of orbital inclination and eccentricity in proxy climate records from Ocean Drilling Program Site 806, *Geology*, 25, 3-6, 1997.

Mwenifumbo, C.J., J.P. Blangy, Short-term spectral analysis of downhole logging measurements from Site 704, *Proc. ODP, Sci. Results*, 114, 577-585, 1991.

Paillard, D., The timing of Pleistocene glaciations from a simple multiple-state climate model, *Nature*, 391, 1998.

Park, J., S.L. D'Hondt, J.W. King and C. Gibson, Late Cretaceous precessional cycles in double time: a warm-Earth Milankovitch response, *Science*, 261, 1431-1434, 1993.

Park, J. and K.A. Maasch, Plio-Pleistocene time evolution of the 100-kyr cycle in marine paleoclimate records, *J. Geophys. Res.*, 98, 447-461, 1993.

Pätzold, J. und Fahrtteilnehmer, Bericht und erste Ergebnisse über die METEOR-Fahrt M15/2, Rio de Janeiro – Vitoria, 18.1. – 7.2.1991, *Ber. FB Geow. Univ. Bremen*, 17, 46 pp, 1993.

Pätzold, J. and cruise participants, Report and preliminary results of METEOR cruise M41/3, Vitória – Salvador de Bahia, 18.4.1998 – 15.5.1998, *Ber. FB Geow. Univ. Bremen*, in press, 1999.

Pestiaux, P. and A. Berger, An optimal approach to the spectral characteristics of deep-sea climatic records, in *Milankovitch and Climate Part 1* edited by A. Berger, J. Imbrie, J.

Hays, G. Kukla and B. Saltzman, Reidel, Dordrecht, pp 417-445, 1984.

Petersen, N., T. von Dobeneck and H. Vali, Fossil bacterial magnetite in deep-sea sediments from the South Atlantic Ocean, *Nature*, 320, 611-615, 1986.

Pisias, N.G. and T.C. Moore, The evolution of Pleistocene climate: a time series approach, *Earth. Planet. Sci. Lett.*, 52, 450-458, 1981.

Prell, W.L., Oxygen and carbon isotope stratigraphy for the Quaternary of Hole 502B: evidence for two modes of isotopic variability, *Initial Rep., DSDP*, 68, 455-464, 1982.

Raymo, M.E., The timing of major climate transitions, *Paleoceanography*, 12, 577-585, 1997.

Raymo, M.E., Glacial puzzles, *Science*, 281, 1467-1468, 1998.

Raymo, M.E., W.F. Ruddiman, J. Backman, B.M. Clement and D.G. Martinson, Late Pliocene variation in northern hemisphere ice sheets and North Atlantic deep water circulation, *Paleoceanography*, 4, 413-446, 1989.

Raymo, M.E., D.W. Oppo and W. Curry, The mid-Pleistocene climate transition: a deep-sea carbon isotopic perspective, *Paleoceanography*, 12, 546-559, 1997.

Robinson, S.G., Applications for whole-core magnetic susceptibility measurements of deep-sea sediments, *Proc. ODP, Sci. Results*, 115, 737-771, 1990.

Robinson, S.G., M.A. Maslin and I.N. McCave, Magnetic susceptibility variations in Upper Pleistocene deep-sea sediments of the NE Atlantic: implications for ice rafting and paleocirculation at the last glacial maximum, *Paleoceanography*, 10, 221-250, 1995.

Rossignol-Strick, M., M. Paterne, F.C. Bassinot, K.-C. Emeis and G.J. DeLange, An unusual mid-Pleistocene monsoon period over Africa and Asia, *Nature*, 392, 269-272, 1998.

Round, F.E., R.M. Crawford and D.G. Mann, The diatoms: biology and morphology of the genera, Cambridge Univ. Press, Cambridge, 747 pp, 1990.

Ruddiman, W.F., M.E. Raymo, D.G. Martinson, B.M. Clement and J. Backman, Pleistocene evolution: northern hemisphere ice sheets and North Atlantic ocean, *Paleoceanography*, 4, 353-412, 1989.

Saltzman, B. and M.Y. Verbitsky, Multiple instabilities and modes of glacial rhythmicity in the Plio-Pleistocene: a general theory of late Cenozoic climatic change, *Clim. Dyn.*, 9, 1-15, 1993.

Schmidt, A., T. von Dobeneck and U. Bleil, Magnetic characterization of Holocene sedimentation in the South Atlantic, submitted.

Schulz, H.D. und Fahrtteilnehmer, Bericht und erste Ergebnisse über die METEOR-Fahrt M20/2, Abidjan – Dakar, 27.12.1991 – 3.2.1992, *Ber. FB Geow. Univ. Bremen*, 25, 173 pp, 1992.

Shackleton, N.J., A. Berger, W.R. Peltier, An alternative astronomical calibration of the lower Pleistocene timescale based on ODP Site 677, *Trans. Royal Soc. Edinburgh: Earth Sci.*, 81, 251-261, 1990.

Stabell, B., Variations of diatom flux in the eastern equatorial Atlantic during the last 400,000 years (METEOR cores 13519 and 13521), *Mar. Geol.*, 72, 305-323, 1986.

Thiessen, W., Magnetische Eigenschaften des östlichen Südatlantiks und ihre paläozeanographische Relevanz, Ph.D. thesis, *Ber. FB Geow. Univ. Bremen*, 41, 170 pp, 1993.

Thompson, R. and F. Oldfield, Environmental magnetism, Allen and Unwin, London, 227 pp, 1986.

Tiedemann, R., M. Sarnthein and N.J. Shackleton, Astronomic timescale for the Pliocene Atlantic $\delta^{18}O$ and dust flux records of Ocean Drilling Program site 659, *Paleoceanography*, 9, 619-638, 1994.

Vali, H., O. Förster, G. Amarantidis and N. Petersen, Magnetotactic bacteria and their magnetofossils in sediments, *Earth Planet. Sci. Lett.*, 86, 389-400, 1987.

Villareal, T.A., Abundance of the giant diatom *Ethmodiscus* in the Southern Atlantic Ocean and the central Pacific gyre, *Diatom Res.*, 8, 171-177, 1993.

Volat, J.L., L. Pastouret and C. Grazzini, Dissolution and carbonate fluctuations in Pleistocene deep sea cores: a review, *Mar. Geology*, 34, 1-28, 1980.

von Dobeneck, T. and F. Schmieder, Using rock magnetic proxy records for orbital tuning and extended time series analyses into the super- and sub-Milankovitch bands, in *Use of Proxies in Paleoceanography: Examples from the South Atlantic* edited by Fischer, G. and G. Wefer, Springer-Verlag Berlin Heidelberg, in press, 1999.

Wefer, G. und Fahrtteilnehmer, Bericht über die METEOR Fahrt M 6/6, Libreville – Las Palmas, 16.2.1988 – 24.3.1988, *Ber. FB Geow. Univ. Bremen*, 3, 97 pp, 1988.

Wefer, G. und Fahrtteilnehmer, Bericht über die METEOR Fahrt M12/1 Kapstadt - Funchal, 13.3.1990 – 14.4.1990, *Ber. FB Geow. Univ. Bremen*, 11, 66 pp, 1990.

Wefer, G. and cruise participants, Report and preliminary results of METEOR cruise M34/3, Walvisbay – Recife, 21.2 – 17.3.1996, *Ber. FB Geow. Univ. Bremen*, 59, 153 pp, 1996.

Wiseman, J.D.H. and N.I. Hendey, The significance and diatom content of a deep-sea floor sample from the neighbourhood of the greatest oceanic depth, *Deep-sea Res.*, 1, 47-59, 1953.

Yiou, P., C. Genthon, M. Ghil, J. Jouzel, H. Le Treut, J.M. Barnola, C. Lorius and Y.N. Korotkevitch, High-frequency paleovariability in climate and CO_2 levels from Vostock ice core records, *J. Geophys. Res.*, 96, 20365-20378, 1991.

Yoder, J.A., S.G. Ackleson, R.T. Barber, P. Flament and W.M. Balch, A line in the sea, *Nature*, 371, 689-692, 1994.

Terrigenous flux in the Rio Grande Rise area during the past 1500 ka: Evidence of deepwater advection or rapid response to continental rainfall patterns? *(Paleoceanography, 14, 84-95, 1999)*

Franz X. Gingele,[1] Frank Schmieder,[2] Tilo von Dobeneck,[2] Rainer Petschick,[3] and Carsten Rühlemann[2]

Abstract. Surface sediment samples and three gravity cores from the eastern terrace of the Vema Channel, the western flank of the Rio Grande Rise, and the Brazilian continental slope were investigated for physical properties, grain size, and clay mineral composition. Discharge of the Rio Doce is responsible for kaolinite enrichments on the slope south of 20° and at intermediate depths of the Rio Grande Rise. The long-distance advection of kaolinite with North Atlantic Deep Water from lower latitudes is of minor importance as evidenced by low kaolinite/chlorite ratios on the Mid-Atlantic Ridge. Cyclic variations of kaolinite/chlorite ratios in all our cores, with maxima in interglacials, are attributed to low- and high-latitude forcing of paleoclimate on the Brazilian mainland and the related discharge of the Rio Doce. A long-term trend toward more arid and "glacial" conditions from 1500 ka to present is superimposed on the glacial-interglacial cyclicity.

1. Introduction

The Rio Grande Rise/Vema Channel/Hunter Channel region is a key area in the western South Atlantic to study spatial as well as temporal variations in the history of deepwater masses. Southern source bottom water passes from the Argentine to the Brazil Basin via the Vema and Hunter Channels. Above, southward flowing North Atlantic Deep Water (NADW) is recorded from 4000 to 2000 m water depth, overlain by Upper Circumpolar Water (UCPW) and Antarctic Intermediate Water (AAIW) [*Peterson and Stramma*, 1990]. The Rio Grande Rise (RGR), which reaches water depths of 800 m, offers the opportunity to sample sediments situated in different water masses and look for tracers of changes in thermohaline circulation.

Numerous studies have focussed in particular on variations in the propagation of Antarctic Bottom Water (AABW) and NADW in the South Atlantic using various tracers from benthic foraminifera assemblages [*Mackensen et al.*, 1993; *Schmiedl and Mackensen*, 1997], Cd/Ca ratios in benthic foraminifera [*Boyle*, 1988, 1994; *Oppo and Rosenthal*, 1994], carbon-13 composition [*Curry et al.*, 1988; *Duplessy et al.*, 1988; *Mackensen et al.*, 1994], diatoms [*Jones and Johnson*, 1984], grain size [*Massé et al.*, 1994], and clay minerals [*Biscaye*, 1965, *Chamley*, 1975, *Jones*, 1984; *Diekmann et al.*, 1996].

On the basis of their strong latitudinal and reciprocal distribution patterns in surface sediments of the South Atlantic, kaolinite and chlorite were inferred to be useful tracers of the major deepwater masses in the vicinity of the RGR. An advection of chlorite with southern source deepwater (AABW) was found by *Biscaye* [1965] and confirmed by later studies [*Jones*, 1984; *Petschick et al.*, 1996]. The occurrence of a kaolinite maximum at intermediate depths (above 4000 m) was attributed to advection of this mineral by NADW [*Chamley*, 1975]. The propagation of kaolinite with NADW is a well-documented feature in many cores from the eastern South Atlantic [*Diekmann et al.*, 1996].

Alternatively, *Jones* [1984] suggested an isopycnal transport model for the kaolinite enrichment on the RGR. On the basis of the assumption that the suspension load of the NADW in the western South Atlantic is too small to sustain a substantial enrichment (clearwater minimum), kaolinite input by the Rio Doce, southward transport with the Brazil current, deposition on the Sao Paulo (Santos) Plateau, and resuspension and isopycnal flow to the RGR was proposed. These different interpretations have implications on the evaluation of temporal changes of kaolinite content in sediment cores, which record either oceanic processes such as NADW fluctuations, sea level changes, or variations in fluvial discharge.

We examined 51 surface samples from two transects to evaluate potential sources and recent propagation of clay minerals (Figure 1). One profile samples the continental slope off the Rio Doce. The second transect runs from the slope across the Santos Plateau, the western and eastern flank of the RGR, to the Mid-Atlantic Ridge (MAR).

The temporal variation in the supply of clay minerals during the past 200 kyr was investigated in sediment cores from the slope (GeoB 2110) and the eastern terrace of the Vema Channel (GeoB 2822). A complete record of clay mineral supply covering the past 1500 kyr was found in core GeoB 2821. This core is situated in a key position on the western flank of the RGR just above the present AABW/NADW boundary. Cross-spectral analysis on the kaolinite/chlorite ratio of this core was carried out to determine phase relationships to orbital cycles and compare phase angles of related paleoceanographic and paleoclimatic proxies.

[1] Baltic Sea Research Institute, Rostock-Warnemuende, Germany.

[2] University of Bremen, Bremen, Germany.

[3] University of Frankfurt, Frankfurt, Germany.

Paper number 1998PA900012.
0883-8305/99/1998PA900012$12.00

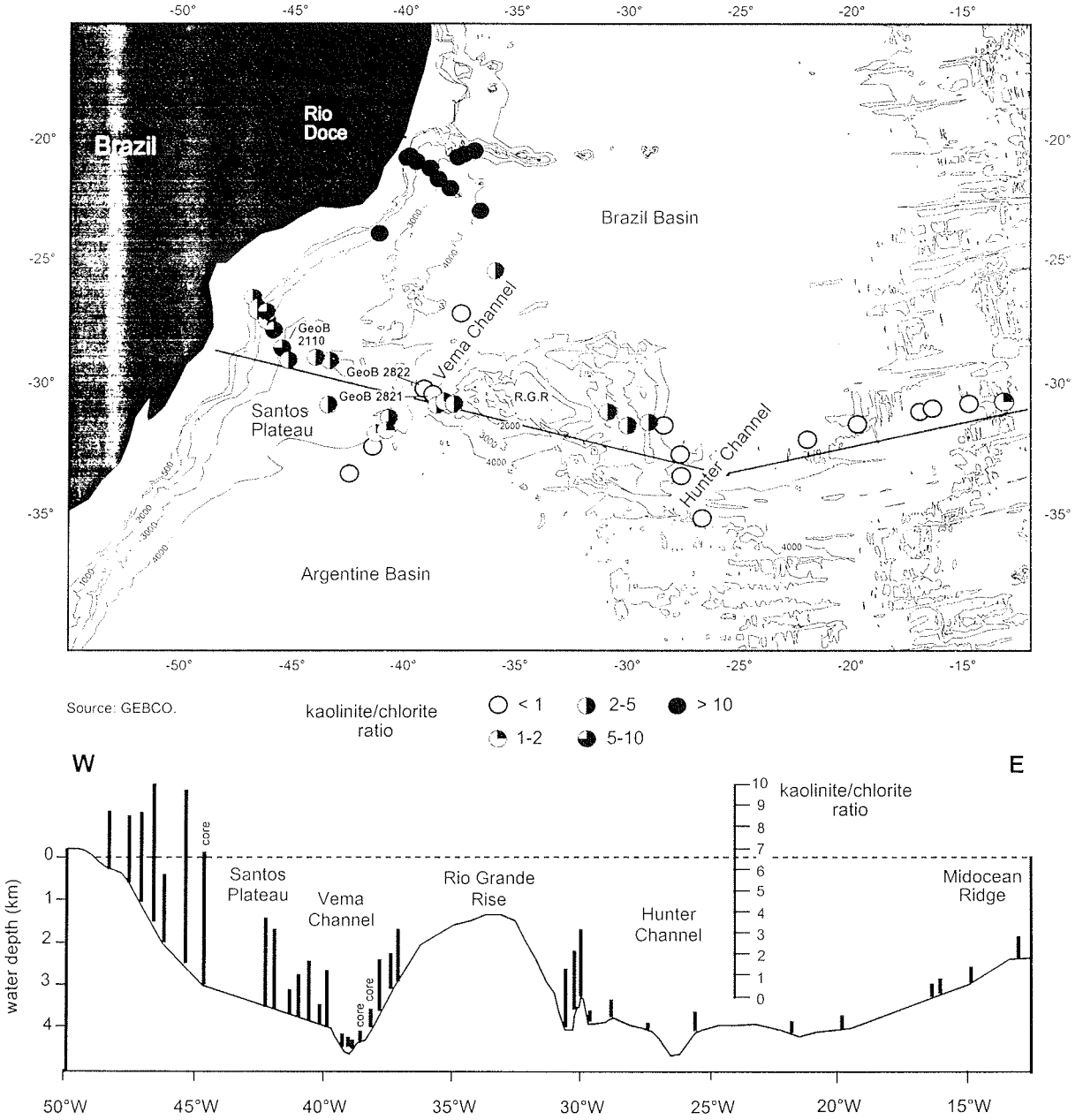

Figure 1. Area of investigation, core locations, and kaolinite/chlorite ratios of 51 surface samples in the investigation area. Depth contours after General Bathymetric Chart of the Oceans (GEBCO). Kaolinite/chlorite ratios are also projected on a hypothetical transect from the Santos Plateau across the Rio Grande Rise (RGR) to the Hunter Channel and Mid-Atlantic Ridge (MAR). Extreme kaolinite/chlorite values (>10) from sites directly off the Rio Doce are excluded from the projection.

2. Material and Methods

Sediment surface samples were recovered with giant box corer and multicorer during *Meteor* cruises M15/2 [*Pätzold et al.*, 1993], M23/2 [*Bleil et al.*, 1993], M29/2 [*Bleil et al.*, 1994], and M34/3 [*Wefer et al.*, 1996]. Sample treatment and clay mineral analyses are given in detail by *Petschick et al.* [1996]. Sediment cores (Table 1) were retrieved with a gravity corer on cruises M23/2 (GeoB 2110-3/4) and M29/2 (GeoB 2821-1 and GeoB 2822-2). Core GeoB 2110 from 3008 m water depth on the continental slope above the Santos Plateau (Figure 1) consists of grey hemipelagic clays with varying amounts of carbonate. Core GeoB 2822 from the eastern terrace of the Vema Channel (4267 m water depth) comprises terrigenous muds with small amounts of calcareous nannofossils and foraminifera. Increasing amounts of carbonate characterize core GeoB 2821 from the western flank of the RGR (3927 m water depth).

The cores were sampled at 5 cm intervals. Samples were treated with 10% acetic acid to remove carbonate, sieved over a 63 µm mesh, and split into >2 µm and <2 µm fractions by settling technique. The weight percentage of the sand fraction (>63 µm) was negligible. Weight percentages of the silt (2-63 µm) and clay fraction (<2 µm) were used to compute a silt/clay ratio.

Table 1. Location of Sediment Cores

Core	Water Depth, m	Latitude, Longitude	Cruise Report	Age Model
GeoB 2110-3/4	3008	28°38.9'S, 45°31.2'W	*Bleil et al.* [1993]	*Bleil et al.* [1993] and C. Rühlemann, (unpublished data, 1993)
GeoB 2821-1	3927	30°27.1'S, 38°48.1'W	*Bleil et al.* [1994]	F. Schmieder, (unpublished data, 1994)
GeoB 2822-2	4267	30°14.3'S, 39°08.5'W	*Bleil et al.* [1994]	*Bleil et al.* [1994]

The clay fraction (<2 μm) was analyzed by X-ray diffraction (CoK_α radiation) on oriented mounts for the four clay mineral groups kaolinite, smectite, illite, and chlorite following standard procedures given in detail by *Petschick et al.* [1996]. These procedures assume that the four main clay mineral groups add up to 100% in the fraction <2 μm and involve the use of the weighting factors of *Biscaye* [1965]. As a consequence our absolute percentages for the individual clay minerals cannot be compared to those of *Jones* [1984], who used weighting factors of *Heath and Pisias* [1979]. However, general patterns of clay mineral distribution are similar.

Magnetic susceptibility was measured on the archive halves of the cores at a 1 cm spacing using a Bartington Instruments M.S.2.C loop sensor. Lomb-Scargle Fourier transform [*Lomb*, 1976; *Scargle*, 1982, 1989] embedded in the Spectrum program [*Schulz and Stattegger*, 1997] was used for all spectral analysis. This spectral estimation method can be directly applied to unevenly spaced geological times series. Cross-spectral analysis for GeoB 2821 was performed using *Welch's* [1967] overlapped segment average (WOSA) procedure to reduce spectral peaks originating from random fluctuations.

2.1. Stratigraphy of GeoB 2110

A preliminary stratigraphic framework was established on shipboard counts of the planktonic foraminifera *Globorotalia menardii* [*Mulitza*, 1993]. On the basis of the cyclic appearance of this species, *Ericson and Wollin* [1968] defined a biostratigraphic zonation scheme using a letter notation from Z (Holocene) to Q in order of increasing ages. Zones Z to U can be directly correlated to oxygen isotope stages with following ages at zone boundaries: Z/Y, 12 ka; Y/X, 80 ka; X/W, 130 ka; W/V, 185 ka; and V/U, 370 ka. Though minor shifts in stage boundaries occur because of the poor resolution of the *G. menardii* counts, the preliminary stratigraphic framework was confirmed for site GeoB 2110 by carbonate stratigraphy after *Damuth* [1977]. Oxygen isotope measurements on planctic and benthic foraminifera were carried out on a Finnegan mass analyzing technique (MAT) 251 mass spectrometer (Figure 2). The measurements of the planktonic foraminifera *Globigerinoides sacculifer* were partly complicated by low sedimentation rates and enhanced carbonate dissolution but enabled identification of oxygen isotope stages 6.0, 6.2, 7.0, and 7.1. Supplementary measurements of *Uvigerina* spp. near isotope stage 4 clarified the stratigraphic position of stages 4.0 and 5.0. In addition to isotope stratigraphy, some characteristic patterns of the high-resolution magnetic susceptibility record were correlated to the SPECMAP stack [*Imbrie et al.*, 1984] and supplied four more tie points (near oxygen isotope stages 2.2, 3.0, 5.5, and 6.4). Because of different phase lags of plánktonic and benthic foraminifera and magnetic susceptibility, no phase information can be deduced from this combined age model.

2.2. Stratigraphy of GeoB 2821

The *G. menardii* counts for core GeoB 2821 did not produce a reasonable pattern. This is due to the wide sample spacing of the shipboard samples and the low sedimentation rates of this core. Since no $\delta^{18}O$ stratigraphy is available an age model derived by orbital tuning of the susceptibility record was used here. This cyclostratigraphy was established in the framework of a stratigraphical synthesis of 12 sediment cores from the subtropical South Atlantic Ocean (subtropical South Atlantic susceptibility (SUSAS) stack) [*von Dobeneck and Schmieder*, 1998], based on cyclic and highly coherent magnetic susceptibility logs. The correlation of susceptibility and carbonate content is inverse as in many marine environments [e.g., *Robinson*, 1990]. This indicates that the rock magnetic signal is a result of varying dilution of the (terrigenous) magnetic sediment fraction by glacial-interglacial carbonate dissolution cycles. On the basis of a detailed stepwise alternating field demagnetization of the Natural Remanent Magnetization (NRM), three paleomagnetic age marks could be identified for GeoB 2821 (Figure 2). A simple age model generated by linear interpolation of these reversal ages already shows spectral characteristics of Milankovitch cyclicity (100 and 41 kyr cycles), suggesting climatic forcing. Correlation to a precisely dated paleoclimate record was necessary to improve the age-depth relation prior to orbital tuning. The $\delta^{13}C$ record of South Pacific Ocean Drilling Program (ODP) Site 806 (T. Bickert, unpublished manuscript, 1998) exhibits a continuously high pattern similarity with the susceptibility record of GeoB 2821 and was therefore used as age reference. The predominant 40 kyr cyclicity of susceptibility was then synchronized with astronomically calculated obliquity variations [*Berger and Loutre*, 1991] as a target curve. A phase shift of -30° (-3.4 kyr) was found by cross-spectral analysis of magnetic susceptibility and $\delta^{18}O$ for one of the SUSAS records [*von Dobeneck and Schmieder*, 1998] ($\delta^{18}O$ data by *Bickert* [1992]). This value corresponds to those calculated by *Imbrie et al.* [1993] for early proxy responses in the Southern Hemisphere. As the SPECMAP stack [*Imbrie et al.*, 1984] is assumed to lag obliquity by 7.9 (7.4 - 8.2) kyr, a net lag of 4.5 kyr was applied for the tuning of magnetic susceptibility.

From the observation that faintly visible precessional peaks in the spectra gradually sharpened at both refinements of the age model the obliquity-tuned primary susceptibility record was filtered (15 - 47 kyr) to extract obliquity and precession cycles and matched to a composed target curve of normalized obliquity and precession.

2.3. Stratigraphy of GeoB 2822

According to *G. menardii* stratigraphy [*Jahn*, 1994] core GeoB 2822 reaches zone V of *Ericson and Wollin* [1968]. No isotope data were available to confirm these ages. Paleomagnetic measurements showed a uniform normal polarity throughout the core. The more detailed glacial-interglacial cycles revealed by the susceptibility record justify minor shifts of assumed stage boundaries Z/Y (isotope stages 1/2) and W/V (6/7). As in the other cores, kaolinite/chlorite and silt/clay (grain size) ratios generally correlate with the glacial-interglacial susceptibility re-

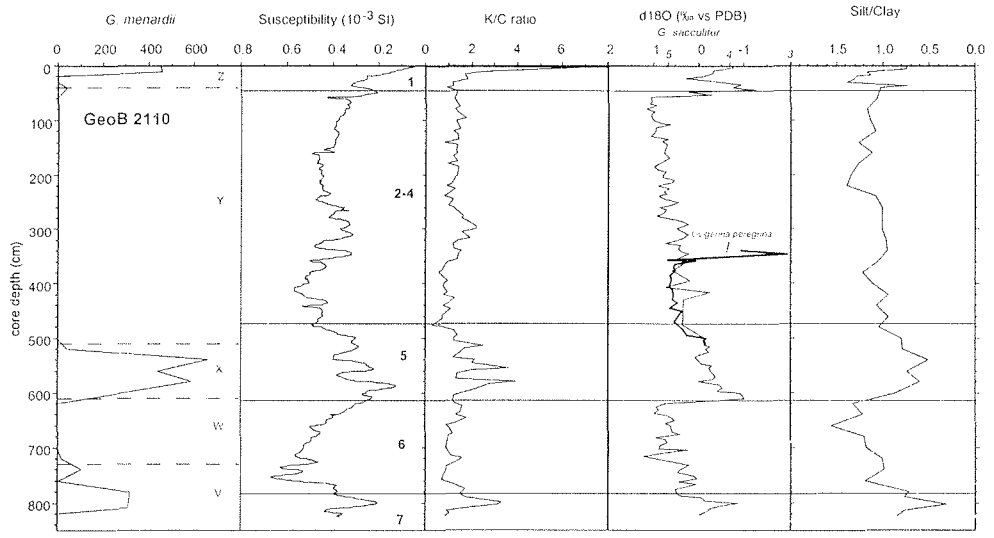
G. menardii
Susceptibility (10-3 SI)
K/C ratio
d18O (‰ vs PDB)
G. sacculifer
Silt/Clay
GeoB 2110
core depth (cm)
Z
Y
X
W
V
1
2-4
5
6
7
G. gomitulus peregrina

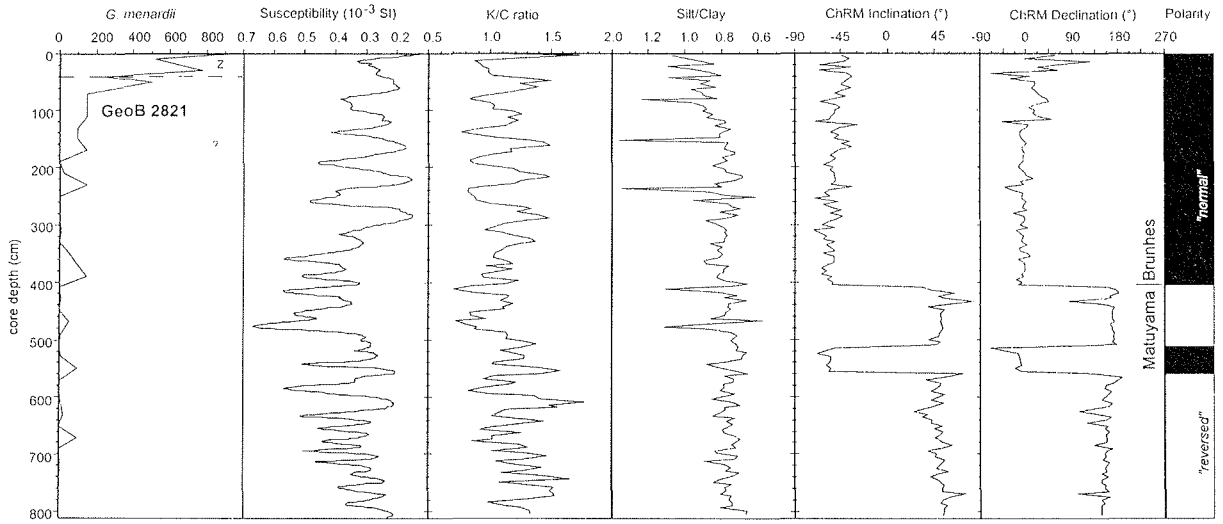
G. menardii
Susceptibility (10-3 SI)
K/C ratio
Silt/Clay
ChRM Inclination (°)
ChRM Declination (°)
Polarity
GeoB 2821
core depth (cm)
Z
Y
Matuyama
Brunhes
"normal"
"reversed"

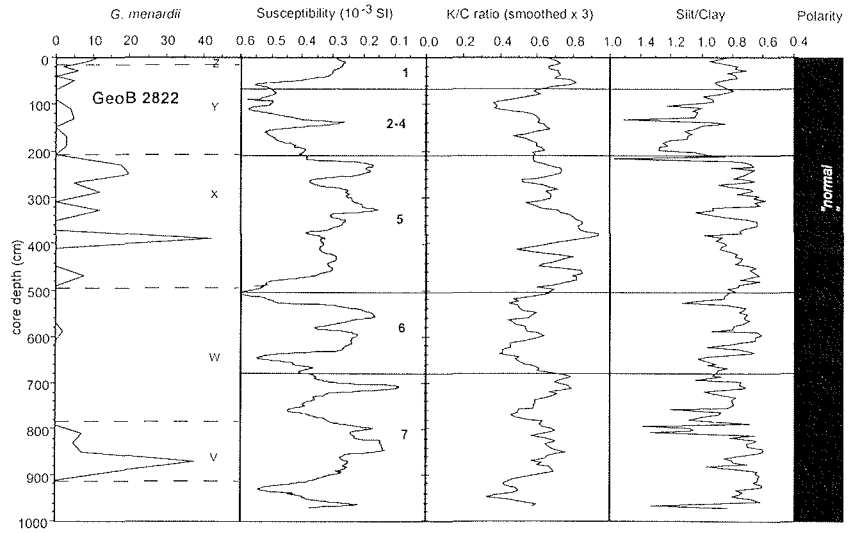
G. menardii
Susceptibility (10-3 SI)
K/C ratio (smoothed x 3)
Silt/Clay
Polarity
GeoB 2822
core depth (cm)
Z
Y
X
W
V
1
2-4
5
6
7
"normal"

Table 2. Data of Cross Spectral Analysis

	100 kyr^{-1} Band		41 kyr^{-1} Band		23 kyr^{-1} Band		T_r	Δt,
	k	°Phi	k	°Phi	k	°Phi	kyr	kyr
			Versus Reversed SPECMAP Stack $\delta^{18}O$					
Kaolinite/chlorite (GeoB 2821-1), 0-500 ka	0.99	-5±3(5)	0.99	-32±3(5)	-	-	500	5.0
Maximum δD Vostok ice core [*Jouzel et al.*, 1994]		-	0.93	-46±12	-	-	220	1.0
%NADW index [*Raymo et al.*, 1990]	0.87	16±15	0.86	5±16	0.83	41±17	400	3.0
Kaolinite/chlorite 43° S [*Diekmann et al.*, 1996]	0.96	-6±7	0.87	11±14	-	-	388	2.0
			Versus Reversed ODP677 $\delta^{18}O$					
Kaolinite/chlorite (GeoB 2821-1), 0-1500 ka	0.96	-33±8(13)	0.94	-31±10(15)	-	-	1525	5.0
Kaolinite/chlorite (GeoB 2821-1), 0-500 ka		-2±2(3)	0.95	-42±10(13)	-	-	500	5.0

Abbreviations are k, coherency; °Phi, phase angle with 80% confidence interval (in parentheses 95%); T_r maximum age used in the calculation; Δt, sample interval. The $\delta^{18}O$ SPECMAP stack was taken from *Imbrie et al.* [1984], and the $\delta^{18}O$ record Ocean Drilling Program Site (ODP) 677 from *Shackleton et al.* [1990].

cord with the exception of stage 6 (Figure 2). Still, individual maxima in the susceptibility record within stage 6 correspond to maxima in the precessional index around 133, 160, and 185 ka. Minima can be related to precessional minima and peaks in the kaolinite/chlorite record. Nevertheless, absolute values for the minima in susceptibility are rather low for a glacial stage. Since this is a feature unparalleled in the other cores it cannot be satisfactorily explained by a common mechanism. Further detailed paleomagnetic investigations would be required to investigate this local, time-restricted phenomena. The final age models of all cores were obtained by linear interpolation between stratigraphic tie points (Figure 3).

3. Results and Discussion

3.1. Surface Distribution

Since kaolinite and chlorite are the proxy clay minerals commonly associated with propagation of NADW and AABW we use the kaolinite/chlorite ratio to delineate the extension of the deepwater masses as demonstrated in the approach of *Petschick et al.* [1996]. Additional sources of kaolinite should reflect in exceptionally high kaolinite/chlorite ratios. Kaolinite/chlorite ratios of the surface samples are depicted in Figure 1 and reveal some characteristic features of sediment input and distribution. Extremely high values between 10 and 80 are recorded off the mouth of the Rio Doce and confirm the role of this river as an important kaolinite source as already stated by *DeMelo et al.* [1975]. The highest values are found on the shelf and upper slope. However, it is important to note that enough river suspension is carried through the water column to keep kaolinite/chlorite ratios above 10 at 4000 m water depth. Even south of 25°, values exceed 2 below 4000 m water depth. Below 4000-4100 m in the Vema and Hunter Channels and the abyssal plains of the Argentine and Brazil Basins, kaolinite/chlorite ratios fluctuate from 0.5 to 1 and confirm the concept of AABW as a source and carrier of chlorite [*Biscaye* 1965; *Jones*, 1984; *Petschick et al.*, 1996]. Some of the river suspension introduced by the Rio Doce is carried south by the Brazil current. Scavenging and incorporation into fecal pellets are believed to remove most of the fine-grained material from the water column rather rapidly [*Deuser et al.*, 1983]. Accumulations of kaolinite-rich sediments are found on the continental slopes off Cabo Frio and with decreasing values above and on the Sao Paulo and Santos Plateaus from 2500 to 3000 m. Since the rivers south of Cabo Frio contain relatively little kaolinite the Rio Doce has to be regarded as the major source for these deposits [*Jones*, 1984].

A characteristic enrichment of kaolinite was also found at intermediate depths (3000-4000 m) on the RGR by *Chamley* [1975] and *Jones* [1984], with the maximum centered at 3300 to 3600 m. Such an enrichment is confirmed by our samples, which cover a depth range from 4500 to 2900 m water depth on the western flank of the RGR. A similar feature is observed on the transect from the eastern slope of the RGR to the Hunter Channel. East of the Hunter Channel toward the MAR kaolinite/chlorite ratios are lower (<1) at comparable water depths (Figure 1). Only on the top of the ridge maximum values of 1.0 are reached. This has important implications concerning the origin and propagation of kaolinite.

Jones [1984] proposed two models to explain the kaolinite enrichment at mid-depths of the RGR: (1) advective transport of kaolinite from low latitudes with NADW and (2) advection of kaolinite along isopycnals from resuspension of kaolinite-rich deposits on the Sao Paulo Plateau. Though he did not rule out the NADW transport model completely, the isopycnal mixing model was better suited to explain his observed clay mineral dis-

Figure 2. (opposite) Parameters used for the stratigraphic classification of the cores. Age models for cores GeoB 2110 and GeoB 2821 are based on shipboard counts of *Globorotalia menardii*. Oxygen isotopes in core GeoB 2110 were measured on the planctic foraminifera *Globigerinoides sacculifer* and some benthic *Uvigerina peregrina*. The stratigraphic framework of GeoB 2821 is based on paleomagnetic analyses and orbital tuning of the magnetic susceptibility record. Also depicted arekaolinite-chlorite ratios and grain size (ratio of silt/clay weight percentages), which fluctuate in a glacial-interglacial pattern. Note that the records of susceptibilty and grain size are reversed for better graphic correlation.

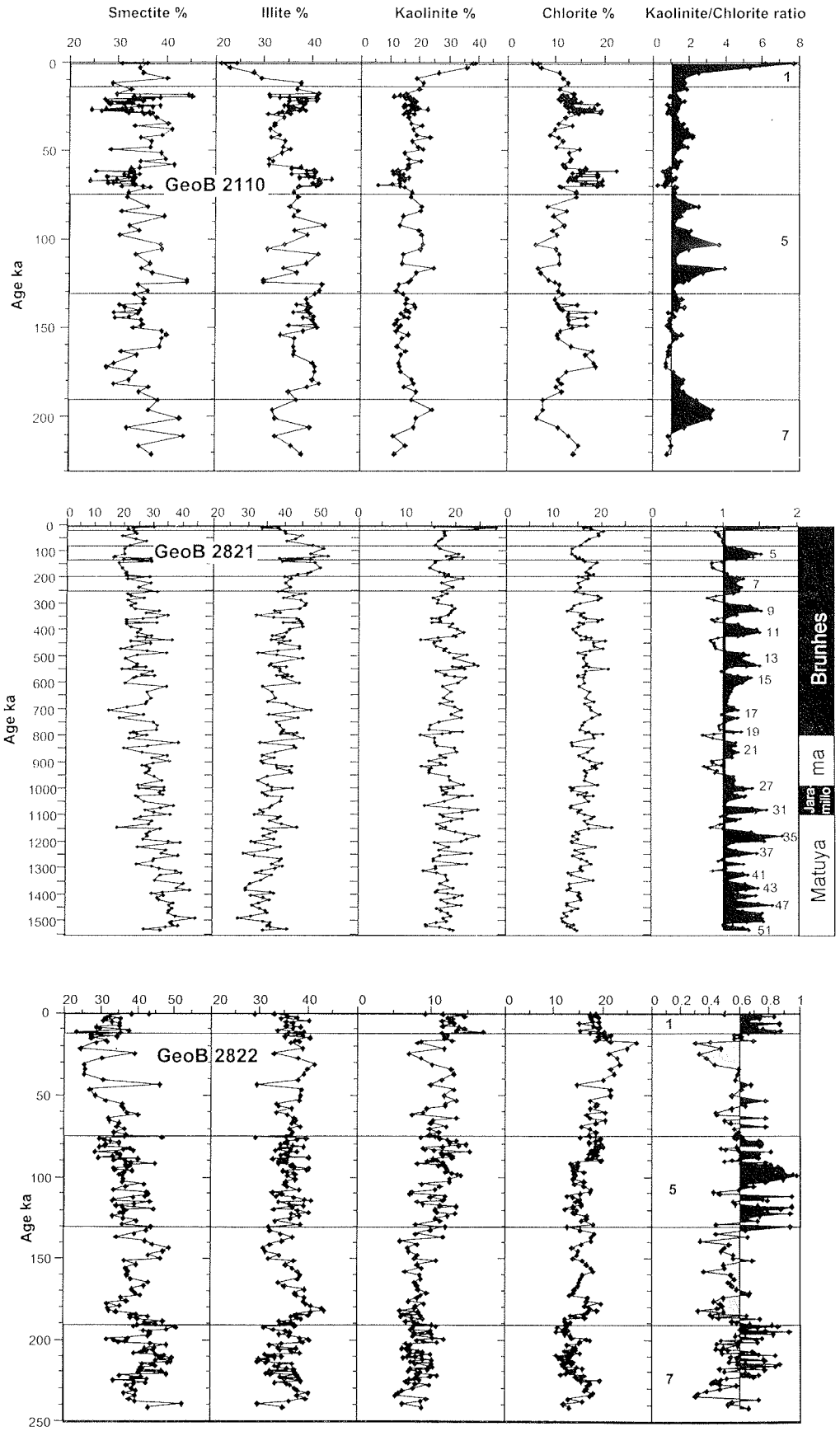
Smectite %
Illite %
Kaolinite %
Chlorite %
Kaolinite/Chlorite ratio
GeoB 2110
GeoB 2821
GeoB 2822
Age ka
Brunhes
ma
Jaramillo
Matuya

tribution. Kaolinite/chlorite ratios determined on our sediment surface sample set yield arguments for both transport models. The symmetrical nature of the kaolinite enrichment at middepths of both sides of the RGR could support the concept of advective transport of kaolinite from low latitudes with NADW. Consequently, similar kaolinite/chlorite ratios should be expected at comparable depths of the MAR. However, only a slight rise in kaolinite/chlorite values is recorded on the top, which may result from minor advection of kaolinite from low latitudes. On the other hand, although the transport of kaolinite to the western slope of the RGR along isopycnals from the Sao Paulo or Santos Plateaus may explain the kaolinite enrichment on the western side of the RGR, it is hard to imagine a mechanism that transports kaolinite-rich suspensions around or across the RGR to the "backside." To explain the symmetrical nature of the kaolinite enrichment on the RGR, we alternatively suggest the injection of kaolinite-rich suspensions into intermediate depths of the NADW off the mouth of the Rio Doce and short-distance transport southward instead of long-distance advection from lower latitudes. This idea is supported by high kaolinite/chlorite ratios down to 4000 m water depth off the river mouth, demonstrating that kaolinite-rich suspensions are able to reach deepwater levels. Injected at 20°S, these suspensions could be advected south with the NADW and be deposited on the first obstacle, which is the RGR.

Our results suggest that a substantial part of the terrigenous sedimentation on the RGR originates from freshwater input and suspension supply by the Rio Doce as evidenced by the kaolinite enrichment at intermediate depths of the RGR. The question arises of whether temporal variations in kaolinite supply primarily record pulses of fluvial discharge or rather represent varying intensities of short-distance NADW flow. To address this problem and look at the temporal variations of the kaolinite/chlorite ratios, we investigated three sediment cores.

3.2. Temporal Variations of Clay Mineral Input

Core GeoB 2110 was taken from 3000 m water depth at the continental slope above the Santos Plateau. Kaolinite/chlorite ratios in surface sediments reach a maximum at this depth (Figure 1) because of advection and deposition of kaolinite from the north with the Brazil current. Significant fluctuations of chlorite flux can be ruled out for this site because the only potential carrier of chlorite, AABW, always stayed well below these depths in the southwestern Atlantic [*Curry*, 1996]. Site GeoB 2110 shows highest kaolinite/chlorite ratios (4-8) in interglacial stages 1, 5 and 7 and lowest ratios (±1) in glacial sections (Figure 3). This is still in accordance with the model of *Jones* [1984], who proposed a southward transport of kaolinite from the mouth of the Rio Doce only during times of high sea level (interglacials) and a direct injection of the river load into intermediate and deepwater levels during times of low sea level (glacials). However, our surface data show high kaolinite/chlorite ratios down to 4000 m water depth also in recent (interglacial) sediments off the Rio Doce. Furthermore, if sea level exerts a major control on the input of kaolinite from the Rio Doce, minima in kaolinite/chlorite ratios could be also expected at the deep sites GeoB 2822 and 2821 during high stands. However, both deep sites show high kaolinite/chlorite ratios during interglacials. Therefore we hypothesize that a potential effect of sea level changes on the input of kaolinite to all our core sites is overridden by fluctuations in the total amount of river discharge.

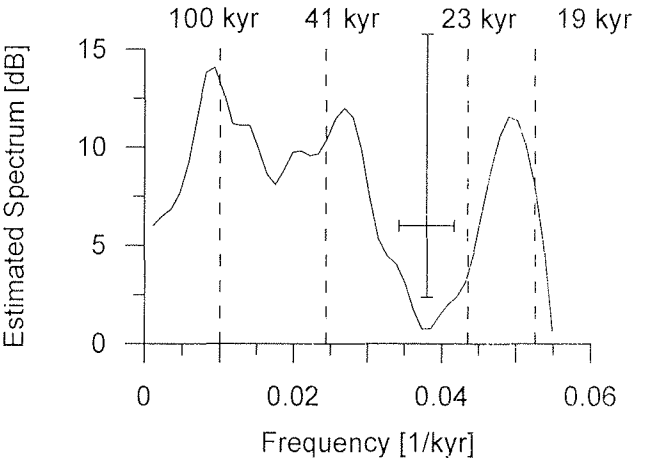

Figure 4. Spectral analysis of kaolinite/chlorite ratio of core GeoB 2110. In addition to spectral peaks near 100 and 41 kyr, strong response to precessional forcing becomes visible in the modified periodogram calculated by Lomb-Scargle Fourier transform using a Welch window. The cross depicts 6 dB bandwidth (horizontal) and 80% confidence interval (vertical).

Spectral analysis of the kaolinite/chlorite ratio of core GeoB 2110 (Figure 4) strengthens this assumption. Although the combined chronostratigraphy described above does not preserve the exact phase relation of different proxies, a Fourier transform yields information on spectral characteristics within the uncertainties of the dating procedure. The resulting spectrum indicates that there is a strong response of the kaolinite/chlorite ratio to precessional forcing. There is abundant evidence (summarized by *DeMenocal* [1995] and *Gingele et al.* [1998]) that low-latitude aridity-humidity cycles documented in eolian flux, monsoon intensity, or river discharge respond to variations in low-latitude insolation, which in turn result from Earth's orbital precession. Therefore we conclude that the kaolinite/chlorite ratio at site GeoB 2110 is significantly influenced by low-latitude river discharge.

The spectrum also documents 100 and 41 kyr variance (Figure 4). The dual nature of high- and low-latitude forcing of low-latitude climate has been recognized by *DeMenocal* [1995] in various sites around the African continent. Mechanisms transporting high-latitude signals, namely the pronounced 100 and 41 kyr cycles, to low latitudes are believed to be cooling North Atlantic surface water and fostering shifts in atmospheric circulation and migration of vegetation belts. Especially the 100 kyr frequency of eccentricity is prominent in many aridity-humidity records [*Pastouret et al.*, 1978; *DeMenocal et al.*, 1993; *Gingele et al.*, 1998].

Figure 3. (opposite) Relative clay mineral percentages and kaolinite/chlorite ratios of cores GeoB 2110, GeoB 2821, and GeoB 2822 versus age. In order to produce a maximum glacial-interglacial contrast the cutoff for the shading of kaolinite/chlorite ratios was set at an average value of 1.0 for the cores within the North Atlantic Deep Water (NADW) (GeoB 2110 and GeoB 2821) and at 0.6 for the core within the Antarctic Bottom Water (AABW) (GeoB 2822). Isotope stages 1-7 [*Imbrie et al.*, 1984] are shaded.

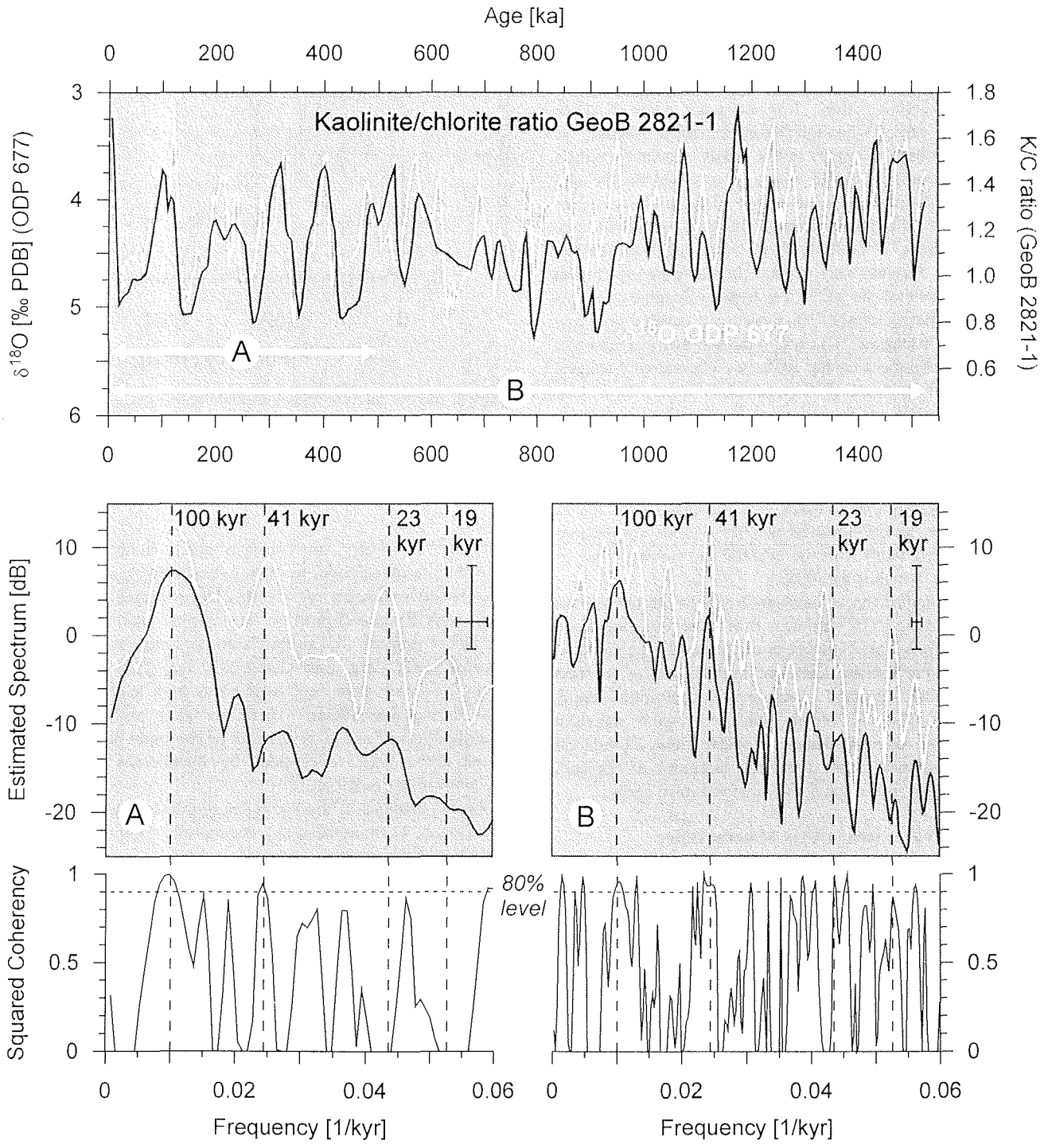

Figure 5. Cross-spectral analysis of kaolinite/chlorite ratio of core GeoB 2821 (black lines) and the reversed $\delta^{18}O$ record of Ocean Drilling Program (ODP) Site 677 (white lines) [*Shackleton et al.*, 1990]. While the past 500 kyr are dominated by eccentricity-related 100 kyr cycles (A), an increased amount of variance in the obliquity band near 41 kyr appears in the spectra of the 0-1500 ka records (B). Both time series are interpolated to 5 kyr steps, the average time resolution of the kaolinite/chlorite record of GeoB 2821. The analysis was performed using *Welch's* [1967] overlapped segment average (WOSA) procedure with two overlapping segments and a Welch window. The sign of the $\delta^{18}O$ record of ODP 677 was inverted to attain directly interpretable phase relations. Crosses depict 6 dB bandwidth and 80% confidence interval. The resulting negative phase angles shown in Table 2 indicate a lead with respect to $\delta^{18}O$. High squared coherency is calculated in the 100 and 41 kyr band.

Core GeoB 2822 from the eastern terrace of the Vema Channel (4300 m water depth) is believed to represent sedimentation within the AABW during interglacial as well as glacial times. The advection of chlorite from the south is documented in the lowest kaolinite/chlorite ratios (<1) of all investigated cores. Although of low amplitude, a significant glacial-interglacial pattern in the kaolinite/chlorite signal can be recognized, with higher values in the interglacial sections (Figure 3). Evidence from grain size and sediment texture from the area [*Johnson and Rasmussen*, 1984; *Massé et al.*, 1994] indicates a more vigorous flow of AABW at the transition from warm to cold periods and within glacials. Increased advection of chlorite with intensified AABW activity during glacials could explain the observed fluctuations in kaolinite/chlorite ratios of core GeoB 2822. Since the site is well below the direct influence of NADW the advection of kaolinite from low latitudes is an unlikely source for GeoB 2822. Therefore we remain with the Rio Doce as the primary kaolinite source also for this core.

Cyclic variations are also recorded in kaolinite/chlorite ratios of core GeoB 2821 (Figure 3). High values correspond to lows in the susceptibility record (Figure 2) and thus interglacial stages (Figure 3). The clay mineral proxy fluctuates in tune with many paleoclimate proxies dominated by high-latitude orbital forcing. A shift in the dominant period of variation from 41 to 100 kyr is visible near 1000 ka (Figure 3).

Cross-spectral analysis of the kaolinite/chlorite ratio of core GeoB 2821 was performed versus the reversed SPECMAP $\delta^{18}O$ stack and reversed $\delta^{18}O$ record of ODP 677 for the past 500 kyr and and versus the reversed $\delta^{18}O$ record of ODP 677 for the past 1500 kyr. It appears that the clay mineral proxy is coherent with global ice volume in the 41 and 100 kyr periods of obliquity and eccentricity (Table 2 and Figures 5 and 6). Resolution and sedimentation rates of the core are too low to investigate a precession-related variability. Moreover, statistical data (Table 2) for the complete kaolinite/chlorite record are difficult to interpret since significant variation in the 100 kyr band occurs only during the past 350 kyr, where 41 kyr cycles, dominating the older section, are reduced (Figure 5). As a consequence of this reflection of the mid-Pleistocene climate transition [e.g., *Ruddiman et al.*, 1989] we concentrate on the section from 0 to 500 ka for the 100 kyr cycle and make use of the whole record for the 41 kyr period. As statistical data (Table 2) and phase wheels (Figure 6) indicate, maxima in GeoB 2821 kaolinite/chlorite ratios lead maxima in NADW flux by 5800 years in the 100 kyr cycle (0 to 500 ka) and 4100 years in the 41 kyr cycle (0 to 500 and 0 to 1500 ka). These results are consistent with characteristic values of early proxy responses in the Southern Hemisphere [*Imbrie et al.*, 1993].

NADW production and propagation have varied in orbital time scales, though the relation to climate is not simple [*Curry*, 1996]. In the western Atlantic (Ceará Rise), only NADW was recorded in some peak interglacials, whereas in some glacials, southern source deepwater reached 3200 m water depth [*Curry*, 1996]. Investigations in the eastern part of the South Atlantic [*Diekmann et al.*, 1996] have shown that the propagation and southward extension of northern source deepwater (NADW) were more pronounced during interglacials, thus providing more kaolinite during warm periods. At first glance, kaolinite/chlorite ratios of core GeoB 2821 fit nicely in the concept of alternating intensities of interglacial NADW [*Diekmann et al.*, 1996] and glacial AABW [*Massé et al.*, 1994] flow. Within the error margins (Table 2), phase angles of kaolinite/chlorite ratios in the 100 kyr band of eccentricity are similar in the eastern and western Atlantic. The implications for the RGR are that either the kaolinite/chlorite ratio is controlled by changes in deepwater flux or that the high-latitude forcing mechanisms, which control deepwater flux and low-latitude climate in the eccentricity band, do not show a significant time lag. However, there are strong arguments opposing an exclusively deepwater-controlled clay mineral supply for sites GeoB 2821 as well as GeoB 2822.

First, AABW activity was strongly reduced after 350 [*Massé et al.*, 1994] or 275 ka [*Johnson and Rasmussen*, 1984], respectively, which would lead to rising kaolinite/chlorite ratios from 350 ka to present. Instead, we find decreasing kaolinite/chlorite ratios in core GeoB 2821.

Second, in the 41 kyr band, maxima of kaolinite/chlorite ratios of core GeoB 2821 significantly lead minima in ice volume, maxima in %NADW flux [*Raymo et al.*, 1990] and maxima in kaolinite/chlorite ratios in the eastern South Atlantic [*Diekmann et al.*, 1996] (statistical data in Table 2). Moreover, the phase angle of kaolinite/chlorite ratios of core GeoB 2821 in the 41 kyr period is close to the maxima of ∂D (deuterium) in the Vostok ice core [*Jouzel et al.*, 1994]. Maxima in the ∂D record indicate periods of increased atmospheric temperatures in Antarctica [*Waelbroeck et al.*, 1995], which are related to intensified evaporation and precipitation in lower latitudes. Consequently, we suggest that temporal changes in the kaolinite/chlorite ratio of the RGR cores may be rather interpreted as an atmospheric signal of precipitation and river input than as a proxy of deepwater fluctuations.

4. Paleoceanographic and Paleoclimatic Implications

Summarizing the evidence from clay mineralogy, grain size, and magnetic susceptibility, we find that the flux of terrigenous matter on the RGR shows cyclic variations at least in the 100 and 41 kyr periods. Interglacial stages are characterized by the deposition of fine-grained, kaolinite-rich terrigenous matter of low magnetic susceptibility. They record periods of increased humidity on the South American mainland and runoff of the Rio Doce. High fluvial discharge was also recorded for the Orinoco and Amazon Rivers during interglacials [*Bowles and Fleischer*, 1985]. *Clapperton* [1993] reported more humid conditions for interglacial stage 5 in Patagonia. The concept of increased humidity in interglacial periods (100 kyr period) is in accordance with results from multiple investigations on the African continent (summary in *DeMenocal* [1995]). Runoff of major African rivers and monsoon intensity fluctuates in the 100 kyr period of global ice volume and 23 kyr period of low-latitude insolation [*Pastouret et al.*, 1978; *Zachariasse et al.*, 1984; *Rossignol Strick*, 1985; *Pokras*, 1987; *Gingele et al.*, 1998]. Our data from the RGR yield similar results for the South American continent at 20°S in the 100 and 41 kyr periods. In core GeoB 2110 the resolution is sufficient to record fluctuations of kaolinite flux in the 23 kyr precessional band. They are believed to represent humidity and discharge variations of the Rio Doce initiated by low-latitude insolation changes.

Minima in the precessional index correspond to increased input of kaolinite and may be interpreted in terms of higher

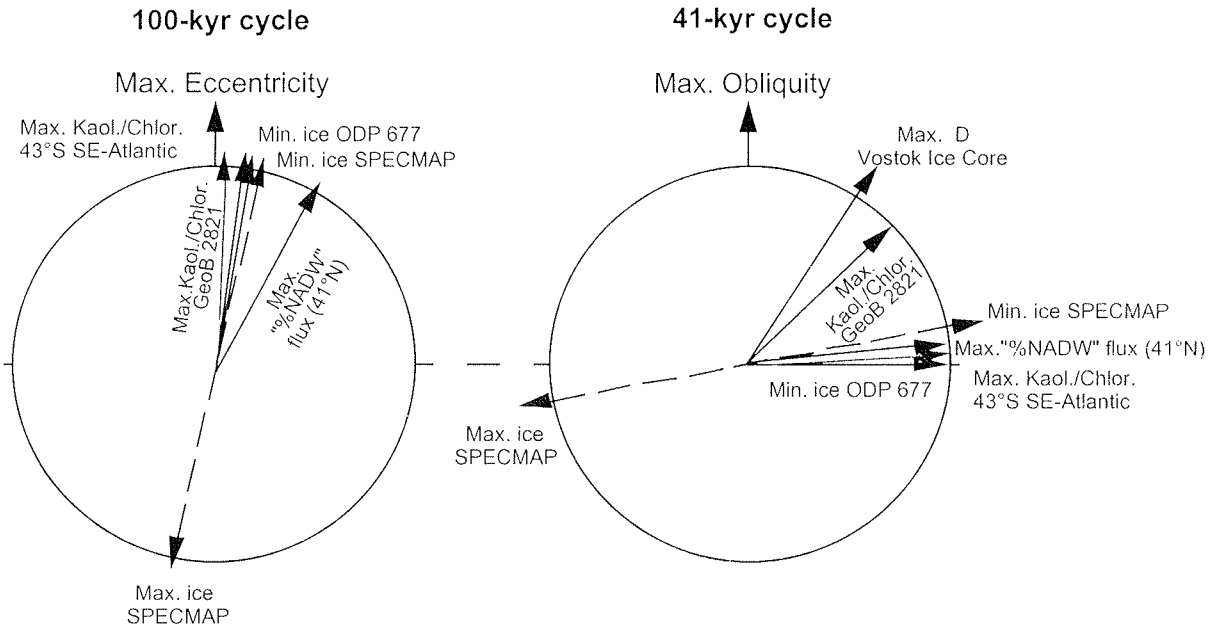

Figure 6. Phase relationships between kaolinite/chlorite ratios of core GeoB 2821 (0-500 ka), % NADW flux [*Raymo et al.*, 1990]kaolinite/chlorite ratios of a core 43°S in the SE Atlantic [*Diekmann et al.*, 1996], and the maximum of δD (deuterium) in the Vostok ice core [*Jouzel et al.*, 1994] in the 100 and 41 kyr periods of eccentricity and obliquity (statistical data see Table 2).

humidity in the drainage area of the Rio Doce. It is interesting to note that at about the same latitude west of the Andes in northern Chile, precession-related humidity/aridity cycles are recorded, which show exactly the opposite pattern [*Lamy, et al.* 1998]. There, maxima in the precessional index correspond to more humid conditions in the sediment record. Increased precipitation there is related to a shift in the position of the southern westerlies and indicates a nonsynchronous behavior of South American paleoclimate on an orbital timescale.

Glacial stages are characterized by maxima in magnetic susceptibility, illite, and grain size (more silt) and lows in kaolinite supply. Cold and dry conditions have been reported for the headwaters of the Rio Doce during the last glacial [*Behling and Lichte*, 1997]. The lack of dilution by fine-grained river suspensions, a more vigorous AABW flow, and the increased input of silt-sized dust, rich in magnetic particles and illite, may have combined to form the terrigenous signal of the cold periods. Previous studies have shown that major fluctuations in dust flux appear to be of global significance with maximum inputs during cold and arid periods [*Clemens and Prell*, 1990; *DeMenocal et al.*, 1993]. A potential source area for dust in the southwestern Atlantic is Patagonia. Patagonian dust is derived from loess deposits, which contain a high percentage of titanomagnetite and illite [*Teruggi*, 1957; *Bonorino*, 1966; *Zarate and Balsi*, 1993]. Although insignificant for the total terrigenous mass balance, the input of Patagonian dust in cold periods could selectively enhance the susceptibility signal preformed by glacial carbonate dissolution events. It may also contribute to an illite enrichment of glacial core sections.

It appears that the composition of the terrigenous matter on the Brazilian slope and also on the RGR responds to changes in humidity/aridity on the adjacent South American continent rather than to variations in deepwater advection. The dual influence of high- and low-latitude forcing on the paleoclimate in the Brazilian hinterland is believed to result in periodical discharge of the Rio Doce. Consequently, the supply and deposition of kaolinite on the slope and the RGR are recorded for the major Milankovitch periodicities.

Multiple potential sources complicate the interpretation of the main clay mineral components smectite and illite. Nevertheless, individual peaks in the downcore record of smectite in core GeoB 2821 are frequently associated with maxima in kaolinite/chlorite ratios and thus with warm and humid periods, whereas illite shows a reciprocal pattern. More evident is a long-term trend in smectite and illite percentages (Figure 3). Illite percentages increase while smectite percentages, as well as average kaolinite/chlorite ratios, decrease from 1500 ka to present. If the paleoclimatic interpretation of the clay mineral proxies is correct, a trend toward more arid and glacial conditions during the Pleistocene is evident. These findings are consistent with results from the African continent [*DeMenocal*, 1995]. Here proxies for African aridity reconstructed from various ODP sites around the continent show a gradual trend toward more arid and cooler conditions from the Pliocene to present with prominent shifts around 2800, 1700, and 1000 ka [*DeMenocal*, 1995].

5. Conclusions

Clay mineral analyses revealed that the Rio Doce (Brazil) is a major source of kaolinite for marine sediments at 20°-30°S in the western Atlantic. Characteristic enrichments of kaolinite are observed at intermediate depths of the continental slope and on the flanks of the RGR at 3000-4000 m water depth.

The supply of kaolinite with NADW is minor as evidenced by the comparison of kaolinite/chlorite ratios from the MAR and

the RGR. Consequently, patterns of terrigenous sedimentation in this part of the Atlantic record climatic conditions on the South American hinterland.

Low-latitude insolation fosters periodical discharge of the Rio Doce in the precessional 23 kyr band, as evidenced in kaolinite/chlorite ratios on the Brazilian slope. Cyclic variations of kaolinite/chlorite ratios on the slope and in a core from the western flank of the RGR are coherent with global ice volume in the 41 and 100 kyr periods. They are also believed to record fluctuations in the discharge of the Rio Doce and mirror humidity conditions on the adjacent South American hinterland. Humid periods are coeval with warm interglacial phases, whereas arid periods correspond to cold, glacial stages. The dual mode of high- and low-latitude forcing of low latitude climate is consistent with similar findings from the African continent. A long-time decrease in smectite content and kaolinite/chlorite ratios from 1500 ka to present is believed to document a trend toward more arid and cooler climate conditions for subtropical southern latitudes of South America.

Acknowledgments. The dedication and effort of crew and master of R/V *Meteor* is greatly acknowledged. We are grateful to F. Bassinot and D. Dobson for constructive reviews and helpful comments. All the data used in this manuscript are archived in the information system PANGAEA/SEPAN (www.pangaea.de). F. Schmieder was supported by the Deutsche Forschungsgemeinschaft in the framework of Graduiertenkolleg 221. This is contribution 249 of special research project SFB 261.

References

Balsam, W. L., B. L. Otto-Bliesner, and B. C. Deaton, Modern and Last Glacial Maximum eolian sedimentation patterns in the Atlantic Ocean interpreted from sediment iron oxide content, *Paleoceanography, 10,* 493-507, 1995.

Behling, H., and M. Lichte, Evidence of dry and cold climatic conditions at glacial times in tropical southeastern Brazil, *Quat. Res., 48,* 348-358, 1997.

Berger, A., and M.F. Loutre, Insolation values for the climate of the last 10 million years, *Quat. Sci. Rev., 10,* 297-317, 1991.

Bickert, T., Rekonstruktion der spätquartären Bodenwasserzirkulation im östlichen Südatlantik über stabile Isotope benthischer Foraminiferen, *Ber. Fachbereich Geowiss. Univ. Bremen, 27,* 205, 1992.

Biscaye, P. E., Mineralogy and sedimentation of recent deep-sea clay in the Atlantic Ocean and adjacent seas and oceans, *GSA Bull., 76,* 803-832, 1965.

Bleil, U., and Cruise Participants, Report and preliminary results of *Meteor* cruise 23/2 Rio de Janeiro - Recife, 27.2.1993 - 19.3.1993, *Ber. Fachbereich Geowiss. Univ. Bremen, 43,* 133, 1993.

Bleil, U., and Cruise Participants, Report and preliminary results of *Meteor* cruise 29/2 Montevideo - Rio de Janeiro, 15.7.1994 - 08.08.1994, *Ber. Fachbereich Geowiss. Univ. Bremen, 59,* 153, 1994.

Bonorino, F. G., Soil clay mineralogy of the Pampa Plains, Argentia, *J. Sediment. Res., 36,* 1026-1035, 1966.

Bowles, F. A., and P. Fleischer, Orinoco and Amazon River sediment input to the eastern Caribbean Basin, *Mar. Geol., 68,* 53-72, 1985.

Boyle, E. A., Cadmium: Chemical tracer of deep-water paleoceanography, *Paleoceanography, 3,* 471-489, 1988.

Boyle, E. A., A comparison of carbon isotopes and cadmium in the modern and glacial maximum ocean: Can we account for the discrepancies? *Carbon Cycling in the Glacial Ocean: Constraints on the Ocean's Role in Global Change, NATO ASI Ser. C,* vol. 117, edited by R. Zahn et al., pp. 105-144, Springer, New York, 1994.

Chamley, H., Influence des courants profonds au large du bresil sur la sedimentation argeleuse recent, *IXe Congr. Int. Sedimentol. Nice, Abstracts,* 13-19, 1975.

Clapperton, C. M., *Quaternary Geology and Geomorphology of South America,* 779 pp., Elsevier, New York, 1993.

Clemens, S. C., and W. L. Prell, Late Pleistocene variability of Arabian Sea summer monsoon winds and continental aridity: Eolian records from the lithogenic component of deep-sea sediments, *Paleoceanography, 5,* 109-145, 1990.

Curry, W. B., Late Quaternary deep circulation in the western equatorial Atlantic, *The South Atlantic: Present and Past Circulation,* edited by G. Wefer et al., pp. 577-598, Springer-Verlag, New York, 1996.

Curry, W. B., J. C. Duplessy, L. D. Labeyrie, and N. J. Shackleton, Changes in the distribution of $\delta^{13}C$ of deep water $\sum CO_2$ between the last glaciation and the Holocene, *Paleoceanography, 3,* 317-341, 1988.

Damuth, J. E., Late Quaternary sedimentation in the western equatorial Atlantic, *Geol. Soc. Am. Bull., 88,* 695-710, 1977.

DeMelo, U., C. P. Summerhayes, and J. P. Ellis, Salvador to Vitoria, southeastern Brazil, IV, *Contrib. Sedimentol., 4,* 78-116, 1975.

DeMenocal, P., Plio-Pleistocene African climate, *Science, 270,* 53-59, 1995 .

DeMenocal, P. B., W. F. Ruddiman, and E. M. Pokras, Influences of high- and low-latitude processes on African terrestrial climate: Pleistocene eolian records from equatorial Atlantic Ocean drilling program site 663, *Paleoceanography, 88,* 209-242, 1993.

Deuser, W. G., P. G. Brewer, T. D. Jickells, and R. F. Commeau, Biological control of the removal of abiogenic particles from the surface ocean, *Science, 219,* 388-391, 1983.

Diekmann, B., R. Petschick, F. X. Gingele, D. K. Fütterer, A. Abelmann, R. Gersonde, U. Brathauer, and A. Mackensen, Clay mineral fluctuations in late Quaternary sediments of the southeastern South Atlantic: Implications for past changes of deepwater advection, *The South Atlantic: Present and Past Circulation,* edited by G. Wefer et al., pp. 621-644, Springer-Verlag New York, 1996.

Duplessy, J. C., N. J. Shackleton, R. G. Fairbanks, L. D., Labeyrie, D. Oppo, and N. Kallel, Deep water source variations during the last climatic cycle and their impact on the global deep water circulation, *Paleoceanography, 3,* 343-360, 1988.

Ericson, D. B., and G. Wollin, Pleistocene climates and chronology in deep-sea sediments, *Science, 162,* 1227-1234, 1968.

Gingele, F. X., P. J. Müller, and R. R. Schneider, Orbital forcing of freshwater input in the Congo-Fan area: Clay mineral evidence from the last 200 kyr, *Paleogeogr. Paleoclimatol. Paleoecol., 138,* 17-26, 1998.

Griffin, J. J., H. Windom, and E. D. Goldberg, The distribution of clay minerals in the World Ocean, *Deep Sea Res. Oceanogr. Abstr., 15,* 433-459, 1968.

Heath, G. R., and N. G. Pisias, A method for the quantitative estimation of clay minerals in North Pacific deep-sea sediments, *Clays Clay Miner., 27,* 175-184, 1979.

Imbrie, J., J. D. Hays, D. G. Martinson, A. McIntyre, and A. C. Mix, The orbital theory of Pleistocene climate: Support from a revised chronology of the marine $\delta^{18}O$ record, in *Milankovitch and Climate, Part 1,* edited by A. Berger et al., pp. 269-305, D. Reidel, Norwell, Mass., 1984.

Imbrie J., et al., On the structure and origin of major glaciation cycles, 2, The 100,000-year cycle, *Paleoceanography, 8,* 699-735, 1993.

Jahn, B., Menardii stratigraphy, in *Report and Preliminary Results of Meteor Cruise 29/2 Montevideo - Rio de Janeiro, 15.7.1994 - 08.08.1994.*, edited by U. Bleil and Cruise Participants, *Ber. Fachbereich Geowiss. Univ. Bremen, 59,* 153, 1994.

Johnson, D. A., and K. A. Rasmussen, Late Cenozoic turbidite and contourite deposition in the southern Brazil Basin, *Mar. Geol., 58,* 225-262, 1984.

Jones, G. A., Advective transport of clay minerals in the region of the Rio Grande Rise, *Mar. Geol., 58,* 187-212, 1984.

Jones, G. A., and D. A. Johnson, Displaced Antarctic diatoms in Vema Channel sediments: Late Pleistocene/Holocene fluctuations in AABW flow, *Mar. Geol., 58,* 59-88, 1984.

Jouzel, J., C. Lorius, J. R. Petit, C. Ritz, M. Stievenard, P. Yiou, N. I. Barkov, V. M. Kotlyakov, and V. Lipenkov, The climatic record from Antarctic ice now extends back to 220 kyr BP, in *Long-term Climatic Variations, NATO ASI Ser., I,* vol. 22, edited by J.-C. Duplessy and M.-T. Spyridakis, pp. 213-237, Springer, New York, 1994.

Lamy, F., D. Hebbeln, and G. Wefer, Late Quaternary precessional cycles of terrigenous sediment input off the northern Chico, Chile (27.5°S) and paleoclimatic implications, *Paleogeogr. Paleoclimatol. Paleoecol., 141,* 233-251, 1998.

Lomb, N.R., Least-squares frequency analysis of unequally spaced data, *Astrophys. Space Sci., 39,* 447-462, 1976.

Mackensen, A., D. K. Fütterer, H. Grobe, and G. Schmiedl, Benthic foraminiferal assemblages from the eastern South Atlantic Polar Front region between 35° and 57°S: Distribution, ecology and fossilization potential, *Mar. Micropaleontol., 22,* 33-69, 1993.

Mackensen, A., H. Grobe, H.-W. Hubberten, and G. Kuhn, Benthic foraminiferal assemblages and the $\delta^{13}C$-signal in the Atlantic sector of the Southern Ocean, *Carbon Cycling in the Glacial Ocean: Constraints on the Ocean's Role in Global Change, NATO ASI Ser. C,* vol. 117, edited by R. Zahn et al., pp. 105-144, Springer, New York, 1994.

Massé, L., J.-C. Faugères, M. Bernat, A. Pujos, and M.-L. Mézerais, A 600,000-year record of Antarctic Bottom Water activity inferred from sediment textures and structures in a sediment core from the Southern Brazil Basin, *Paleoceanography, 9*, 1017-1026, 1994.

Mulitza, S., Stratigraphy, in *Report and Preliminary Results of Meteor Cruise 23/2 Rio de Janeiro - Recife, 27.2.1993 - 19.3.1993*, edited by U. Bleil, and Cruise Participants, *Ber. Fachbereich Geowiss. Univ.Bremen, 43*, 133, 1993.

Oppo, D. W., and Y. Rosenthal, Cd/Ca changes in a deep Cape Basin core over the past 730,000 years: Response of circumpolar deepwater variability to Northern Hemisphere ice sheet melting?, *Paleoceanography, 9*, 661-675, 1994.

Pastouret, L., H. Chamley, G. Delibrias, J. C. Duplessy, and J. Thiede, Late Quaternary climatic changes in western tropical Africa deduced from deep-sea sedimentation off Niger delta, *Oceanol. Acta, 1*, 217-232, 1978.

Pätzold, J., and Cruise Participants, Berichte und erste Ergebnisse über die *Meteor*-Fahrt M15/2 Rio de Janeiro - Vitoria, 18.1.1991 - 7.2.1991, *Ber. Fachbereich Geowiss. Univ. Bremen, 17*, 46, 1993.

Peterson, R. G., and L. Stramma, Upper-level circulation in the South Atlantic Ocean, *Progr. Oceanogr., 26*, 1-81, 1990.

Petschick, R., G. Kuhn, and F. X. Gingele, Clay mineral distribution in surface sediments of the South Atlantic: Sources, transport and relation to oceanography, *Mar. Geol., 130*, 203-229, 1996.

Pokras, E. M., Diatom record of late Quaternary climatic change in the eastern equatorial Atlantic and tropical Africa, *Paleoceanography, 2*, 273-286, 1987.

Raymo, M. E., W. F. Ruddiman, N. J. Shackleton, and D. W. Oppo, Evolution of Atlantic-Pacific $\delta^{13}C$ gradients over the last 2.5 m.y., *Earth Planet. Sci. Lett., 97*, 353-368, 1990.

Robinson, S. G., Applications for whole-core magnetic susceptibility measurements of deep-sea sediments, *Proc. Ocean Drill. Program Sci. Results, 115*, 737-771, 1990.

Rossignol-Strick, M., Mediterranean Quaternary sapropels: An immediate response of the African monsoon to variation of insolation, *Paleogeogr. Paleoclimatol. Paleoecol., 49*, 237-263, 1985.

Ruddiman, W.F., M.E. Raymo, D.G. Martinson, B.M. Clement, and J. Backman, Pleistocene evolution: Northern Hemisphere ice sheets and North Atlantic ocean, *Paleoceanography, 4*, 353-412, 1989.

Scargle, J.D., Studies in astronomical time series analysis, II, Statistical aspects of spectral analysis of unevenly spaced data, *Astrophys. J., 263*, 835-853, 1982.

Scargle, J.D., Studies in astronomical time series analysis, III, Fourier transforms, autocorrelation functions, and cross-correlation functions of unevenly spaced data, *Astrophys. J., 343*, 847-887, 1989.

Schmiedl, G., and A. Mackensen, Late Quaternary paleoproductivity and deep water circulation in the eastern South Atlantic Ocean: Evidence from benthic foraminifera, *Paleogeogr. Paleoclimatol. Paleoecol., 130*, 43-80, 1997.

Schulz, M., and K. Stattegger, Spectrum: Spectral analysis of unevenly spaced paleoclimatic time series, *Comp. Geosci., 23*, 929-945, 1997.

Shackleton, N. J., A. Berger, and W. R. Peltier, An alternative astronomical calibration of the lower Pleistocene timescale based on ODP site 677, *Trans. R. Soc. Edinburgh Earth Sci., 81*, 251-261, 1990.

Teruggi, M. E., The nature and origin of Argentine Loess, *J. Sedimentol. Petrol., 27/3*, 322-332, 1957.

von Dobeneck, T., and F. Schmieder, Using rock magnetic proxy records for orbital tuning and extended time series analysis into the super and sub-Milankovitch bands, *Proxies in Paleoceanography*, edited by G. Fischer and G. Wefer, Springer, New York, in press, 1998.

Waelbroeck, C., J. Jouzel, L. Labeyrie, C. Lorius, M. Labracherie, M. Stievenard, and N. I. Barkov, A comparison of the Vostok ice deuterium record and series from Southern Ocean core MD 88-770 over the last two glacial-interglacial cycles, *Clim. Dyn., 12*, 113-123, 1995.

Wefer, G., and Cruise Participants, Report and preliminary results of *Meteor*-cruise M34/3 Walvis Bay - Recife, 21.02. - 17.03.1996, *Ber. Fachbereich Geowiss. Univ. Bremen. 79*, 168, 1996.

Zachariasse, W. J., R. R. Schmidt, and R. J. W. Van Leuwen, Distribution of foraminifera and calcareous nannoplankton in Quaternary sediments of the eastern Angola Basin in response to climatic and oceanic fluctuations, *Neth. J. Sea Res., 17*, 250-275, 1984.

Zarate, M., and A. Balsi, Late Pleistocene-Holocene eolian deposits of the southern Buenos Aires province, Argentina: A preliminary model, *Quat. Int., 17*, 15-20, 1993.

F. X. Gingele, Baltic Sea Research Institute, Seestraße 15, D-18119 Warnemünde, Germany. (e-mail: franz.gingele@io-warnemuende.de)

R. Petschick, Fachbereich Geowissenschaften, Universität Frankfurt Senckenberganlage 32-34, D-60325 Frankfurt, Germany.

C. Rühlemann, F. Schmieder, and T. von Dobeneck, Fachbereich Geowissenschaften, Universität Bremen, Bibliotheksstrasse, D-28334 Bremen, Germany.

(Received April 9, 1998;
revised October 23, 1998;
accepted October 27, 1998.)

Summary and perspectives

Two closely related main objectives delineate the framework of this thesis:

- Establishing representative age models for sediment series from the South Atlantic Ocean based on high-resolution magnetic measurements.
- Extracting paleoceanographic and paleoclimatic information from the climatically controlled magnetic signals by means of specially adapted statistical analyses.

The results achieved substantiate magnetic cyclostratigraphy as a potentially very powerful tool for detailed, accurate age modeling. Proceeding from magnetostratigraphic or oxygen isotope dating high-resolution chronostratigraphies were established by orbital tuning of susceptibility records. In the subtropical and western tropical South Atlantic Ocean as in many other open ocean environments these signals reflect the varying ratio of climatically modulated terrigenous and biogenic sediment accumulation.

While the SUSAS records are essentially dominated by carbonate dissolution cycles due to enhanced influence of southern source waters during glacials, the CEARIS series primarily mirror sea-level related changes in terrigenous input. These regional depositional settings had to be taken into account in the tuning procedure as they affect the phase relations between driving orbital variations and environmental magnetic response and therefore the definition of suitable target signals.

Age control is a crucial precondition for every paleoceanographic study. Consequently, the magnetic cyclostratigraphies presented led to several interdisciplinary co-operations. They enabled a temporal analysis of clay mineral input during Pleistocene times recorded in a SUSAS core from the western Rio Grande Rise. In this area surface samples identify the Rio Doce as a major source of kaolinite. Cyclic variations of kaolinite/chlorite ratios in the 41 and 100 kyr bands were shown to be coherent with global ice volume. They are interpreted to originate from increased humidity in the South American hinterland and enhanced runoff of the Rio Doce during interglacials. Due to low sedimentation rates, the strong precessional component which must be expected under these conditions as a result of low-latitude insolation changes is not preserved in this core. However, for sediments from the Santos Plateau high-resolution susceptibility measurements permitted the refinement of an oxygen isotope stratigraphy and the identification of a strong 23 kyr periodicity in kaolinite/chlorite ratios. This finding validates the link between low-latitude climate changes and kaolinite input.

Extended time series analyses of magnetic susceptibility focused on climate variability in the frequency bands above and below the main Milankovitch frequencies. Higher sedimentation rates allowed a detailed investigation of sub-Milankovitch phenomena for sediments from the Ceará Rise. Using techniques of bandpass filtering, spectral and bispectral analysis high frequency patterns could be related to periodic harmonics and combination tones of orbital frequencies as well as to millennial Dansgaard-Oeschger cycles. The direct linkage of terrigenous sedimentation to tropical climate mirrored in environmental magnetic data opens promising perspectives for sub-Milankovitch reconstructions in these latitudes.

Magnetic cyclostratigraphy also enabled detailed age modeling for the low sedimentation rate deposits from the oligotrophic 'ocean desert' of the subtropical South Atlantic yielding complete Pleistocene time series. The main, still enigmatic feature of this interval of Earth's climate history is the change from variations with a period of 41 kyr to the late Pleistocene 100 kyr ice age cycles in the course of the mid-Pleistocene climate transition

(MPT). Visualized by evolutionary spectral analysis the changing frequency content of the SUSAS cores reproduce in great detail the Pleistocene climate evolution known from benthic oxygen isotopes.

Compared to a stationary ETP model the magnetic proxy signals document an alternating exchange of spectral energy between the 41 and 100 kyr bands. Preceded by the occurrence of a single 100 kyr cycle at about 1150 ka, the major shift towards reduced response to obliquity forcing occurred at about 650 ka, synchronous with the onset of 100 kyr cyclicity. These results substantiate threshold models which explain the late Quaternary 100 kyr cycles by postulating a decreasing atmospheric pCO_2 level.

In addition, magnetic mineral concentrations recorded an important paleoceanographic feature not reported from oxygen isotopes and hence obviously not directly related to global ice volume. In the middle Pleistocene average susceptibilities are enhanced by 40%, a consequence of reduced carbonate deposition as magnetite accumulation remained constant. Temporal analysis of the SUSAS west-east asymmetry permits to define a MPT interim state of increased carbonate dissolution, most likely resulting from enhanced influence of southern source deep waters. This interval exactly fills the time span between the first occurrence of larger glacial ice shields at about 920 ka and the onset of the 100 kyr cyclicity.

At the end of the MPT interim state, a terminal event documented by various unusual lithologies was observed in several cores. This '530 ka event' is presumably related to strong changes in the ocean circulation system. A global character of this event is suggested as it occurs coincidentally with other unusual climate excursions which hint at extremely warm and humid climates in Asia and Africa.
These new insights to the nature of the MPT were essentially drawn from a rock magnetic view on Quaternary marine sediment series. Magnetic cyclostratigraphy and advanced signal analyses were the tools to decipher the sediment history of a key region for the understanding of the global thermohaline circulation which, due to very low sedimentation rates, had been largely excluded from earlier paleoceanographic studies.

Danksagung

Herrn Professor Dr. Ulrich Bleil danke ich für die Vergabe und Betreuung der Dissertation, sein stetes, anregend kritisches Interesse am Fortgang der Arbeiten und ganz besonders für das mir in schwierigen Zeiten entgegengebrachte Verständnis.

Für die freundliche Übernahme des zweiten Gutachtens danke ich Herrn Professor Dr. Gerold Wefer.

Die intensive Zusammenarbeit mit Dr. Tilo von Dobeneck hat mir große Freude bereitet. Gut, daß wir die gleiche 'Wellenlänge' haben und so manches Mal zur richtigen Zeit 'in Phase' gedacht und gehandelt haben! Danke, Tilo!

Für die nette Arbeitsatmosphäre geht ein dickes 'Dankeschön' an meine Kolleginnen und Kollegen in der Marinen Geophysik, an die Techniker Liane Brück, Heike Piero und Christian Hilgenfeldt, unsere Mädels Katharina Däumler und Andrea Schmidt, den unvergessenen 'Ehemaligen' Dr. Harald 'Harri' Petermann, Dr. Thomas Frederichs, Dr. Karl Fabian und natürlich an meinen lieben Zimmerkollegen Jens Funk. Ein 'Danke' auch an Professor Dr. Volkhard Spieß und seine Arbeitsgruppe für die gute und produktive Nachbarschaft, an Dr. Franz Gingele für die gute Zusammenarbeit am Rio Grande Rise und an Dr. Torsten Bickert für seine stete Diskussionsbereitschaft und auch dafür, daß er mir zum Teil unveröffentlichte Daten zur Verfügung gestellt hat. Stellvertretend für all' die anderen netten Leute im Fachbereich Geowissenschaften der Universität Bremen, die das Arbeiten hier im Hause und auf dem Schiff so angenehm gestalten, möchte ich an dieser Stelle der 'guten Seele' des SFB's, Gisela Boelen, danken, die wir alle kennen und lieben und die hier insbesondere für die jungen Leute (und zum Glück auch für die nicht mehr ganz so jungen) so viel tut.

Petra, Dirk und Sebastian Rahe haben mir manch' erholsame Stunde in der Heide geschenkt und waren immer für mich da, wenn mir der Himmel auf den Kopf zu fallen drohte. Einen ganz lieben Dank dafür!

Nicht zuletzt möchte ich von Herzen den Menschen danken, die in den Jahren meiner Dissertation mit mir zusammen gewohnt und gelebt haben: Eleonora Uliana, Andrea Spies, André Janke, Bernd Laser und Markus Josten.